

# THE RADIO AND ELECTRONIC ENGINEER

The Journal of the Institution of Electronic and Radio Engineers

FOUNDED 1925 INCORPORATED BY ROYAL CHARTER 1961

*"To promote the advancement of radio, electronics and kindred subjects by the exchange of information in these branches of engineering."*

---

VOLUME 30

JULY 1965

NUMBER 1

---

## A MINISTRY OF COMMUNICATIONS

THE wide ranging proposals now being made in Parliament and the Press for the reorganization of the British Post Office may well lead to alteration of ministerial responsibility for Britain's communication services.

Under the Wireless Telegraphy Act of 1904 the Post Office is established as the British national communications organization. For example it handles the allocation of frequencies and in this respect it must often be placed in an invidious position since it is both the authority and an important user of the frequencies it allocates. The Post Office is also invariably responsible for nominating representatives of Great Britain at international discussions.

These functions were reviewed in the Institution's survey 'Radio and Television Broadcasting in Great Britain'† which recommended that in all international communications matters Great Britain should be represented by a National Communications Authority. Nationally this would provide for representation of all classes of users of communication systems, including the defence services, so that they could make their claims for various frequency allocations. The Authority would be served also by a Systems Committee to deal with such technical problems as systems of colour and monochrome television, sound and wired broadcasting, the radio and telephone services, etc.

The British Post Office has to its credit outstanding achievements in the development of all forms of communication, both by wire and radio. It has contributed greatly by providing a national network for distribution of television, but the pace of modern advance calls for quite independent control of a modern communications system. The tremendous possibilities in the field of satellite communication have often been referred to in this *Journal* and it is true that the original *Telstar* project called for great efficiency from British Post Office engineers who designed and built the Goonhilly earth station.

The present Minister—the Postmaster General—is not only responsible for communications, including telephone and telegraph services, but is also responsible for a Savings Bank and all postal services. All this in an age when electronics, which derived from and is increasingly responsible for all forms of communication services, is ranked as one of the country's most important industries!

Some separation of these ministerial responsibilities is therefore inevitable. It is not the function of this *Journal* to comment on rumours and manifestos on extending public ownership by the establishment of state enterprise, linked with existing nationalized industries. We may, however, note that the Post Office Engineering Union has already advocated separation of the telephone service.

Certainly the other services of the Post Office could in themselves benefit from wider adoption of modern methods of automation such as automatic sorting methods, and computer oriented banking techniques. These modern technological aids could be better studied by a Minister free of the responsibilities of a Britain committed to an age of space communication.

Apart from the international problems of direct and shared satellite communication facilities, Commonwealth and international standardization of equipment, and research, a future Minister of Communications will immediately have the problem of improving Britain's internal communications and ensuring adequate facilities for communication in the Europe of the future. An extremely worthwhile job, calling for a Minister with a vision of the future.

G. D. C.

---

† *J. Brit. I.R.E.*, 21, pp. 379–87, May 1961.

## INSTITUTION NOTICES

### Election of Honorary Members

At an Institution meeting held in London on 26th May 1965 the Council's recommendation that Admiral of the Fleet The Earl Mountbatten of Burma, K.G., should be elected Honorary Member, was approved with acclamation.

Lord Mountbatten was presented with his scroll of Honorary Membership and signed the Roll of Honorary Members on the occasion of the Institution's Dinner in London on 24th June. In presenting the scroll the President, Colonel G. W. Raby, C.B.E., paid tribute to Lord Mountbatten's services to the Institution as President and subsequently Charter President.

During the Reception preceding the Dinner, Sir Gordon Radley, K.C.B., C.B.E., also signed the Roll of Honorary Members and received his scroll of Honorary Membership from the Immediate Past President, Mr. J. Langham Thompson. Members will recall that Mr. Thompson placed the Council's recommendation for the election of Sir Gordon as an Honorary Member before the Membership at a meeting in London on 26th May, 1964. This was the date on which Sir Gordon gave his Clerk Maxwell Memorial Lecture. (See *The Radio and Electronic Engineer*, June 1964.)

### Annual General Meeting

The 4th Annual General Meeting of the Institution since its incorporation by Royal Charter, will be held at the London School of Hygiene and Tropical Medicine, Gower Street, W.C.1, on Monday, 13th December, 1965 at 6 p.m.

The formal Notice of Meeting and Agenda will be published in the *Proceedings* of the Institution.

### The British Association for the Advancement of Science

This year's Annual Meeting of the British Association for the Advancement of Science will be held at Cambridge from 1st to 8th September.

The programme of this famous scientific meeting this year shows much evidence of the Association's intention to give more attention than formerly to technology as distinct from the pure sciences. In the field of electronics, for instance, the Association's Kelvin Lecture will be on "Thin films and their role in computers", to be given by Dr. Martin Prutton.

Further information may be obtained from the British Association offices at 3 Sanctuary Buildings, 20 Great Smith Street, London, S.W.1.

### Earl Mountbatten of Burma

Her Majesty The Queen has appointed Admiral of the Fleet Earl Mountbatten of Burma, K.G., to the Order of Merit. Lord Mountbatten retired on 16th July from the post of the Chief of the Defence Staff which he has held for the past six years.

### Proposed French Section of the Institution

At a meeting of members held in Paris on 10th April last, during the International Components Exhibition, it was unanimously agreed to set up a small committee to organize meetings and other functions for members in France. M. Mstislas Martinoff (Associate Member) is Chairman of the committee, and M. P. J. C. Prevost (Associate Member) is the Secretary. Other members of the committee are: Dr. A. V. J. Martin and Wing Commander G. E. Trevains (Associate Members) and M. N. C. Sen (Graduate).

The committee hopes that its activities during the coming months will justify the Council approving the formal establishment of a French Section.

Information on the committee's plans may be obtained from M. Prevost, whose address is 29 Rue Victor Massé, Paris 9.

### International Conference on Microwave and Optical Generation and Amplification

The Sixth International Conference on Microwave and Optical Generation and Amplification (formerly known as the Conference on Microwave Tubes) will be held at Cambridge University from 12th to 16th September 1966. The Conference, which is sponsored jointly by the Electronics Division of the Institution of Electrical Engineers and the I.E.R.E., is intended to stimulate the exchange of ideas on the research which will have taken place since the Fifth Conference in Paris in September 1964 in the fields of microwave and optical generation, amplification and other active processes. Contributions on recent outstanding scientific and technical progress in these fields will be presented and discussed.

The programme will cover microwave and optical generation by solid state, plasma and other active devices, as well as by the classical forms of microwave tubes. In addition it will include the application of various principles and phenomena relevant to the generation and amplification of coherent electromagnetic waves without strict frequency limitation.

Offers of papers and requests for further information when available should be sent to the Conference Secretariat (Reference MOGA), Institution of Electrical Engineers, Savoy Place, London, W.C.2.

# Distributed CR Cross-coupling Circuits for Multivibrators

By

K. G. NICHOLS, M.Sc.

(Associate Member)†

**Summary:** The use of uniformly distributed capacitance-resistance lines as cross-coupling circuits for transistor multivibrators is considered. The differential equation which governs the voltage across the line at any point is set up; this equation is the one-dimensional heat conduction equation. Boundary conditions are derived corresponding to the different parts of the multivibrator cycle. A numerical method of solving the equation for the base and collector waveforms is given. An approximation is introduced to deal with the effects of stored base charge on the multivibrator waveforms. The results of specimen calculations are discussed. Some details of the numerical analysis technique, and of the programming details, are presented in an appendix.

## 1. Introduction

The possibility of using distributed capacitance-resistance networks as the cross-coupling elements for multivibrator circuits has been suggested elsewhere.<sup>1, 2</sup> Such coupling elements may find application in thin-film microcircuits and integrated solid circuits, for the combination of resistive and capacitive elements may effect a saving of substrate area.

In a thin-film microcircuit the distributed CR line would consist of a dielectric layer sandwiched between two thin film nichrome resistors.<sup>3</sup> In integrated solid circuits the line would consist of a reverse-biased p-n junction. The lateral resistance of the semiconductor on either side of the junction would form the resistors of the line. The junction capacitance would be distributed along the line between the two resistors. Such structures form four-terminal networks which are represented by the symbol<sup>3, 4</sup> of Fig. 1.

In the present paper, consideration is restricted to uniform lines, that is, to lines having a constant resistance and capacitance per unit length. Referring to Fig. 1, the total resistance of the lower arm is taken as  $R$ , that of the upper arm as  $NR$ , and the total capacitance between them as  $C$ . The quantity  $N$  is thus the ratio between the two resistances. Throughout it is convenient to assume that the line has unit length, and to refer to any point of the line by means of a fraction of its length, referred to one end.

A further restriction of the present paper is the limiting of the resistance and capacitance values to constants independent of voltage. This is certainly not true of the integrated circuit line, where the capacitance of the p-n junction is function of the junction voltage, and where also the resistances on either side of the junction may be somewhat changed by space-charge depletion effects. It is hoped to investigate lines with

voltage-dependent capacitance at some later date.

Nevertheless, in a qualitative way, the results obtained from the restricted analysis here presented throw some light on the somewhat more involved case of voltage-dependence.

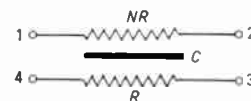


Fig. 1. Uniform, distributed CR line.

## 2. The Multivibrator Circuit and Equivalent Circuits

The connections to the line so that it may be used as a cross-coupling network of a multivibrator type circuit are shown in Fig. 2. The resistance  $R$  is the collector load of the transistor Tr 1, and the resistance  $NR$  is the base leak of the transistor Tr 2. The capacitance  $C$  cross-couples the collector of transistor Tr 1 to the base of transistor Tr 2. The collector of Tr 2 and the base of Tr 1 are also cross-coupled, either by a conventional, lumped parameter,  $CR$  network, or by a second distributed line. The circuit may be biased as a univibrator by making positive either  $-V_{BB}$ , or the equivalent supply to the base of Tr 1. As a multivibrator both these supplies are negative in polarity.

Excluding the relatively short time during which the circuit switches from one state to another, only one transistor of the pair conducts at any instant, the other being held off by a positive voltage on its base. Further, under normal operating conditions, the conducting transistor is in the saturated state. This is essential if the repetition frequency of the multivibrator, or pulse duration of the univibrator, is to be largely independent of the transistor characteristics. All practical multivibrators operate with the conducting transistor saturated, unless extra circuit

† Department of Electronics, University of Southampton.

elements, diodes or Zener diodes, are used to define voltage levels, thereby preventing saturation of the transistors. Circuits of this latter kind will not be considered. In what follows, it will be assumed that the conducting transistor remains saturated until it is switched off by a positive voltage at its base. This is equivalent to assuming a sufficiently high current gain in common emitter configuration.

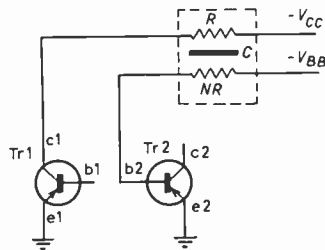


Fig. 2. The line as a cross-coupling network in a multivibrator circuit.

In saturation, the collector-emitter voltage of a transistor is a function of the collector current  $I_c$ , but nevertheless is small, and unlikely to exceed 200 mV in magnitude. In addition the base-emitter voltage of the conducting transistor will not exceed a few hundred millivolts at any base current to be encountered. These voltages will be approximated to by zero voltages in this analysis. Thus the collector-emitter and base-emitter are assumed to be short-circuit paths for the saturated transistor.

In addition, leakage current in the base-collector path of a transistor, cut off by a positive voltage on its base, will be neglected. The cut-off transistor is therefore represented by open-circuits between the three electrodes.

The circuit which may be used to investigate the base-waveform of the cut-off transistor is shown in Fig. 3. Here Tr 1 is conducting and Tr 2 is cut-off, its base voltage being positive. The base voltage of Tr 2 must decay from its positive value towards  $-V_{BB}$  for it is returned to this supply through the resistance  $NR$ . When this base voltage is approximately zero, Tr 2 conducts, and the well-known positive feedback-regenerative action rapidly switches Tr 2 on, and Tr 1 off.

It is usually assumed that this regeneration is so rapid that the energy stored in the cross-coupling networks is unchanged during the switching. The energy stored on the line just before switching becomes the initial condition for the determination of the collector waveform of Tr 1 just after switching. The circuit for this latter case is shown in Fig. 4. The collector voltage of transistor Tr 1, cut off by a positive

voltage on its base, will now decay from zero towards the supply  $-V_{CC}$ . The degree to which it attains this goal depends on how long it takes its base to decay to the cut-on point of approximately zero volts, for the case of the multivibrator, or on the time delay before the advent of another trigger pulse, in the case of the univibrator.

One point worth noting is that although switching from the circuit of Fig. 3 to that of Fig. 4 occurs when the base voltage of Tr 2 is zero, that is, when the voltage across the left-hand end of the line is zero, there is still a voltage across other parts of the line. The conclusion is that it is not possible to assume a uniform distribution of energy along the line at the instant of switching.

The circuits for the two normal states of the multivibrator have been discussed. One further case remains to be considered. Although it has been stated that switching between states is very rapid and, for the purposes of waveform determination, the switching time can be neglected, there is one case where this switching time may be appreciable. More significantly, this case may have a marked effect on the base waveform when distributed coupling networks, as distinct from conventional networks, are used. This occurs when there is appreciable stored base charge in the saturated transistor. Before the base voltage of a transistor can be taken positive, to switch it off, its stored base charge must be neutralized. In the present case, this is carried out at the expense of charge stored in the capacitance of the distributed line. If the transistor is of a slow switching type, its stored base charge when saturated may not be negligible compared with the charge stored on the line. Alternatively, this may be expressed as if the line capacitance is too low, the stored base charge is no longer negligible. In a conventional multivibrator, the lumped parameter cross-coupling capacitance has charge immediately available for neutralization of the stored base charge. Although loss of step-amplitude may occur, the base voltage waveform is unchanged in general shape. In the present case, the neutralizing charge must be drawn through part of the resistance of the line, thereby involving a delay. The base waveform is, in this case, modified in shape. In a later section of the paper, a computed waveform illustrates this effect (see Fig. 15).

Consider the state of affairs just before transistor Tr 1 is switched on by its base voltage dropping to zero. The circuit which is applicable is that of Fig. 4. The collector voltage of transistor Tr 1 will be negative, but not necessarily equal to  $-V_{CC}$  unless a long time has elapsed to allow it to attain this potential. Since the base of Tr 2 is at zero, there will therefore be a potential across the left-hand end of the line. Now when transistor Tr 1 switches on, it will go into

saturation and so its collector voltage rises rapidly to zero. In the absence of stored base charge, the positive potential step at the collector of Tr 1 is communicated via the distributed capacitance  $C$  to the base of Tr 2, causing its voltage to go positive, thus cutting Tr 2 off. In the presence of stored base charge, the base of Tr 2 will not go positive until its stored charge has been neutralized by current flow into the base terminal  $b_2$ . Only after this neutralization will the base voltage rise above zero. The equivalent circuit during this neutralization process is shown in Fig. 5. Once neutralization has been effected then the circuit of Fig. 3 is applicable. The initial conditions for this latter circuit will, however, depend on how much charge has been lost from the distributed capacitance, during the neutralization period. This neutralization of the stored base charge is the only switching transient effect which will be considered.

For future reference, the three states under consideration, namely those for which the circuits of Figs. 3, 4 and 5 are applicable, will be referred to as cases A, B and C respectively. All three cases satisfy the same differential equation, which will be derived in the next section, but must be solved subject to different boundary conditions. These latter conditions will be considered in section 4.

### 3. The Line Equation

Inspection of Figs. 3, 4 and 5 shows that the networks to be considered are of the two mesh variety, even though one of the meshes is rather simple, and involves the earth line through the batteries  $V_{CC}$  and  $V_{BB}$ .

In a more complex example, distributed capacitance between the resistance  $R$  and the earth line, and between the resistance  $NR$  and the earth line, would be expected.

For such a system there will, in general, be two simultaneous differential equations to be satisfied corresponding to the two mesh equations of lumped parameter circuit theory. In the present case, it will be shown that a reduction to one equation can be effected, the presence of the second mesh being dealt with by modification of the boundary conditions that the solution must satisfy.

Figure 6 shows an infinitesimal length  $\delta x$  of the line, the earth line completing the second mesh. Since the total length of the line is unity, the elements of the short length are  $R \delta x$ ,  $NR \delta x$  and  $C \delta x$ , where  $R$ ,  $NR$  and  $C$  are the total values. The voltages and mesh currents are shown in the figure.

At a fixed instant of time, the following mesh equations may be written.†

† See also reference 4, wherein an equation for sinusoidal operation is set up.

$$V - IR \delta x - V - \delta V - INR \delta x + I'NR \delta x = 0$$

$$V' - I'NR \delta x + INR \delta x - V' - \delta V' = 0$$

Dropping the restriction to a fixed instant of time, these equations become respectively:

$$\frac{\partial V}{\partial x} = -(N+1)RI + NRI' \quad \dots\dots(1)$$

$$\frac{\partial V'}{\partial x} = NRI - NRI' \quad \dots\dots(2)$$

In addition, the current increment  $\delta I$  in a length  $\delta x$  results from a changing voltage across the capacitance  $C \delta x$ , thus:

$$\delta I = -C \delta x \frac{\partial V}{\partial t}$$

or

$$\frac{\partial I}{\partial x} = -C \frac{\partial V}{\partial t} \quad \dots\dots(3)$$

The absence of distributed capacitance in the other mesh means that  $\delta I'$  is zero, as indicated in the figure, and hence,

$$\frac{\partial I'}{\partial x} = 0 \quad \dots\dots(4)$$

Differentiation of eqns. (1) and (2) followed by substitution from (3) and (4) leads to:

$$\frac{\partial^2 V}{\partial x^2} = (N+1)CR \frac{\partial V}{\partial t} \quad \dots\dots(5)$$

$$\frac{\partial^2 V'}{\partial x^2} = -NCR \frac{\partial V}{\partial t} \quad \dots\dots(6)$$

These are the simultaneous, differential, mesh equations. In a general case both would involve  $V$  and  $V'$ . In this special case only the latter equation involves  $V'$ . The first of the equations is the one-dimensional heat conduction equation, exact solutions of which exist for many particular cases.<sup>5</sup> These exact solutions are difficult to apply when subject to involved boundary and initial conditions, such as exist in the present work. For this reason a numerical technique for the solution of the equation has been adopted. The boundary condition for eqn. (5) arises out of eqn. (6) in the following way; elimination of  $\left(\frac{\partial V}{\partial t}\right)$  between these equations gives:

$$\frac{\partial^2 V'}{\partial x^2} = -\frac{N}{N+1} \cdot \frac{\partial^2 V}{\partial x^2}$$

which integrates twice to:

$$V' = B(t) + A(t)x - \frac{N}{N+1} V \quad \dots\dots(7)$$

$A(t)$  and  $B(t)$  are arbitrary functions of time, independent of  $x$ , which are determined by the initial conditions of the problem.

Thus in this special case, the simultaneous differential equations reduce to one equation, namely (5), for once  $V$  is known  $V'$  can be obtained by use of eqn (7). In order to deal with the stored base charge consideration, case C, expressions for the mesh currents  $I$  and  $I'$  will be required. These can be obtained from eqns. (1) and (2). The terms in  $\left(\frac{\partial V'}{\partial x}\right)$  can be eliminated with the aid of a differentiated version of eqn. (7).

Thus:

$$I = -\frac{1}{R}\left(\frac{\partial V}{\partial x} + \frac{\partial V'}{\partial x}\right) = -\frac{1}{R}\left(\frac{1}{N+1} \cdot \frac{\partial V}{\partial x} + A(t)\right) \dots\dots(8)$$

$$I' = -\frac{1}{NR}\left(N \frac{\partial V}{\partial x} + (N+1) \frac{\partial V'}{\partial x}\right) = -\frac{N+1}{N} \frac{A(t)}{R} \dots\dots(9)$$

It is convenient to have also an expression for  $(I-I')$  for this is the current, evaluated at  $x = 0$ , which flows into the base terminal when dealing with case C. Thus

$$I-I' = -\frac{1}{R}\left(\frac{1}{N+1} \frac{\partial V}{\partial x} - \frac{A(t)}{N}\right) \dots\dots(10)$$

Summarizing, the differential equation to be solved is the one-dimensional heat conduction equation, namely (5), and the equations required for the boundary conditions are (7), (8), (9) and (10).

**4. The Boundary and Initial Conditions**

**4.1. Case A. The Voltage Waveform of the Cut-off Base. (Circuit of Fig. 3.)**

The symbol  $V(x, t)$  is used to represent the voltage across the line at any point  $x$  and any time  $t$ , with similar interpretation of other symbols.

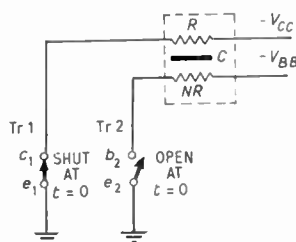


Fig. 3. Equivalent circuit A; Tr 1 conducting, Tr 2 cut-off,  $V_{b2} > 0$ , decaying towards  $-V_{BB}$ .

At the right-hand end, the line voltage must equal the difference in the battery voltages at all times:

$$V(1, t) = V_{BB} - V_{CC} \dots\dots(11)$$

In addition, at this end of the line, the voltage  $V'$  is equal to  $V_{BB}$  at all times, and so by eqn. (7), and

subsequently (11):

$$V'(1, t) = -V_{BB} = B(t) + A(t) - \frac{N}{N+1}(V_{BB} - V_{CC}) \dots\dots(12)$$

Again, referring to Fig. 3, it is seen that the current out of terminal  $b_2$  is zero at all times, whence by eqn. (10);

$$I'(0, t) - I(0, t) = \frac{1}{R}\left(\frac{1}{N+1} \frac{\partial V}{\partial x}(0, t) - \frac{1}{N} A(t)\right) = 0 \dots\dots(13)$$

Also, from Fig. 3, since the terminal  $c_1$  is grounded, the voltage  $V + V'$  is zero, for all time, at the left-hand end of the line; hence, using eqn. (7);

$$V(0, t) + V'(0, t) = V(0, t) + B(t) - \frac{N}{N+1} V(0, t) = 0 \dots\dots(14)$$

Equations (12) and (14) can be solved for  $A(t)$  and the solution substituted into eqn. (13) to give the derivative boundary condition;

$$\frac{\partial V}{\partial x}(0, t) - \frac{V(0, t)}{N} = -V_{CC} - \frac{V_{BB}}{N} \dots\dots(15)$$

This equation is the boundary condition at the left-hand end of the line ( $x = 0$ ), and eqn. (11) is the boundary condition at the right-hand end of the line ( $x = 1$ ).

It remains to consider the initial condition of the line. Referring to Fig. 4, it is seen that if the circuit has been in this state for a sufficiently long time, the collector terminal  $c_1$  of Tr 1 will be at a potential  $-V_{CC}$  and the voltage distribution along the line will be given by  $(xV_{BB} - V_{CC})$ . This is a linear distribution from  $-V_{CC}$  at the left-hand end to  $(V_{BB} - V_{CC})$  at the right-hand end. In the absence of stored base charge effects, if now the circuit switches to its other state (Fig. 3) then this distribution along the line becomes the initial condition for the case A problem. The initial condition is therefore:

$$V(x, 0) = xV_{BB} - V_{CC} \dots\dots(16)$$

Strictly then, this condition would apply for a univibrator whose stable state is Tr 1 off and Tr 2 on, and which is only triggered to its astable state after it has attained quiescence in its stable state. In the more general case of a multivibrator, it is to be expected that the circuit will switch from case B (Fig. 4) to case A (Fig. 3) before the transients in Fig. 4 have died out to leave the linear distribution of eqn. (16) along the line. In this case the initial condition  $V(x, 0)$  for the case A solution must be taken as the final condition of the case B solution. If there is any appreciable stored base charge, the distribution along the line is modified, as a result of the neutralization of the stored charge, before the case A problem is entered. In this

circumstance, the initial condition  $V(x, 0)$  is taken as the final condition of the case C solution.

Two computer programs have been written to solve the case A problem, one uses the initial condition of eqn. (16), and the other, a slight modification of the first, is arranged to read in the initial condition  $V(x, 0)$  as data. These programs are arranged to compute the line voltages until such time as the base voltage of Tr 2 becomes zero. The distribution on the line at this instant is then arranged to be available as the initial condition input for the case B problem. The two case A programs will be referred to as A' and A respectively, and further details of them will be given in a later section and in the appendices.

4.2. Case B. The Voltage Waveform of the Cut-off Collector. (Circuit of Fig. 4.)

Reference to Fig. 4 shows that the boundary condition at the right-hand end of the line is identical to that for the case A problem; namely,

$$V(1, t) = V_{BB} - V_{CC} \quad \dots\dots(11)$$

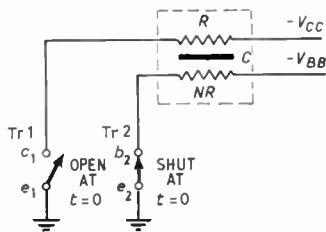


Fig. 4. Equivalent circuit B; Tr 2 conducting, Tr 1 cut-off,  $V_{c1}$  decaying towards  $-V_{CC}$ .

The boundary condition, eqn. (12), of case A is also valid for the present case.

At the left-hand end of the line the boundary conditions are:

$$V'(0, t) = B(t) - \frac{N}{N+1} V(0, t) = 0 \quad \dots\dots(17)$$

$$I(0, t) = -\frac{1}{R} \left[ \frac{1}{N+1} \frac{\partial V}{\partial x}(0, t) + A(t) \right] = 0 \quad \dots\dots(18)$$

Between eqns. (12) and (17) the function  $B(t)$  can be eliminated and the function  $A(t)$  determined. Substitution of  $A(t)$  into eqn. (18) gives,

$$\frac{\partial V}{\partial x}(0, t) - NV(0, t) = NV_{CC} + V_{BB} \quad \dots\dots(19)$$

This is the boundary condition for the left-hand end of the line.

The initial condition  $V(x, 0)$  for a case B problem is always the distribution along the line at the end of a case A solution. That is, a case A line distribution at

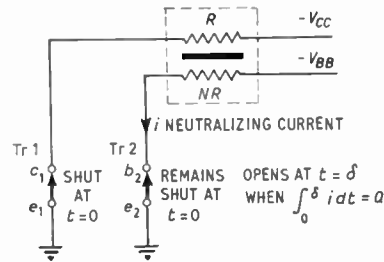


Fig. 5. Equivalent circuit C; Tr 1 and Tr 2 conducting while stored base charge of Tr 2 is neutralized.

the instant the base voltage of Tr 2 becomes zero.

A program, referred to as B, has been written to solve the case B problems. This program is arranged to compute for a time specified in its input data. The line distribution after this time is arranged to be available as initial condition input data for a case A problem, or, when stored base charge is appreciable, for a case C problem. The time for which the program is required to compute is taken as the base voltage decay time of the *other* coupling circuit, irrespective as to whether it is a conventional lumped parameter, or a distributed parameter, circuit. The determination of this time interval in the general case will be discussed in a later section.

4.3. Case C. The Neutralization of the Stored Base Charge. (Circuit of Fig. 5.)

Reference to Fig. 5 shows that the boundary condition at the right-hand end of the line is once again given by eqn. (11), namely

$$V(1, t) = V_{BB} - V_{CC} \quad \dots\dots(11)$$

The boundary condition, eqn. (12), is also valid for this case.

At the left-hand end of the line the boundary condition is now simply

$$V(0, t) = 0 \quad \dots\dots(20)$$

with the additional condition:

$$V'(0, t) = 0 \quad \dots\dots(21)$$

The initial condition is either taken as eqn. (16), namely

$$V(x, 0) = xV_{BB} - V_{CC} \quad \dots\dots(16)$$

valid when the cut-off collector circuit has become quiescent before being switched into saturation, or as the final line distribution of a case B calculation. This latter case is applicable when the collector of the cut-off transistor has not become quiescent prior to switching into saturation.

The calculation must be continued until such time as the stored base charge has been neutralized. The stored base charge  $Q$  will be expressed as an equivalent length  $q$  of the line changed to the voltage  $V_{CC}$ . Thus:

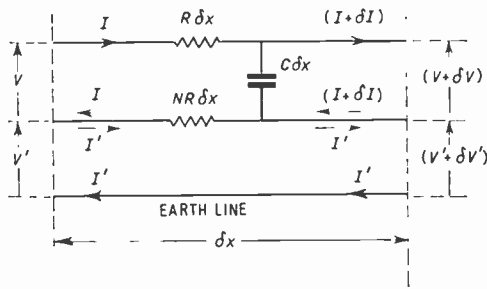


Fig. 6. Infinitesimal length of line showing voltages and mesh currents.

$$Q = qCV_{CC} \quad \dots\dots(22)$$

or

$$q = \frac{Q}{CV_{CC}}$$

After an interval  $\tau$ , the base charge which has been neutralized is

$$Q(\tau) = \int_0^\tau [I(0, t) - I'(0, t)] dt \quad \dots\dots(23)$$

since the integrand here is the current flowing out of the base terminal  $b_2$  (see Fig. 5). When, as  $\tau$  increases, a value of  $Q(\tau)$  equal to  $Q$  is obtained, the computation is to end. This value of  $\tau$  gives the delay before case A commences and the line distribution at this time  $\tau$  becomes the initial condition for the case A problem. Using eqns. (7), (12) and (21),  $B(t)$  is found to be zero and  $A(t)$  is found to be

$$A(t) = -\frac{NV_{CC} + V_{BB}}{N + 1} \quad \dots\dots(24)$$

Substituting eqn. (10) into (23) and using (24), the condition for neutralization of the base charge becomes

$$Q = -\int_0^\tau \frac{1}{R} \left[ \frac{1}{N + 1} \frac{\partial V}{\partial x}(0, t) + \frac{NV_{CC} + V_{BB}}{N(N + 1)} \right] dt$$

Replacing  $Q$  with the equivalent line length  $q$  from eqn. (22),

$$q = -\int_0^\tau \frac{1}{(N + 1)CR} \left[ \frac{1}{V_{CC}} \frac{\partial V}{\partial x}(0, t) + \frac{N + V_{BB}/V_{CC}}{N} \right] dt \quad \dots\dots(25)$$

In the computation,  $\tau$  is increased until eqn. (25) is satisfied. In general, this is possible since the first term in the integrand is negative and causes the integrand to be negative. The right-hand side of the equation is thus positive as required. As  $\tau$  is increased, however, the integrand decreases in magnitude and eventually changes sign. If this occurs before the integral becomes equal to  $q$ , it is impossible to neutralize the stored charge with the charge available on the line.

Then the circuit does not multivibrate and this will be called the 'fail' condition.

The computer programs for this case determine the time  $\tau$  for neutralization of the stored charge or indicate a 'fail' if this should occur. At the instant of neutralization, the distribution along the line is arranged to be available as input data for a case A problem. Two slightly different programs are used, the first, referred to as C', uses eqn. (16) for its initial input data, and the second, referred to as C, accepts the final line distribution of a case B problem for its initial conditions.

### 5. The Computational Method

Some brief details of the computational method and of the computer programs are given in this section. A somewhat more extensive account is presented in the Appendix. In all calculations, the time constant  $(N + 1)CR$ , appearing in eqn. (5), is normalized to 1 second. The differential equation which is solved is therefore:

$$\frac{\partial^2 V}{\partial x^2} = \frac{\partial V}{\partial t} \quad \dots\dots(26)$$

A further normalization used throughout is that of  $V_{CC}$  to 1 volt. The voltage  $V_{BB}$  may then be interpreted as the ratio of  $V_{BB}$  to  $V_{CC}$  and to avoid confusion, this ratio is denoted by the symbol  $S$ .

The differential equation is solved by the implicit difference method of Crank and Nicholson.<sup>6</sup> The line is split into a number of segments and the equation and its boundary conditions are replaced by equivalent difference equations. Up to forty equally-spaced iteration points on the line could be used, but twenty points were found adequate for most cases. Although the Crank-Nicholson method converges for any time step, some oscillation of solution was found for the larger time steps. Where this occurred, the time step was reduced until oscillation was no longer noticeable and then the number of iteration points was doubled, to forty, the time step being halved simultaneously. In all cases, the solution then obtained was in agreement with the twenty-point solution to at least four significant figures. In practice this was a simpler procedure than trying to predict in advance the iteration constants required for a given accuracy.<sup>7</sup> This oscillation of solution was associated with derivative boundary conditions, in particular, those for case B problems. At one time, it was hoped to solve the equation with only ten equally spaced iteration points. In order to do this, the so-called 'high accuracy'<sup>8</sup> derivative approximations were used for the boundary conditions. This was quite successful, but in the long run, the extra difficulty of programming to include these high accuracy derivative approximations into the Crank-Nicholson method was found tedious com-

pared with the simplicity of increasing the number of iteration points. An alternative procedure, which was not tried, would be to make the iteration points at the left-hand end of the line closer than those at the other end.

An ALGOL program, suitable for use on fast modern computers, which automatically adjusts its iteration constants to obtain any desired accuracy has been described<sup>9</sup> for dealing with problems of this kind. Unfortunately, this program was not particularly suited to the present problem nor could it be used with the available computer, a Ferranti *Pegasus*. In any event this latter computer is very slow when operating ALGOL programs.

The time steps can be defined by means of the iteration constant  $r$ :

$$\Delta t = r(\Delta x)^2 \quad \dots\dots(27)$$

where  $\Delta x$  is the interval between iteration points on the line. Although the solution converges for any

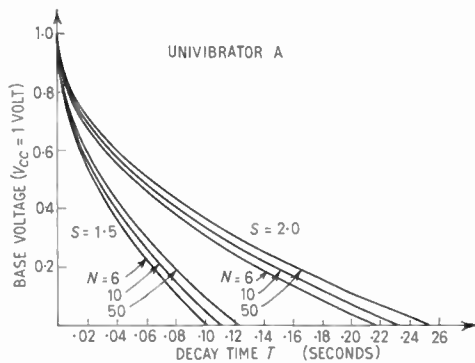


Fig. 7. Univibrator A; voltage waveform of cut-off base.

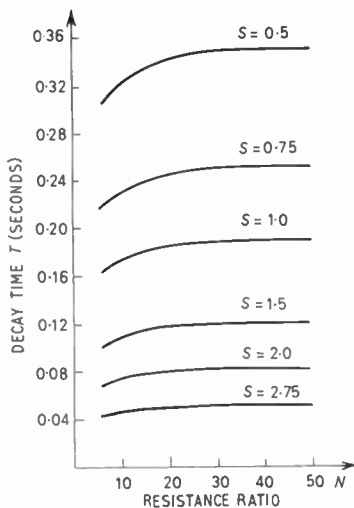


Fig. 8. Univibrator A; decay time  $T$  as a function of resistance ratio  $N$ , parameter supply ratio  $S$ .

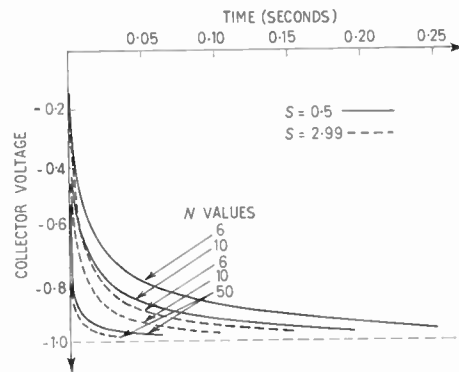


Fig. 9. Univibrator B; voltage waveform of cut-off collector.

value of  $r$ , as already explained, to avoid oscillation of the solution, the value of  $r$  had to be restricted. Using the twenty equally spaced iteration points, values of  $r$  equal to unity were found suitable for most case A solutions except when  $N$ , the ratio of the resistors, exceeded 24 in which case  $r$  was reduced to 0.5. For case B solution  $r$  values of 0.5 and 0.25 were necessary for  $N$  values below and above 24 respectively. For case C solutions, an  $r$  value of 0.25 was used throughout. Case A problems, in the presence of stored base charge, required  $r$  values of 0.25 for the first twenty, or so, time steps, but subsequently  $r$  was increased to unity. This was as much necessary to obtain adequate indication of the initial rapid rise of base voltage as to prevent oscillation of the solution.

### 6. Univibrator Waveforms: Uniform Initial Line Distributions. No Stored Base Charge

In this section, results of computations using program A' are presented. This program uses a uniform initial line distribution, eqn. (16), corresponding to the stable state of a quiescent univibrator.

The final distribution along the line at the end of the A' program is used as initial distribution for program B, which then computes the recovery of the collector waveform in the stable state. The results are presented in order to give an indication of how the waveforms and a stable period depend on the circuit parameters.

Figure 7 shows the voltage waveform of the cut-off base for two different values of  $S$ , and three different values of  $N$ . Figure 8 gives the base waveform decay time  $T$  as a function of  $N$  for a range of  $S$  values. The most marked feature of the base waveforms is the rapid initial decay which then slows up and becomes almost linear with time. It is impossible to fit an exponential curve to these waveforms with any degree of accuracy. It is worth noting that, for a given  $S$ , the decay time  $T$  is approximately independent of the parameter  $N$ , particularly for  $N$  greater than 10.

Figure 9 gives collector recovery waveforms for the normally off transistor. Waveforms for two different  $S$  values and three different  $N$  values are shown. The most noticeable feature of these waveforms is their 'square' appearance; again curve fitting to an exponential is not possible. The collector at first decays very rapidly, particularly for the high  $N$  values, and then it approaches the supply voltage  $-V_{CC}$  asymptotically. This latter approach is very gradual indeed, and a very long time elapses before it reaches 99% of its final value. This very long final recovery has a marked effect on the period when the circuit is used in a multivibrator configuration; this will be explained in the next section.

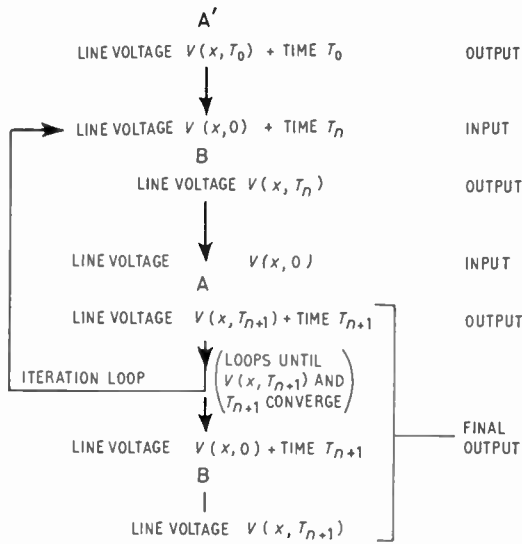


Fig. 10. Iteration loop; symmetrical multivibrator.

7. Multivibrator Waveforms. No Stored Base Charge

The  $A'$  and  $A$  programs compute the time for the base voltage to decay to zero, and make available the line distribution for input to the  $B$  program. The time the  $B$  program is required to operate is determined therefore by the decay time of an  $A$  program. In the case of a symmetrical multivibrator, the procedure is shown in Fig. 10. Initially program  $A'$  is used with the linear initial line distribution, eqn. (16). The decay time  $T_0$  and final line distribution are fed into program  $B$ . The output line distribution of  $B$  is used as initial data for  $A$ , which then computes a new decay time  $T_1$ . This is fed back into  $B$  and the programs loop until the decay times and final line distributions converge. Convergence is assumed when results for successive loops differ in only the fourth significant figures.

The number of loops required for convergence varies with the  $N$  and  $S$  parameters of the computation, but

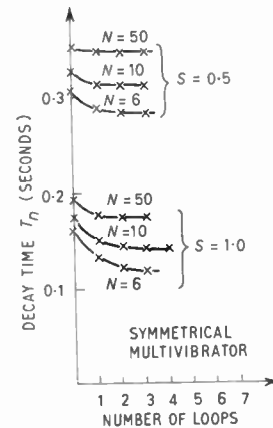


Fig. 11. Convergence of period time  $T_n$ .

is generally between four and nine. Figure 11 shows how the period time  $T_n$  converges with the loop number for a few typical cases. The general conclusion is that convergence is most rapid for small  $S$  and large  $N$ , a trend which might be expected intuitively. When the multivibrator is not symmetric, it is necessary to run two loops of programs, one for each line. The base decay time of one is used to time the collector decay of the other, and vice versa. The arrangement is shown in Fig. 12, in which the  $CR$  product for one line is twice that of the other. In addition, the  $S$  ratio of the former is twice that of the latter and the  $N$  ratios are 9 and 19 respectively. The value of  $(N+1)CR$  for line II is thus four times that

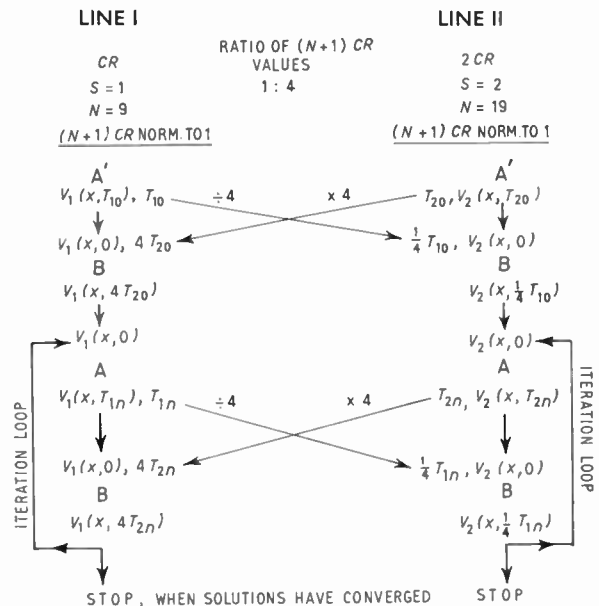


Fig. 12. Iteration loops; asymmetrical multivibrator.

for line I, but since all the programs take  $(N+1)CR$  normalized to unity, the time scale of line II is reduced by a factor of 4 relative to that of line I. It follows that the base decay times  $T_{1n}$  of line I must be divided by 4 before use as input to B programs of line II. Similarly, the times  $T_{2n}$  of line II must be multiplied by 4 before use in line I.

Again, iteration is continued in the two parallel loops until both the line voltages and decay times have converged to an accuracy of a few parts in  $10^4$ . Figure 13 shows the computed waveforms for the data of Fig. 12.

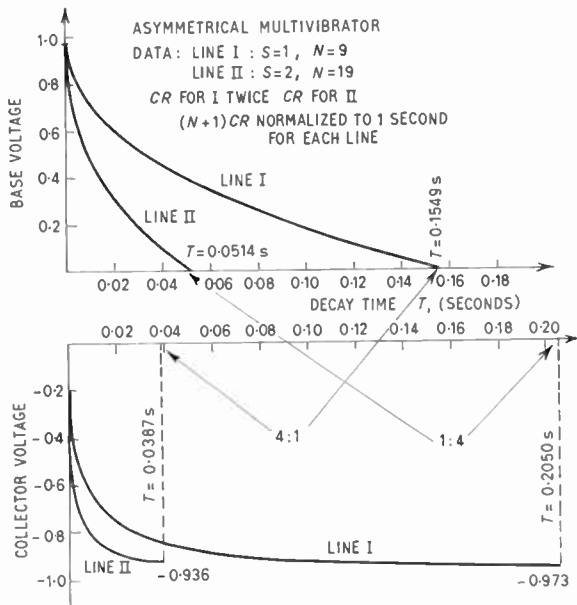


Fig. 13. Waveforms for data of Fig. 12.

**8. Multivibrator Waveforms. With Stored Base Charge**

If there is appreciable stored base charge, program C must be included in the iteration loops. Figure 14 shows the main outline of the computational scheme for this case; otherwise the detail is the same as for Fig. 12.

Figure 15 shows the waveforms resulting from a calculation on a symmetrical multivibrator with an  $S$  ratio of 1,  $N$  ratio of 10, and an equivalent stored base charge  $q$  of 0.01. This calculation, of course, involves only one iteration loop. The initial delay of 0.00084 seconds is the time needed to neutralize the stored base charge. A difficulty which arises is that it is not possible, in theory, to predict the  $q$  value before the waveforms are known, but of course this  $q$  value is required to calculate the waveforms. In practice, however, a

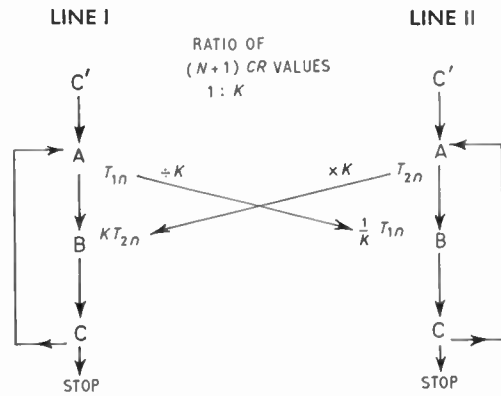


Fig. 14. Iteration loops; asymmetrical multivibrator, with stored base charge.

reasonable estimate of  $q$  might be made in advance of the calculation and this value could be corrected in the light of the results of the calculation. A fresh calculation could then be made with the new  $q$  value. This means, of course, a further iteration loop. Since the calculations for an asymmetric multivibrator with stored base charge take approximately one and a half hours on a *Pegasus* computer, even though all the programs are written in machine code and scaled to avoid the use of floating point arithmetic sub-routines, any further iterations of this kind are better avoided. A more satisfactory arrangement is to compute a solution for several values of  $q$  and graphically interpolate between them to obtain an approximately correct value for  $q$ .

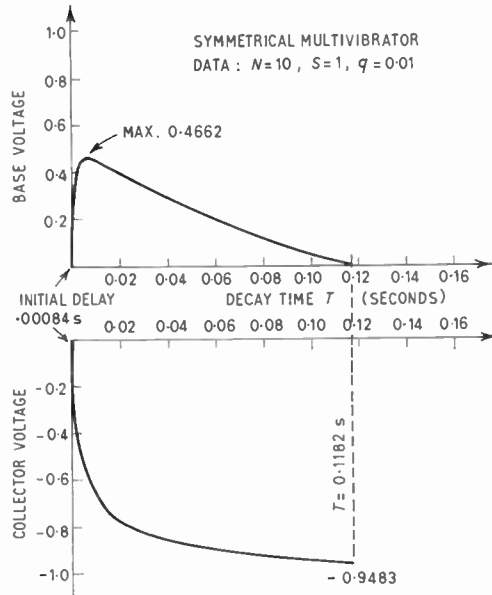


Fig. 15. Waveforms; symmetrical multivibrator, with stored base charge.

Very small values of  $q$ , of the order of 0.005 and less, give rise to a computational difficulty. The exact nature of this problem is difficult to explain in a few paragraphs, but briefly, it arises because the equivalent line length  $q$ , of the stored base charge, becomes small compared with the iteration interval  $\Delta x$ , which is normally 0.05; 20 points on the line. Difficulty might be expected, therefore, whenever  $q$  is less than 0.05. The occurrence of difficulties of this kind, in the solution of partial differential equations for particular boundary conditions, has been pointed out elsewhere.<sup>10</sup> In practice, the method used for testing for troubles of this kind, was to double the number of iteration points to 40, the maximum allowed by the programs. If there was any significant change in the results, due to this doubling of the number of iteration points, the  $q$  value was deemed too low to be reliable. In general, using this test,  $q$  values greater than 0.005 were found reasonably reliable even though this is equivalent to but part of one iteration interval. One way of overcoming this difficulty would be to use more closely spaced iteration points at the transistor end of the line which, as mentioned earlier, would also help in eliminating oscillation of solutions. This requirement was not foreseen at the commencement of the work and the program alteration would now prove too difficult. However, it will be used in future programs.

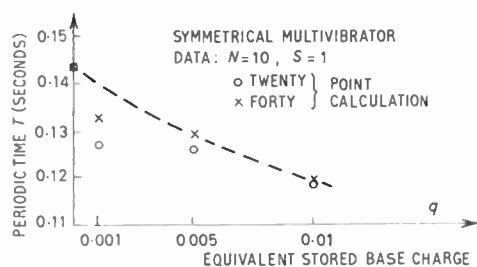


Fig. 16. Typical variation of period time  $T$  with stored base charge  $q$ .

At present, calculations are made for zero  $q$  (reliable since program C is not used), and for  $q$  values of, 0.01, 0.02 and 0.05. Results for smaller values of  $q$  are obtained by interpolation. Figure 16 shows the variation of periodic time with  $q$  for a typical case. In this figure, the points marked with a circle were calculated for 20 segments along the line and those marked with a cross for 40 segments along the line. The case of  $q$  zero was calculated without the use of program C. From the figure it is seen that the cross and circle coincide for the case  $q$  equal to 0.01, and so this period time may be considered reliable. For the lower values of  $q$ , the two calculations diverge and even the forty-point calculation must be treated with suspicion.

In the account of the case C problem given in section 4, it was explained that if  $q$  is too large, the base charge cannot be neutralized. This is indicated by a 'fail' condition in the case C program. With reference to Fig. 14, only for the larger values of  $q$  will this 'fail' occur in the initial program C'. For the more borderline values of  $q$ , the 'fail' may not occur until a number of iteration loops, through the C program, have been completed. In such cases, the period times  $T_{1n}$  and  $T_{2n}$  change appreciably with each loop before failure occurs. Even for values of  $q$  for which neutralization can just be effected, large changes in the period times are experienced before the ultimate convergence of the solution.

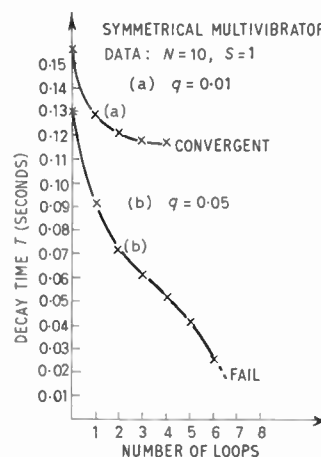


Fig. 17. Change of periodic time with iteration loop number.

Figure 17 shows these effects for the symmetrical multivibrator case of Fig. 15 with a  $q$  of 0.01, case (a), and a  $q$  of 0.05, case (b); the latter fails after a few iteration loops.

### 9. Conclusions

The differential equation governing the use of a uniform distributed CR line as the cross coupling network for multivibrator type circuits has been set up. Boundary conditions applicable to three different states of the multivibrator have been established. A major approximation was made when all switching transients other than that resulting from neutralization of stored base charge, were neglected; further, it has been assumed that the transistor switched off immediately the neutralization is completed. A second approximation made was the assumption of zero  $V_{CE}$  and  $V_{BE}$  for a saturated transistor. Finally, it was assumed that desaturation of a transistor occurs only in response to the start of conduction in the other transistor.

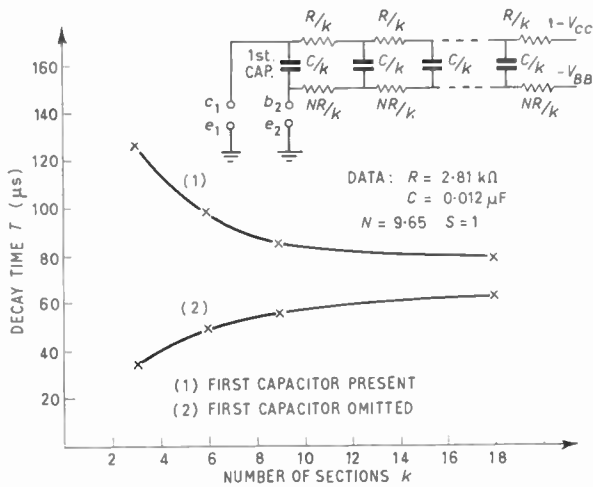


Fig. 18. Decay time as function of number of sections of lumped parameter line.

The numerical method of solution and the computer programs used have been outlined. Certain computational difficulties have been pointed out. Numerical solutions for a number of typical cases have been presented.

In general it has been shown that the transients in the cut-off collector circuit take a very long time to decay, and that the residual energy along the line has a marked effect on the multivibrator period when switching occurs before the decay is complete. Further it has been shown that stored base charge may have a pronounced effect on the multivibrator waveforms and period.

An indirect conclusion of the work concerns the nature of lumped parameter models which might be used to represent the line. It has been suggested<sup>2</sup> that the transient response of distributed CR lines may be predicted with the aid of lumped parameter, two and three section, CR models of the line. The difficulties encountered with oscillation of solutions and neutralization of stored base charge, suggest that at least ten sections would be necessary to represent the distributed line. Figure 18 shows some experimental results obtained when simulating a distributed line of a univibrator by lumped parameter models of different numbers of sections. Curve (1) shows the decay time as a function of the number of sections used to represent the line, the first element of the line being a capacitor while curve (2) shows the same function with the first capacitor omitted. The line was initially quiescent, with a uniform distribution of voltage along its length. These results suggest that the distributed line cannot easily be represented by a lumped parameter model of few sections.

A considerable amount of experimental work has been carried out using 18-section lines with a half-value capacitor ( $C/2k$ ), for the first element. For the negligible stored base charge case, the base and collector voltage waveforms are as predicted in this paper. They have decay times which agree with the calculated times, apart from a few percent which may be taken up in component tolerances. Figure 19 shows photographs of typical voltage waveforms. When stored base charge is appreciable, the 18-section model will only give waveforms of voltage similar to those calculated, if the first capacitor in the line is omitted, as might be expected from intuitive considerations. It is in this circumstance that the model becomes untenable, there seems to be no way of obtaining a useful lumped parameter equivalent circuit.

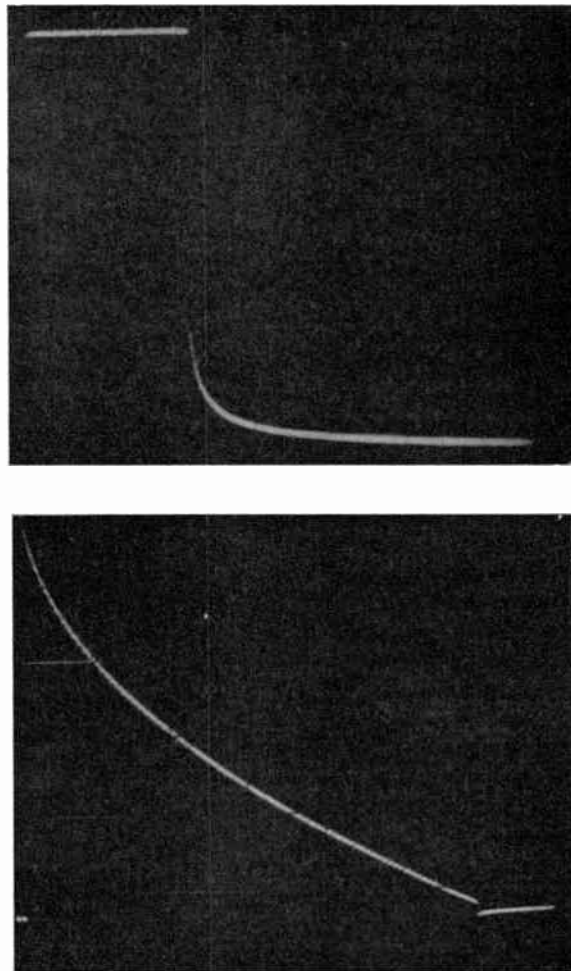


Fig. 19. Base and collector voltage waveforms: 18-section model: half-value first capacitor:

Data:  $S = 1$ ,  $N = 31.3$ . Measured  $T = 0.19$  (normalized)  
 $\left( \begin{array}{l} C/k = 0.043 \mu\text{F} \\ R/k = 150 \Omega \\ k = 18 \end{array} \right) \pm 2\%$  Measured  $T = 12 \text{ ms}$  (actual)

Unfortunately, technological facilities are not available to the author for the construction of distributed lines with sufficiently precise parameters to test the results of this paper. Several attempts have been made at constructing models of a distributed line, on a large scale, with the aid of proprietary, and experimentally prepared resistance papers. Little success was achieved, because of non-uniformity of the sheet resistivity of such papers.

It cannot be claimed that distributed coupling networks for multivibrators offer any significant advantages over lumped parameter networks with regard to multivibrator performance. Indeed, stored base charge effects, generally considered deleterious, are more pronounced for the former type of network. One small advantage is the somewhat more rectangular collector voltage waveform.

However, it is highly probable that distributed networks of this kind will be extensively used in integrated circuits, and thin film circuits, because of their ease of manufacture and economy of substrate space.

### 10. Acknowledgments

The author acknowledges the provision of computational facilities by the University of Southampton, and expresses his thanks to the staff of the computation sub-department for invaluable assistance. In particular, thanks are due to Mr. P. J. Taylor, of the above sub-department, for an excellent course of lectures on the numerical solution of partial differential equations.

### 11. References

1. "Nor Speedup with a distributed Parameter Network", LMSD Tech. Report 895021, Lockheed Aircraft Corp.
2. F. A. Lindholm and W. W. Happ, "Transient analysis of thin film structures", *The Radio and Electronic Engineer*, **26**, pp. 421-35, 1963.
3. W. W. Happ, "Synthesis of distributed parameter RC-networks", *Proc. Inst. Radio Engrs*, **50**, p. 483, 1962 (Letter).
4. P. S. Castro, A. J. Nichols and H. R. Kaiser, "Distributed parameter circuit design techniques", *I.R.E. Wescon Convention Record*, 1962.
5. H. S. Carslaw and J. C. Jaeger, "Conduction of Heat in Solids". (Oxford University Press, 1947.)
6. J. Crank and P. Nicholson, "A practical method for numerical evaluation of solutions of partial differential equations of the heat conduction type", *Proc. Cambridge Phil. Soc.*, **43**, pp. 50-67, 1947.
7. W. R. Wasow, "On the accuracy of implicit difference approximations to the equation of heat flow", *Math. Tables Aids Comp.*, **12**, pp. 43-55, 1958.
9. "PARAB 1", pp. 75-90, "Selected Numerical Methods". Edited by C. Gram, Regnecentralen, Copenhagen, 1962.
8. R. D. Richtmyer, "Difference Methods for Initial Value Problems", pp. 92-96. (Interscience, New York, 1957.)
10. "Modern Computing Methods", Notes on Applied Science, No. 16, Chapter 9, p. 76, H.M. Stationery Office, London.

11. A. N. Lowan, "The Operator Approach to Problems of Stability and Convergence", pp. 13-15. (Scripta Mathematica, New York, 1951.)
12. G. B. Forsythe and W. R. Wasow, "Finite Difference Methods for Partial Differential Equations", p. 236. (Wiley New York, 1960.)
13. "Modern Computing Methods", *ibid.*, pp. 4-6.

### 12. Appendix: The Crank-Nicholson Method

The equation to be solved is eqn. (26); that is:

$$\frac{\partial^2 V}{\partial x^2} = \frac{\partial V}{\partial t} \quad \dots\dots(26)$$

To represent these equations by finite differences the line is split into  $k$  segments (Fig. 20). Each segment is of length  $\Delta x$ , and the voltages at the dividing points are considered at times  $t$  and  $t + \Delta t$ , called the  $s$ th and  $(s+1)$ th iteration steps respectively. The right-hand side of eqn. (26) is represented by the finite difference  $\left(\frac{V_{n,s+1} - V_{n,s}}{\Delta t}\right)$ , while the left-hand side is represented by:

$$\frac{1}{2(\Delta x)^2} \{ (V_{n+1,s+1} - 2V_{n,s+1} + V_{n-1,s+1}) + (V_{n+1,s} - 2V_{n,s} + V_{n-1,s}) \}$$

Equating these expressions for interior points of the line ( $n = 2, 3, \dots, k-1$ ) gives, when expressed in matrix form:

$$\left(-\frac{r}{2}, 1+r, -\frac{r}{2}\right) \begin{pmatrix} V_{n-1,s+1} \\ V_{n,s+1} \\ V_{n+1,s+1} \end{pmatrix} = \left(\frac{r}{2}, 1-r, \frac{r}{2}\right) \begin{pmatrix} V_{n-1,s} \\ V_{n,s} \\ V_{n+1,s} \end{pmatrix} \quad \dots\dots(28)$$

where the iteration constant  $r$  is given by;

$$r = \frac{\Delta t}{(\Delta x)^2} \quad \dots\dots(29)$$

At the right-hand end of the line (Fig. 20),  $V_{k+1}$ , is, by eqn. (11) equal to  $(S-1)$  for all  $s$ . The difference equation corresponding to the line point  $n = k$  is, therefore, by replacing  $V_{n+1,s+1}$  and  $V_{n+1,s}$  of eqn. (28) by  $(S-1)$ :

$$\left(-\frac{r}{2}, 1+r\right) \begin{pmatrix} V_{k-1,s+1} \\ V_{k,s+1} \end{pmatrix} = \left(\frac{r}{2}, 1-r\right) \begin{pmatrix} V_{k-1,s} \\ V_{k,s} \end{pmatrix} + r(S-1) \quad \dots\dots(30)$$

The boundary conditions at the left-hand end of the line depend on whether a case A, B or C solution is sought. Considering, by way of example, a case A problem, eqn. (15) gives the required boundary condition. To treat this as a finite difference equation, a fictitious point is introduced on the line corresponding to  $n = 0$ . The finite difference equation for the boundary condition is then for time step  $s$

$$\frac{V_{2,s} - V_{0,s}}{2\Delta x} - \frac{V_{1,s}}{N} = -\left(1 + \frac{S}{N}\right)$$

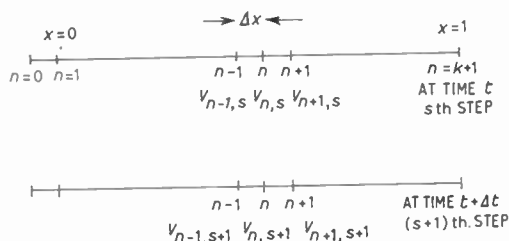


Fig. 20. Iteration points along the line at times  $t$  and  $t + \Delta t$ .

Rearranging,

$$V_{0,s} = V_{2,s} - \frac{2}{kN} V_{1,s} + \frac{2}{k} \left(1 + \frac{S}{N}\right) \dots\dots(31)$$

Elimination of the fictitious voltage  $V_{0,s}$  allows the finite difference equations for the point  $n = 1$ , corresponding to eqn. (26), to be written as

$$\begin{aligned} \left(1 + r + \frac{r}{Nk}, -r\right) \begin{pmatrix} V_{1,s+1} \\ V_{2,s+1} \end{pmatrix} \\ = \left(1 - r - \frac{r}{Nk}, r\right) \begin{pmatrix} V_{1,s} \\ V_{2,s} \end{pmatrix} + \frac{2r}{k} \left(1 + \frac{S}{N}\right) \dots\dots(32) \end{aligned}$$

The left-hand end boundary condition for case B and case C problems can be similarly treated.

Equations (28), (31) and (32) can be combined into a single matrix equation for the whole line, namely

$$(I + M)V^{(s+1)} = (I - M)V^{(s)} + B \dots\dots(33)$$

There  $V^{(s)}$  is the column matrix of the  $k$  line voltages  $V_{n,s} (n = 1, \dots, k)$ ,  $I$  is the  $k$ 'th order unit matrix, and  $M$  and  $B$  are the  $k \times k$  square and  $k$ th order column matrices respectively as given below:

$$M = r \begin{pmatrix} 1 + \frac{1}{Nk}, & -1, & 0, & \dots & \dots & \dots & 0 \\ -\frac{1}{2}, & 1, & -\frac{1}{2}, & 0, & \dots & \dots & 0 \\ 0, & -\frac{1}{2}, & 1, & -\frac{1}{2}, & \dots & \dots & 0 \\ \dots & \dots & \dots & \dots & \dots & \dots & \dots \\ 0, & 0, & \dots, & 0, & -\frac{1}{2}, & 1, & -\frac{1}{2} \\ 0, & 0, & \dots, & \dots, & 0, & -\frac{1}{2}, & 1 \end{pmatrix} \dots\dots(34)$$

$$B = r \begin{pmatrix} 2\left(1 + \frac{S}{N}\right)/k \\ 0 \\ \vdots \\ 0 \\ S-1 \end{pmatrix} \dots\dots(35)$$

The procedure is to commence with the column matrix  $V^{(0)}$  of the initial voltages along the line on the right-hand side of eqn. (33), and then to solve for the matrix  $V^{(1)}$ . This, in turn, is used to find  $V^{(2)}$  and so

on. The solution<sup>6, 7, 11</sup> converges for all  $r$  but the accuracy depends on  $r$ ,  $k$  and the nature of the boundary and initial conditions as detailed in the main text.

A number of methods are available for the solution of sets of equations of the form given by the matrix eqn. (33). One obvious one is the algebraic inversion of the matrix  $(I + M)$ . Computationally this is rather time consuming, although it has the advantage that the inversion need only be carried out once for each problem. This approach was adopted for the earlier work with ten-segment lines. For twenty or more segments, the computing time became prohibitive by this method. It should be noted that although  $(I + M)$  is triple diagonal,  $(I + M)^{-1}$  is not, nor also is  $(I + M)^{-1}(I - M)$ . A large number of multiplication steps are therefore necessary in forming  $(I + M)^{-1}(I - M)V^{(s)}$  in each time step iteration.

Gauss-Seidal<sup>12</sup> and similar iteration processes should also be very effective in solving eqn. (33), since these methods are usually rapidly convergent for triple diagonal matrices. These methods were not, however, tried in the present work.

The method used in the present work to solve eqn. (33), was algebraic reduction of the triple-diagonal set of equations to double diagonal form. The technique is a special case of 'pivotal condensation'<sup>13</sup> applicable to the rather special form of the equations involved. Thus if the last equation of the set from matrix eqn. (33) is multiplied by  $2/(1+r)$  and added to the last but one equation, the  $V_{k,s+1}$  term is eliminated from the latter equation. In a similar way, the new last but one equation can be used to eliminate  $V_{k-1,s+1}$  from the last but two equation. In this way, a new matrix equation is formed, namely:

$$AV^{(s+1)} = b^{(s)} \dots\dots(36)$$

Here  $A$  is a  $k \times k$  matrix having zero elements everywhere except on the diagonal and lower sub-diagonal. The first equation of the set (36) has only one variable  $V_{1,s+1}$  which, therefore, is immediately determined. This is then substituted into the second equation of the set whence  $V_{2,s+1}$  can be found. This procedure is then followed through all the equations in succession.

In practice, it was found that this method of solution was faster than matrix inversion even though the right-hand sides of the equation had to be manipulated, in the manner described above, for each time step iteration. The reason why computational speed was not sacrificed by this method hinges on the relatively few arithmetical steps needed to form each element of  $b^{(s)}$ .

*Manuscript first received by the Institution on 22nd January 1965 and in final form on 17th March 1965. (Paper No. 989.)*

# of current interest . . .

## Prospects for Radio Astronomy

The Report of the Fleck Committee on Radio Astronomy, published by the Science Research Council on 6th April 1965, recommends that Great Britain should press forward with research in radio astronomy at the existing centres and give it generous treatment in order to do so. This, the Committee believes, means that the existing flourishing research groups at Jodrell Bank and Cambridge should be given special encouragement and assistance, and if necessary provided with new radio telescopes by 1972. The cost of such a programme would be about £4M spread over seven years.

The Committee draws special attention to the danger of electrical and radio interference which could severely restrict the use of the existing and planned radio telescopes at Jodrell Bank, Cambridge, and the Royal Radar Establishment, Malvern, unless steps are taken to avoid interference. The Committee would therefore warmly welcome the continued co-operation of the appropriate planning authorities in safeguarding this work because they regard it as of national scientific moment.

## Progress of the International Years of the Quiet Sun (1964–1965)

Since 1st January 1964, scientists in over 70 different countries and at over 2000 separate stations have been making a wide range of special measurements and observations which are related to the enterprise known as the International Years of the Quiet Sun. During this two-year period, investigations are being undertaken to advance our knowledge and understanding of solar-terrestrial relations—that branch of geophysics which is concerned with the influence of the Sun's corpuscular and electromagnetic radiations on the Earth and its environment.

The years 1964 and 1965 were selected since they were expected to span the time when sunspot activity would be at a minimum, thereby making it possible to compare similar or identical measurements made at solar minimum and solar maximum—that is, during the International Geophysical Year, 1957–58. It now appears that the minimum in solar activity occurred some time during the third quarter of 1964 and preliminary quick-look analyses are now being made.

A review of the progress made by the participating countries was given during the 111rd General Assembly of the IQSY, held recently in Madrid, at which Professor W. J. G. Beynon, C.B.E., of the University College of Wales, Aberystwyth, presided. During the conference special review lectures on recent advances in the branches of geophysics represented by the IQSY disciplines were given by invited lecturers.

## International Recommendations for Precision Sound Level Meters

Published by the International Electrotechnical Commission, IEC Publication 179, "Precision sound level meters", applies to sound level meters for high precision apparatus for laboratory use, or for accurate measurements in which stable, high fidelity and high quality apparatus is required. A sound level meter is, generally, a combination of a microphone, an amplifier, certain weighting networks, an attenuator and an indicating instrument having certain dynamic characteristics. The sound level meter covers the frequency range 10 to 20 000 c/s.

The object of Publication 179 is to specify the characteristics of an apparatus for measuring accurately certain weighted sound pressure levels. The instrument described in this Recommendation represents a practical combination of characteristics that will achieve a high degree of stability and accuracy.

Copies of IEC Publication 179 may be obtained from the BSI Sales Branch, 2 Park Street, London, W.1, price £1 5s. each.

## A World Trade Center

To enable trade between any combination of countries to be arranged in a single location is the ideal behind the construction of the World Trade Center which is to occupy a 16-acre site in the commercial heart of New York.

When finally completed, the World Trade Center will comprise over 10 million square feet including a 250-room hotel; parking for 2000 vehicles and the other facilities and services required to cater for an estimated working population of 50,000 persons within the Center, in addition to the many thousands of business visitors who will call daily.

The entire project will be air-conditioned and the two 110-storey tower blocks will be served by a unique express lift system specially designed for the Center. Some 300,000 square feet of specialized exhibition space will be available on permanent or temporary basis. Lecture halls of varying sizes equipped with instantaneous translation facilities are planned. Multilingual secretarial services will be available as well as all normal business facilities.

Work will commence on the construction of the World Trade Center later this year and by mid-1968 the Center will be operational and over 2 million square feet will be ready for occupation by commercial tenants. The entire project will be completed during 1970.

Further information may be obtained from Richard Ellis and Son, Chartered Surveyors, 85 Gracechurch Street, London, E.C.3.

# The Application of Eigen Theory to Filter Networks

By

J. F. REYNOLDS, M.A.  
(Associate Member) †

**Summary:** This note develops the concepts of characteristic impedance and propagation constant using matrix methods. It shows that they can be interpreted in terms of the eigen roots and vectors of the transfer and impedance matrices. It is not suggested that the methods are quicker than the normal ones, but that this approach provides an alternative interpretation of the filter parameters.

## 1. Introduction

In the last few years, a considerable amount of literature has appeared on the application of matrices to four-terminal networks. This technique has the advantage of affording a systematic method of analysis, and it often causes a considerable reduction in algebra. This note develops the basic theory of filters using matrices, and assigns new meanings to the characteristic impedance and propagation coefficient.

## 2. Transfer Matrix Analysis

Consider an elementary filter section of transfer matrix  $A$ .



Suppose also that the input and output curtage vectors are  $C_1$  and  $C_0$  respectively, these being defined as two-dimensional vectors whose elements are the voltage and current. It may be shown ‡ that

$$\begin{bmatrix} V_1 \\ I_1 \end{bmatrix} = \begin{bmatrix} a_{11} & a_{12} \\ a_{21} & a_{22} \end{bmatrix} \begin{bmatrix} V_0 \\ I_0 \end{bmatrix}$$

or in matrix notation

$$C_1 = AC_0 \quad \dots\dots(1)$$

Now, by definition, the characteristic impedance  $z_0$  is that impedance which, when placed between the output terminals, causes the same impedance across the input terminals. Also, the propagation coefficient  $\gamma$  is the natural logarithm of the ratio of input to output voltages (or currents) when the section is terminated by an impedance of value  $z_0$ . When the impedances at input and output are equal

$$\frac{V_1}{I_1} = \frac{V_0}{I_0}$$

both being equal to  $z_0$ .

It follows that

$$\text{and} \quad \left. \begin{matrix} V_1 = \lambda V_0 \\ I_1 = \lambda I_0 \end{matrix} \right\} \quad \dots\dots(2)$$

where  $\lambda$  is some scalar.

Equation (2) can be rewritten in vector form as

$$C_1 = \lambda C_0 \quad \dots\dots(3)$$

But from equation (1),

$$C_1 = AC_0$$

It therefore follows that

$$AC_0 = \lambda C_0 \quad \dots\dots(4)$$

Equation (4) is the equation defining the eigen roots and vectors of  $A$ . The interpretation of an eigen root  $\lambda$  can be obtained from equations (2) which show that it is equal to the ratio  $V_1/V_0$ . The definition of the propagation constant  $\gamma$  shows that

$$\gamma = \log_e \lambda \quad \dots\dots(5)$$

Also, since the determinant of  $A$  is known to be 1, the product of the two eigen roots is unity, which results in two values for  $\gamma$  which are equal in magnitude, but opposite in sign. These two values correspond to propagation in the two possible directions, and the positive one is evaluated by taking the value of  $\lambda$  greater than 1.

The significance of the corresponding eigen vector is that its elements represent the voltage and current at the output terminals, so that the ratio of the elements gives the characteristic impedance  $z_0$ .

## 3. Impedance Matrix Analysis

Consider now the same problem using the impedance matrix  $Z$ . It can be shown that, using the same sign convention as in Section 2,

$$V_1 = z_{11}I_1 + z_{12}I_0$$

$$V_0 = z_{21}I_1 + z_{22}I_0$$

In matrix notation, this becomes

$$V = ZI \quad \dots\dots(6)$$

† Glamorgan College of Technology, Treforest, Pontypridd, Glamorgan.

‡ K. G. Nicholls, "A matrix representation of linear amplifiers", *J. Brit.I.R.E.*, 21, pp. 517-33, June 1961.

G. Zelinger, "Basic Matrix Algebra and Transistor Circuits". (Pergamon Press, Oxford, 1963.)

Suppose that the impedances at the input and output terminals are equal. In this case

$$\frac{V_1}{I_1} = \frac{V_0}{I_0} = \lambda$$

where  $\lambda$  is some scalar.

It follows that

$$\left. \begin{aligned} V_1 &= \lambda I_1 \\ V_0 &= \lambda I_0 \end{aligned} \right\} \dots\dots(7)$$

Using vector notation, this becomes

$$V = \lambda I \dots\dots(8)$$

But, using eqn. (6), eqn. (8) can be rewritten

$$ZI = \lambda I \dots\dots(9)$$

This is the equation defining the eigen roots and vectors of  $Z$ . The physical significance is deduced from equations (7) which show that an eigen root  $\lambda$

represents the characteristic impedance  $z_0$ . Since it can be shown for a symmetric filter that the trace of  $A$  (i.e. the sum of the diagonal elements) is zero, the two eigen roots of  $Z$  are equal in magnitude and opposite in sign. Only the positive root is relevant in this case.

The significance of the corresponding eigen vector is that its elements represent the input and output currents. The propagation constant  $\gamma$  is given by the natural logarithm of their ratio.

If these methods are applied to any of the standard filter sections, it will be found that the usual results can quickly be obtained.

*Manuscript first received by the Institution on 30th September 1964, and in final form on 29th March 1965. (Contribution No. 85.)*

© The Institution of Electronic and Radio Engineers, 1965

## STANDARD FREQUENCY TRANSMISSIONS

(Communication from the National Physical Laboratory)

Deviations, in parts in  $10^{10}$ , from nominal frequency for June 1965

June 1965	GBR 16kc/s 24-hour mean centred on 0300 U.T.	MSF 60 kc/s 1430-1530 U.T.	Droitwich 200 kc/s 1000-1100 U.T.	June 1965	GBR 16 kc/s 24-hour mean centred on 0300 U.T.	MSF 60 kc/s 1430-1530 U.T.	Droitwich 200 kc/s 1000-1100 U.T.
1	- 150.1	- 150.8	+ 2	16	- 148.5	- 149.8	- 2
2	- 150.6	- 150.8	+ 2	17	- 149.9	- 150.2	- 2
3	- 150.2	- 150.5	+ 3	18	- 150.0	- 149.7	- 1
4	- 150.0	- 149.8	-	19	- 149.4	- 150.0	-
5	- 149.1	- 149.0	+ 4	20	- 151.0	- 151.5	-
6	- 149.6	- 149.9	- 7	21	- 150.4	- 149.7	+ 1
7	- 149.0	- 149.8	- 6	22	- 149.7	- 151.1	+ 2
8	- 148.3	- 150.1	- 7	23	- 150.1	- 149.3	+ 2
9	- 150.2	- 150.8	- 7	24	- 149.6	- 150.6	+ 5
10	- 150.9	- 150.6	- 6	25	- 150.2	- 150.6	+ 3
11	- 150.2	- 150.5	- 5	26	- 150.2	- 150.4	+ 5
12	- 149.1	- 149.2	- 4	27	- 150.4	- 149.8	+ 8
13	- 149.8	- 150.0	- 5	28	- 149.7	- 151.7	0
14	- 149.9	- 150.2	- 3	29	- 149.6	- 149.3	0
15	- 148.5	- 149.0	- 3	30	- 148.6	- 150.7	- 1

Nominal frequency corresponds to a value of 9 192 631 770 c/s for the caesium F.m (4,0)-F.m (3,0) transition at zero field.

Note: The phase of the GBR/MSF time signals was retarded by 100 milliseconds at 0000 U.T. on 1st July 1965.

# A New Television Test Card for Trade Test Transmissions

By

G. HERSEE (*Member*) †,

A. JAMES ‡,

T. N. J. ARCHARD §,

D. H. RUMSEY §, R. SIMS §,

G. S. ASHBURNER || and

A. PORT ||

*Presented at a meeting of the Television Group of the Institution in London on 7th May, 1964.*

**Summary:** This paper describes the design and the manufacturing techniques necessary for the accurate reproduction of high grade test transparencies using resolution bars of sine-wave cross-section.

Part 1 discusses the design and specification, and how the latter is affected by the manufacturing difficulties.

Part 2 discusses earlier methods of producing sine-wave resolution bars, together with the defects of these techniques. A modified form using rotating polaroid filters and a travelling slit is then described, and is shown to give results within the specified tolerances.

Part 3 shows that more than a straight photographic copy is involved for high-precision work, and describes the new techniques devised for the purpose.

## Part 1

### THE DESIGN OF THE NEW TEST CARD

G. Hersee and A. James

#### 1. Introduction

A general purpose test card originally introduced by the British Broadcasting Corporation and known as Test Card C has been in use in Great Britain for almost two decades. Some years ago, largely as a result of the improvements in television equipment and the distribution links, certain disadvantages of Test Card C became apparent. A new design was formulated, taking into account the difficulties of reproducing transparencies with a high order of accuracy.

This paper describes the problems encountered in designing and writing the specification for these test cards, with particular emphasis on those aspects of the design directly determining the characteristics of the video signal produced.

#### 2. Defects of Test Card C

Various designs of pattern have been produced for the testing of television equipment, the most well

known being Test Card C, originally introduced by the B.B.C. in 1947. (Fig. 1.) Although nowadays it is usually made as a transparency it has become a convention in the industry to refer to these patterns and their reproductions as 'cards' because for many years they were made as opacities.

Test Card C has now been in use for about two decades, but with the improvement in transmission equipment certain disadvantages have become apparent. For example, the frequency or resolution gratings are of rectangular cross-section when density is plotted against distance, and have rapid transitions with full modulation depth. When these are scanned in a modern wide-band slide scanner, signals are generated well outside the band-width of the system. In transmission through the networks these higher frequencies are attenuated, and the resultant fundamental is increased in amplitude. Starting with a square wave, and removing all except the fundamental, results in it being increased to a value of  $4/\pi$  times the original amplitude.

There are other disadvantages of Test Card C. A grid of white lines is used to divide the background into squares but the dimensions of these were not chosen to fit the available area. Again, the black and white 'pole pieces' provided at either side of the circle give an optical illusion causing the circle to

† British Broadcasting Corporation, Planning and Installation Department, London, W.1.

‡ Independent Television Authority, Brompton Road, London, S.W.1.

§ British Broadcasting Corporation Research Department, Kingswood Warren, Surrey.

|| Colour Centre Ltd., Farnham Royal, Bucks.

appear squashed. Finally, the grey scale or step-wedge used in some versions of Test Card C is seriously at fault, neither the total contrast range nor the density changes between intermediate steps being standardized.

### 3. Standardization

This last point underlines the need for standardization. In the course of years various 'masters' of Test

Card C have been drawn or painted. Apart from the variations in grey scale already referred to, some of these differ significantly in their general dimensions as well as in the accuracy (both in frequency and modulation depth) of the frequency gratings. Further inaccuracies have been introduced in the photographic reproductions. It was therefore highly desirable for any new design to be very precisely specified so that such errors are eliminated.

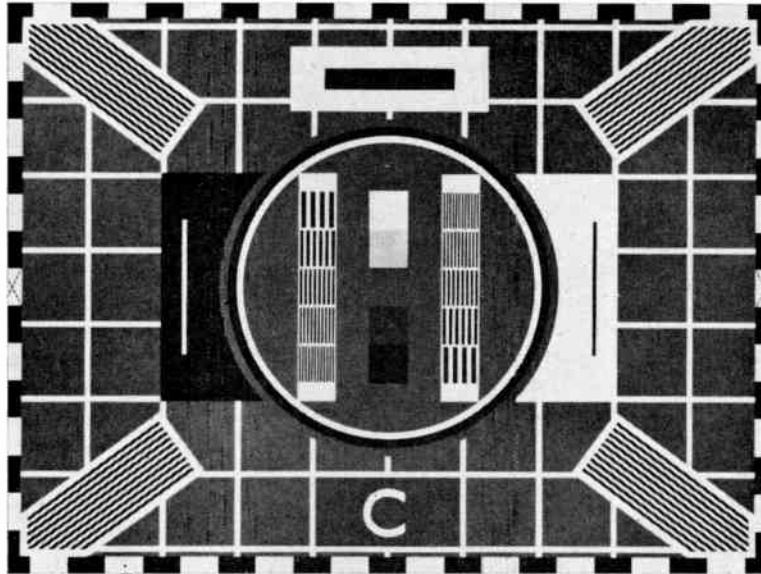


Fig. 1. Test Card C.

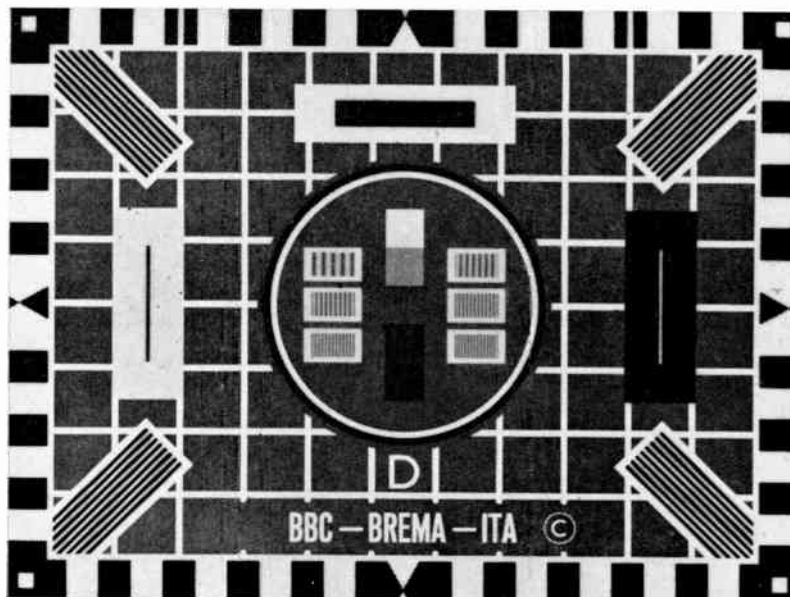


Fig. 2. Test Card D.

#### 4. Objectives and General Design Considerations

In late 1959 a committee representing the B.B.C., the British Radio Equipment Manufacturers' Association (B.R.E.M.A.), and the Independent Television Authority was set up to study what changes should be made in the design.

This committee consulted with other interested bodies and during discussions it became clear that an entirely new design of test card would be desirable, which should be suitable for use by the receiver trade not only to demonstrate receivers for sale but also as an aid in receiver and aerial adjustment. Members of the public would also expect to find the card useful in tuning their receivers and perhaps eventually to identify the desired channel.

The test card should give a clear and pleasant picture from a correctly-adjusted installation but defects in the aerial and receiver should be apparent irrespective of transmitter and channel. This would require that a tight specification is adhered to, including transmission modulation levels. The design should therefore result in a signal easily measured and adjusted by the broadcaster.

#### 5. Copyright

The copyright of the design (Fig. 2, designated Test Card D for the 405-line version, and E for the 625-line version) is vested jointly in the B.B.C., B.R.E.M.A., and the I.T.A. Copies will be readily available but to avoid the confusion experienced with Test Card C the owners will only authorize the issue of copies which are manufactured to the specification.

It should be noted that the only difference between the D and E versions is in the frequency gratings, suitable frequencies being substituted for the system in use.

#### 6. The New Design

##### 6.1. General

In considering the design to be adopted, several with radically different features were considered. For instance, horizontal arrangements of gratings and grey step wedges, omission of the diagonal corner bars, and omission of the circle were among ideas suggested. However, it was considered that dealers and engineers were so familiar with the Test Card C that the new design should follow it as far as possible. Eventually a layout was agreed, and a specification drawn up.

##### 6.2. Black and White Areas

###### 6.2.1. Grid pattern

A white grid pattern is used to form a background eleven squares wide and eight high, surrounded by a border of castellations. These are each one half a

square wide, making the total area twelve by nine, i.e. the correct aspect ratio.

###### 6.2.2. Castellations

These are black and white rectangles which surround the pattern, and are used to test for synchronization defects in receivers.

###### 6.2.3. Scan amplitude

It is essential that the scanning raster has its width and height set accurately to that for which the pattern was designed. Any variation in these dimensions will cause corresponding variations in the frequency of the signals from the gratings. Errors of up to 5% can be obtained from the variations in the blanking pulse width supplied to the scanner, so means should be provided to reduce any further errors due to wrong raster amplitude. This is easily done by the use of darts (sometimes referred to as 'egg-timers'), the scanning raster being set so that the crossover point is just at the edge of the scanned area.

###### 6.2.4. Corner diagonal gratings

In the corners of the pattern black and white gratings of rectangular cross-section are provided to check focusing and linearity of scanning in the corners. They are at 45 deg to the edges and are such dimensions that a 1 Mc/s square wave is generated when scanned on the 405-line system.

###### 6.2.5. Streaking rectangles

These (colloquially referred to as the 'letter box') are situated above the large circle, and consist of a black rectangle surrounded by a large white one. Any defects in the low-frequency response of the system then shows up as poor reproduction of the tones of these areas. The rectangles are slightly larger in the new design, as it was felt that this would make the defects easier to detect.

###### 6.2.6. The circle

Consideration was given to increasing the size of the large circle in the new design, but the receiver side of the industry were not in favour of this so it is retained at about the same size as before. Aesthetically it forms a useful division between the main area with its white grid background and the central area with its frequency gratings and step wedge.

###### 6.2.7. Pulse bars

Many measurements of lines and amplifiers are now made with the 'pulse and bar' technique. It was suggested that the narrow bars in the pole pieces on either side of the circle should be made with a sine-squared cross section. Accurate reproduction of this proved to be impossible however, due to limitations in the photographic process which becomes more

severe when an attempt is made to reproduce accurately cross-sections of large modulation depth. By restricting the minimum density to 0.5 it has been proved possible to make pulses which bear some resemblance to the sine-squared cross section.

#### 6.2.8. Captions

Below the circle there is an area where the white grid has been omitted to provide a space where captions may be inserted.

### 6.3. Central Areas

#### 6.3.1. The frequency gratings

The Test Card C has two sets of five frequency gratings. They are rather narrow resulting in a 3-microsecond signal when scanned in the 405-line system. This is found to be insufficient to allow a steady state output to be obtained. In order to provide space for longer gratings in D the number has been reduced. For aesthetic reasons an additional grating is provided, each frequency appearing once only. The six gratings are arranged in groups of three at either side of the vertical step wedge. Their length has been increased to approximately 6 microseconds in the 405-line system. The additional grating has a frequency of 2.75 Mc/s, just below the system cut-off frequency.

To alleviate the difficulties mentioned in Section 2 and because transmission equipment often has a restriction on the input level of signals above 1.75 Mc/s, the modulation range of the grating was originally restricted to 50% of the black-white transition. Later it proved possible to increase this to 70% of the black-white transition. A new generating process was devised and is described in Part 2. By very careful control and selection of the photographic conditions, described in Part 3, it has been possible to make the grating of sine-wave shape. As a result of these changes, ringing is normally avoided following the gratings.

Nevertheless it should be realized that sine-wave patterns can be misleading in their subjective appearance, tending to give a false impression of picture softness.

The frequencies finally chosen for both versions of the design are given in Section 9.

Note that Test Card E does not have any 3 Mc/s gratings, as these can cause trouble by the second harmonic beating with inter-carrier sound signals to give interfering beat signals.

#### 6.3.2. The step-wedge

It is desirable that the step-wedge when reproduced on a receiver should give equal changes of subjective brightness. The top and bottom steps are respectively

white and black, and contain small circular areas of slightly lower density to show when crushing occurs. The precise densities were chosen after a series of subjective tests were carried out by the B.B.C. Research Department.<sup>1</sup>

### 7. Choice of Densities and Modulation Levels

In selecting the densities several factors have to be considered including the contrast range of normal programme material, the maximum and minimum densities usually reached in release prints, and the fog and base densities of dyed-base film stock. These were among the factors considered in compiling the British Standard on densities of films and slides for television.<sup>8</sup> This specifies densities of 0.4 for white areas and 2.0 for black areas. S.M.P.T.E. recommended practice R.P.7 gives similar figures, as does modern telerecording practice. These densities were therefore adopted for these cards.

Mention has already been made of the need to restrict the density range of the pulse bars. The values of the intermediate densities have to be chosen carefully, and this involves consideration of the characteristics of the television system. The picture tube in the receiver has an incremental light output which is proportional to an increment of the input voltage raised to the power  $\gamma$ . The camera tube input light to output voltage has a similar transfer function. All other parts of the system have a linear characteristic. It is necessary for the overall  $\gamma$  to be approximately unity. Now the picture tube has a  $\gamma$  value of approximately 2.5 and to correct for this it is conventional for the transmitting equipment to pre-distort the signal so that it has an effective  $\gamma$  value of about 0.4, giving the overall  $\gamma$  value of unity. These values are not precise, so that the  $\gamma$  value of the transmitted signal can vary in the range 0.4 to 0.6, film scanning equipment (telecine) tending to have the lower value and cameras the higher. Consequently, there is some difficulty in selecting a value for the transparency which may be used with either type of equipment. Since both types of equipment have their own correction incorporated, particularly vidicon camera tubes which have an inherent gamma of about 0.6, it is desirable to make the gamma of the card unity. This also means that the appearance of the card will be the same when seen through the television system as when viewed by optical projection.

The signal levels from the various densities can be calculated assuming that the minimum density is set to the peak white level of 0.7 V and that the required value of gamma is 0.5. These voltages are given in Appendix 2.

Initially it was forecast that spurious effects would be caused unless the background grey of each set of

bars was made to be the mid-density of the bars, and the width of the block adjusted so that the transition from background to bars occurred at this value, i.e. there was no sudden jump. The bar patterns for Test Card E were made in this form, but when viewed on receivers the low tone of the background gave the subjective appearance of very poor frequency re-

sponse. This design was therefore withdrawn pending some months experience with Test Card D, where the grey background is that of the minimum density of the bars. It is now proposed to amend Test Card 'E' so that it has the same background density to the bars as Test Card 'D' and to increase the modulation depth of these bar patterns to 70% on both cards.

Part 2

THE PRODUCTION OF SINUSOIDAL RESOLUTION BAR PATTERNS FOR INCLUSION IN THE TELEVISION TEST CARDS D AND E

T. N. J. Archard, D. H. Rumsey and R. Sims

8. Introduction

In any optical image-forming system it is usual to describe the performance in terms of resolution in patterns per unit dimension and in image acutance. It is an accepted practice in image assessment to use resolution bars having a rectangular profile, but varying in mark/space ratio and density range. One of the attendant problems associated with the electrical signals generated by the scanning of resolution bars having a rectangular profile is that unless unlimited bandwidth is used, some form of harmonic distortion is unavoidable. It is therefore desirable to use a form of resolution pattern that has a sinusoidal profile, thus overcoming this distortion. If a system is tested using sinusoidal bar patterns, the limiting resolution is revealed by a progressive decrease of modulation as bar patterns of increasing frequency are used. The use of sinusoidal bar patterns is therefore highly desirable, but unfortunately their photographic production presented a number of problems which are discussed in this paper.

9. Initial Requirements

A series of bar patterns having sinusoidal distribution was required for inclusion in Test Cards D and E. They were to be produced in blocks of different frequencies and they were to conform to a specified density range. A specification for these bars is shown in Table 1. (See also Appendix 1.)

Table 1  
Sinusoidal Resolution Bar Patterns

Reflexion Density Range	Frequencies Mc/s	
White 0.5	1.0, 1.5, 2.0, 2.5, 2.75, 3.0	Test Card D
Black 1.05	1.5, 2.5, 3.5, 4.0, 4.5, 5.25	Test Card E

The final bars were to be printed on single-weight glossy bromide paper. The densities quoted are single-diffuse.

10. Experimental Production Techniques

10.1. Previously used Methods of Production

Various techniques have been used previously to produce, by photo-mechanical means, sine-wave bars on a photographic emulsion. One method referred to by Kapany and Pike<sup>2</sup> shows how a static and a rotating polaroid screen can together be used to produce sinusoidal modulation of a beam of light. If a rotating slit is placed in front of these screens and then photographed, sinusoidal bar patterns would be obtained. These patterns would however be in the form of radials and therefore unsuitable for the proposed test cards. An electronic method utilizing a television display has been used by Hersee<sup>3</sup> to produce the sine-wave bar patterns for B.B.C. Test Card 51. It would, nevertheless, have been extremely difficult to have adopted this system and to have met the present specification.

There are other purely optical methods, but in general their instrumentation is rather elaborate and they tend to be somewhat inflexible; therefore, in

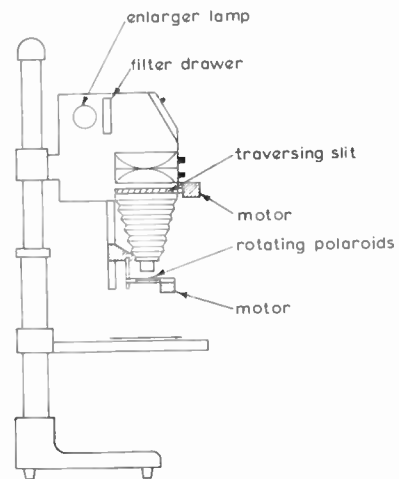


Fig. 3. Initial layout of enlarger.

order to produce a range of bar patterns and maintain close control over the density range, it was decided to use the method of rotating polaroid screens referred to by Kapany and Pike, but with a modified system of scanning.

### 10.2. Equipment

As the task in hand required the use of what was basically photographic equipment, it was decided to undertake some experiments for converting a Model 3.S Durst Laboratory enlarger to take rotating polaroid screens, and to mount a traversing slit in the plane of the photographic negative. The layout is shown in Fig. 3.

### 10.3. Rotating Polaroid Screens

Measurements of the polaroid screens revealed that a high overall density range could be obtained, and initially it was decided to situate the rotating mechanism under the lens. One screen was fixed and the other rotated by a lightweight synchronous motor having torque of approximately 4 g-cm. The rotating drive was effected through a 200 : 1 gear reduction train to the rim of the polaroid screen; power for the motor was obtained from an amplifier which in its turn was driven by a generator capable of giving an output having a variable frequency. By this means the speed of rotation of the polaroid filter could be varied with precision between 1 and 6 rev/min by altering the frequency of the generator output from 50 to 300 c/s.

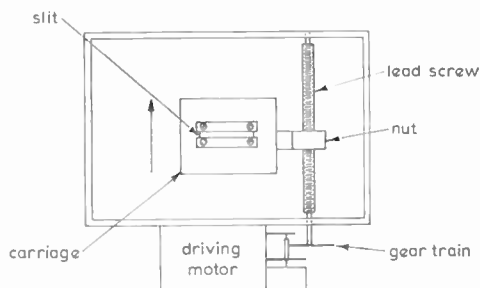


Fig. 4. Lead screw and nut.

### 10.4. Slit Mechanism

The scanning device was mechanical and took the form of a slit of variable width mounted on a carriage that required to be moved across the negative plane of the enlarger at a constant velocity. The original drive for this carriage was a lead screw and nut made specially for the purpose, the layout of which is shown in Fig. 4. To enable the slit velocity to be evaluated when using this drive, a slit width of only 0.01 mm was first employed. The enlarger lamp was fed from a stabilized source and the image of the slit projected on

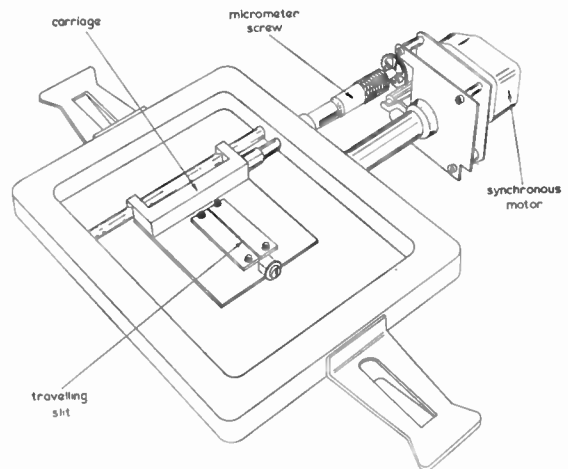


Fig. 5. Slit carriage with micrometer lead screw.

to bromide paper fixed to the enlarger baseboard. The slit was then allowed to traverse the length of the lead screw whilst the enlarger continuously exposed the image of the slit on the bromide paper. It was found on development of the print that the recorded image revealed not a perfect overall grey, but a series of bars of different densities and widths. These were, in fact, a record of minor inaccuracies in the lead screw and nut. To overcome this difficulty the lead screw and nut were replaced by a standard micrometer screw of 0.5 mm pitch and the slit mechanism was lightly loaded against the head of the screw to minimize back-lash as shown in Fig. 5. The results obtained from this modified drive were a great improvement over those obtained from the original system. The screw was driven through a gear train by a similar motor to that used for the polaroid screen so that both movements could be synchronized or bear a constant preset relationship to one another. In practice, it was found beneficial to run the slit drive motor at a constant speed of 200 rev/min using stabilized electricity supply voltage at a frequency of 50 c/s and restrict the use of the variable-frequency output from the generator to the polaroid drive motor alone. This gave a slit speed of 1.875 mm/min.

### 10.5. Experimental Results

Having obtained a constant velocity for the slit, a series of tests was commenced to evaluate the photographic record of the resultant bars. As the initial tests were to explore the basic idea, the principal objective was to ascertain that a series of recorded bar patterns had a sinusoidal distribution throughout. Unfortunately, although the waveform was approximately correct, the resultant bars appeared to be pairing over the whole of the area exposed.

A further problem was that small particles of dust became lodged between the blades of the very narrow slit used. This caused a series of lines to be drawn across the image recorded on the photographic plate.

10.6. Bar Pairing

The effect of bar pairing proved to be an elusive problem to solve. Upon measurement it was discovered that two consecutive cycles of polarization were unequal in their effect. Attempts were made to correct this by placing the stationary polaroid at various positions in the enlarger's optical system. A third polaroid was introduced to lie over the traversing slit, but although it diminished the effect, the pairing was still apparent. A solution was eventually found by dispensing with the rotating polaroids under the lens and situating them next to the enlarging lamp. The pairing effect had been caused by a partial polarization of the light in the enlarger optics and it

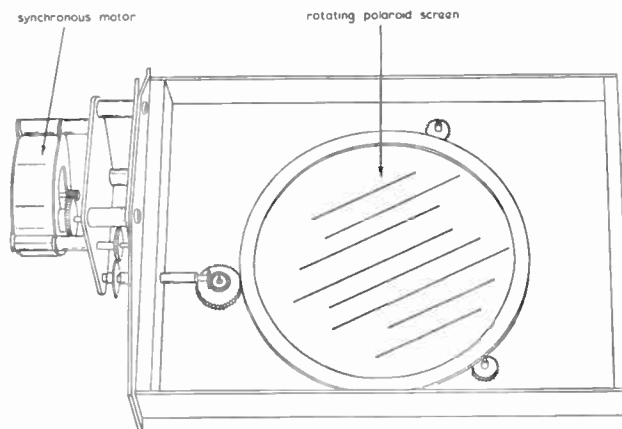


Fig. 6. Rotating polaroid assembly.

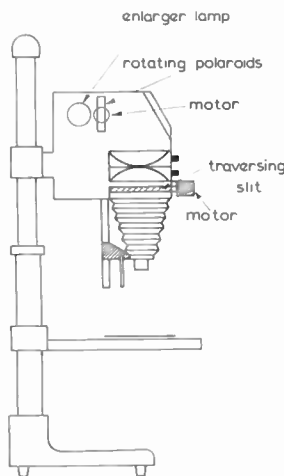


Fig. 7. Final layout of enlarger.

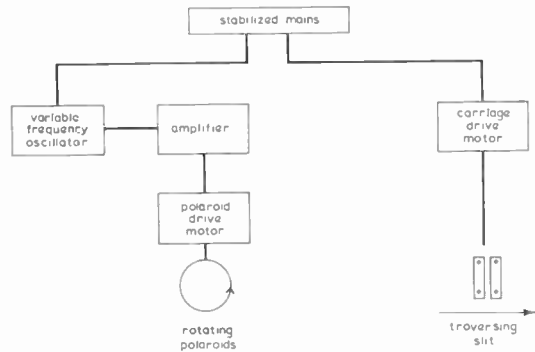


Fig. 8. Equipment layout—block schematic.

was therefore necessary to polarize the light at its source. As this particular enlarger had a colour filter drawer immediately in front of the lamp, it was convenient to redesign the rotating polaroids so that a compact assembly could be mounted in place of the filter drawer. This assembly is shown in Fig. 6, and the final mechanical arrangements employed are shown in Figs. 7 and 8. They gave a flexible system of production having the following features:

- (a) Variable speed of polaroid rotation. This controlled the number of bar patterns recorded.
- (b) Uniform speed of slit traverse.
- (c) Variable slit width controlling depth of modulation.
- (d) Variable magnification, also controlling (b) and (c).

11. Theoretical Considerations

If light of intensity  $I$  is sinusoidally modulated into the form  $I_m \uparrow$  (see Fig. 9(a)), by means of the polaroid filter and travelling slit, and in this form is projected on to a photographic emulsion, then on development this emulsion will have a transmission characteristic in the form of  $1/I_m$ , (Fig. 9(b)). If this recorded image is exposed to a uniform light source and a print obtained, then this print will have a transmission characteristic, Fig. 9(c), similar to that given by the original light and slit combination, providing the following conditions are fulfilled:

- (a) That the emulsion used has a density/log exposure characteristic that is linear over the range required.
- (b) That the overall processing is controlled to a gamma of one.

$\uparrow I_m = k + \sin 2\pi x/\lambda$  where  $I_m$  is the intensity at a distance  $x$  from the start of the scan and  $\lambda$  is the distance corresponding to one cycle of intensity variation. As the intensity cannot have a negative value for any value of  $x$ ,  $k$  is a constant equal to or greater than 1.

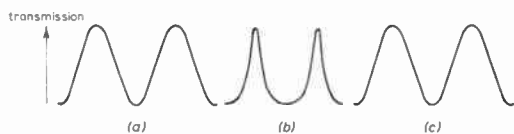
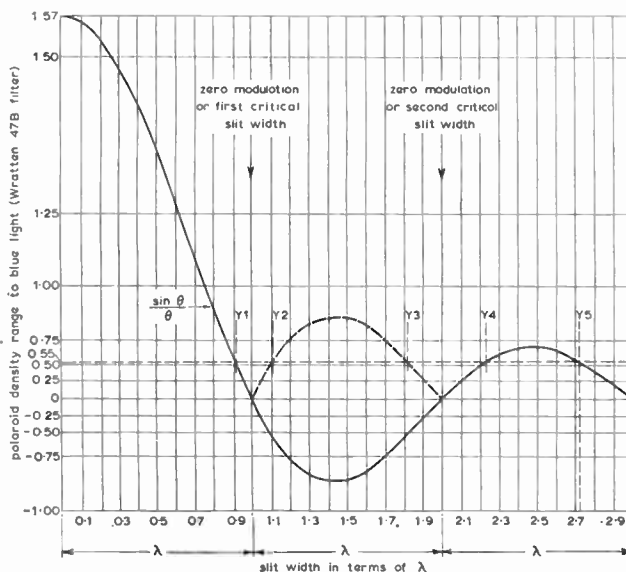


Fig. 9. A plot of sine-wave profiles.  
 (a)  $I_m$  from polaroid assembly  
 (b)  $1/I_m$  from intermediate negative  
 (c)  $I_m$  from final print

Fig. 10. A plot of density range versus slit width  $\frac{(\sin \theta)}{\theta}$ .



## 12. The Production of the Master Intermediate Negative

### 12.1. Exposure

It was determined empirically that the final master negative from which all the bars could be produced would be one containing 24 sinusoidal cycles and be 75 mm long overall. This number of cycles was in excess of those necessary to cover both the maximum frequencies required on Test Cards D and E, but it was anticipated that they would be needed for other specialized test patterns. The overall length of 75 mm was chosen because it was a convenient size to handle in the enlarger and a wide range of photographic materials was available in this size from which the master negative could be reproduced. By setting the enlarger at a 5 : 1 ratio between the negative holder containing the slit and the copy board, the slit travel to produce this master negative 75 mm long would therefore be reduced by the enlarger ratio, i.e. 75/5 mm to a dimension of 15 mm; this was well within the limits of the micrometer screw actuating mechanism of the slit. From the mode of operation of the equipment it may be seen that the wavelength,  $\lambda$ , of the bar patterns is inversely proportional to the frequency of modulation,  $f_m$ , given by the rotating polaroid screen and directly proportional to the velocity,  $v$ , of the slit, i.e.

$$\lambda = \frac{v}{f_m} \dots (1)$$

In the case under review,  $\lambda$  may be simply determined from the ratio of the total length of slit travel to the total number of patterns, i.e.

$$\lambda = \frac{15}{24} = 0.625 \text{ mm}$$

If  $v = 1.875$  mm per minute and  $\lambda = 0.625$  mm, then

from eqn. (1),

$$f_m = \frac{1.875}{0.625} = 3 \text{ cycles per minute}$$

As there are two cycles of modulation for each complete rotation of the polaroid screen, this gives the screen a final drive speed of 1.5 rev/min. As discussed in Section 10.3, the overall gear reduction employed from the motor to the polaroid screen was 200 : 1, therefore, for 1.5 rev/min of the polaroid, the motor speed had to be 300 rev/min. The normal synchronous motor speed was 200 rev/min at 50 c/s, it was therefore necessary to adjust the frequency of the supply generator to 75 c/s to give the required 300 rev/min.

From the specification given in Table 1, the density of the bars was 0.5 min. to 1.05 max., a range of 0.55. For ease of working it was decided that the master negative would be made by blue light on a blue-sensitive material.† The density range of the polaroids to blue light was therefore measured and the results are given in Table 2. These are diffuse densities to blue light using a Wratten 47B Filter.

Table 2

Measured density range of polaroid screen unit

minimum	0.7
maximum	2.27
density range	1.57

Using the polaroid filter and travelling slit a series of exposures was made on B40 plates with a finite

† Of the various materials tested, Kodak B40 plates were one type found to be suitable.

increase in slit width for each exposure. From the measurements obtained a curve was plotted relating the range of densities produced for a given width of slit, the velocity of the slit and speed of rotation of the polaroid filters remaining constant. It was observed that this curve followed the form of  $\sin \theta/\theta$  (where  $\theta$  is expressed in radians), as shown in Fig. 10. The geometrical and mathematical treatments from which this form of curve may also be derived are adequately described elsewhere<sup>4, 5</sup> as similar conditions apply in the scanning of variable-width sound tracks on cine film and in aperture distortion in television camera tubes.

From Fig. 10 it will also be seen that the curve descends from a maximum density of 1.57 and crosses the line of zero density range (zero modulation) when the slit covers its own width in the time taken for one complete cycle of modulation produced by the polaroid filters or when  $\lambda = \text{slit width}$ ; this zero modulation or critical slit width occurs for any integer relationship of slit width to pattern wave-length. Between these points of zero modulation there exist therefore along the curve a number of points  $Y_1$  to  $Y_5$  where the density range required, i.e. 0.55 may be obtained. In practice, for the reasons given in Section 10.5, the widest slit possible was preferred, so point  $Y_5$  was chosen, giving a slit width of  $2.75\lambda$ , or 1.7 mm where  $\lambda = 0.625$  mm.

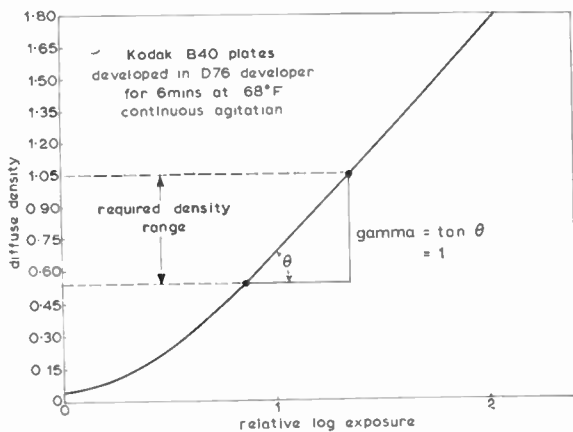


Fig. 11. A characteristic curve of Kodak B40 plates.

12.2. Development

To achieve a gamma of 1 on the B40 plates a development time of six minutes in Kodak D76 at 68°F (20°C) was found to be optimum, this time being long enough to enable an accurate and reproducible result to be obtained with controlled manual agitation. The characteristic curve of the Kodak B40 plates under these conditions is shown in Fig. 11.

12.3. Density Measurement

As the image density of the bars on the master negative varied continuously, it was necessary to use a microdensitometer to carry out the measurements. In order to relate the specular density readings obtained by a microdensitometer to the single-diffuse density required, a graduated series of exposures was also made on a Kodak B40 plate which was similarly developed to a gamma of 1. This plate was then measured using a microdensitometer and also a densitometer capable of measuring diffuse density.

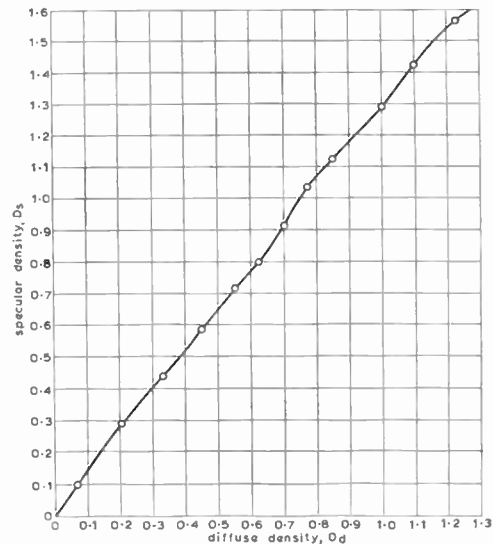


Fig. 12. A plot of the Callier coefficient of a processed B40 plate.

The results are shown in Fig. 12. The relationship between diffuse density  $D_d$  and specular density  $D_s$  is known as the Callier coefficient  $D_s/D_d$  and varies according to the density being measured.

13. The Production of Sine-Wave Bars of Reflectance: Test Cards D and E

13.1. Practical Considerations

The final requirement for the sine-wave bars was their production on bromide paper to the specification given in Table 1. As a master negative had now been obtained with the correct density range, it was necessary to print from it the different frequency bars at the correct magnification. It was also essential that the bromide print obtained should be developed to a gamma of 1.

13.2. Print Material and Processing

An inspection of manufacturers' curves showing the characteristics of printing papers revealed that with certain chlorobromide emulsions it should be possible

to achieve unity gamma. It was found experimentally that by using Kodak Bromesko WSG.1S paper and developing it as shown below, a gamma of 1 could be achieved:

- Developing agent: Kodak Soft Gradation
- Dilution by volume: 1 : 3
- Time: 1½ minutes
- Temperature: 68°F (20°C)

From a range of density steps produced on the B40 plate it was found that the straight line portion encompassed the density range required of 0.5 to 1.05, as shown in Fig. 13.

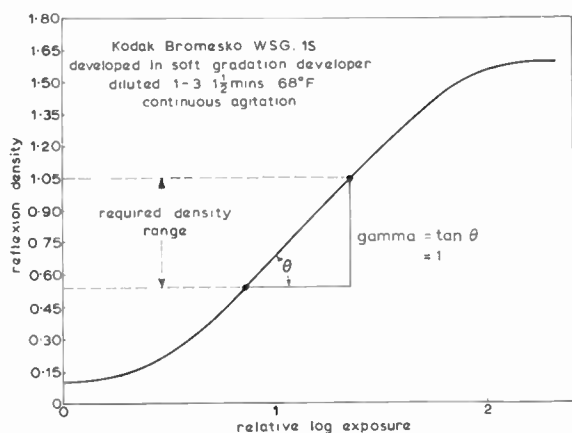


Fig. 13. A characteristic curve of Kodak Bromesko WSG.1S paper.

In an attempt to ensure consistent results the exposure and processing conformed to the following conditions:

- (a) The enlarger lamp was fed from a stabilized supply.
- (b) All the chlorobromide paper came from the same batch.
- (c) All the exposed prints were first soaked in water before processing.
- (d) Fresh developer was used for each print.
- (e) The method of agitation was strictly controlled so as to be the same for each development.

13.3. Measurement

One of the more difficult problems encountered was the task of measuring the variable reflexion densities of the sine-wave bar patterns. The reflexion densitometer available could measure a minimum width of approximately 1 cm; but on the bar patterns the distance to be measured to disclose the different density levels had, in theory, to be infinitesimal. As it

was possible to produce relatively large area density patches and these could be calibrated, it was decided to use a comparative system of reflexion density measurement.

A Zeiss binocular microscope was obtained which enabled a specimen area of only 1 mm in diameter to be measured. A built-in tungsten light source was used to illuminate the specimen. A photo-resistive cell was fitted to one of the eyepieces and its output fed to a microammeter. Using this apparatus it was possible to effect a comparison between the specimen and the previously calibrated density patches. It was essential to use a glazed paper specimen, as serious trouble was encountered when using unglazed material owing to the random specular highlights caused by the irregular surface of the paper.

Although this technique had its limitations, it enabled a close method of density determination to be made on a comparative basis. The final measurements were made by displaying the known density patches alongside the blocks of bars in front of an image-orthicon television camera. This camera was operating in a linear mode under carefully controlled conditions of illumination. The electrical output waveform was displayed on an oscilloscope from which measurements could be made. Table 3 indicates the results that were obtained for Test Card E.

Table 3

Frequency	White level	Black level	Modulation
1.5 Mc/s	12.5	1.3	11.2
2.5 Mc/s	12.4	1.2	11.2
3.5 Mc/s	12.3	1.2	11.1
4.0 Mc/s	12.3	1.2	11.1
4.5 Mc/s	12.5	1.4	11.1
5.25 Mc/s	12.2	1.2	11.0

Density 0.5 = 12.3 arbitrary units  
 Density 1.05 = 1.2 arbitrary units

13.4. Bar Pattern Dimensional Measurements

The bar patterns were checked overall by a travelling microscope, and they were found to be within 2% of the required dimensions.

13.5. Final Bar Patterns

The need for optimum quality bar patterns meant that in some instances re-washing and drying a print could make it acceptable. In many cases chemical reduction of the image was used to remove density and bring the bars within the specified range. Figure

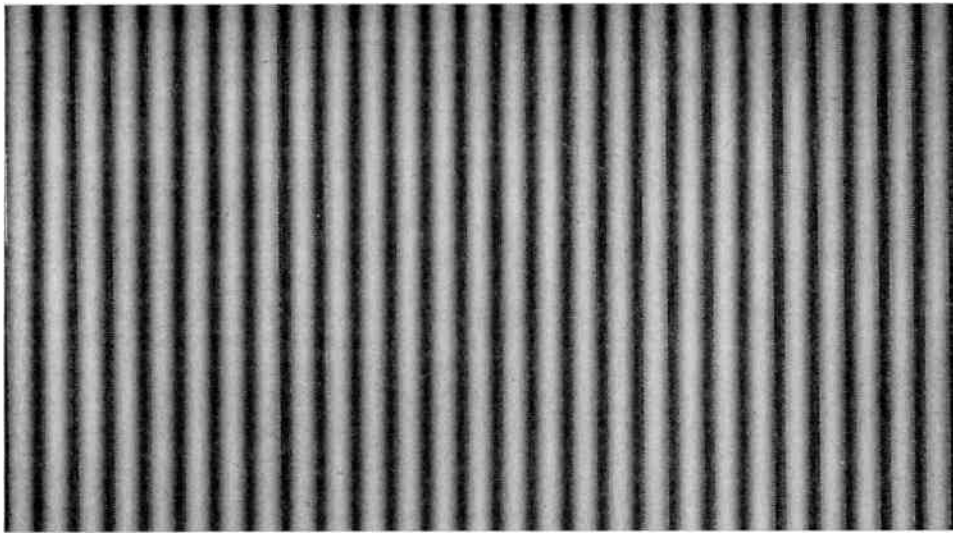


Fig. 14. An example of the final sine-wave bar patterns.

14 shows one example of the final sine-wave bar patterns.

#### 13.6. *The Mounting of the Bar Patterns and Background: Test Card E*

Owing to some problems envisaged in the transmission of Test Card D, it was decided that each block

of bar patterns for Test Card E should commence and finish at the mid-specific density value of 0.72; the blocks of patterns were therefore mounted on a grey background of this density. After a period of use this was found to cause greater difficulties to the viewer, and a background similar to that of D will be substituted. (See Sect. 7.)

### Part 3

#### THE METHOD OF PRODUCING 2 in × 2 in SLIDES

G. S. Ashburner and A. Port

##### 14. Introduction

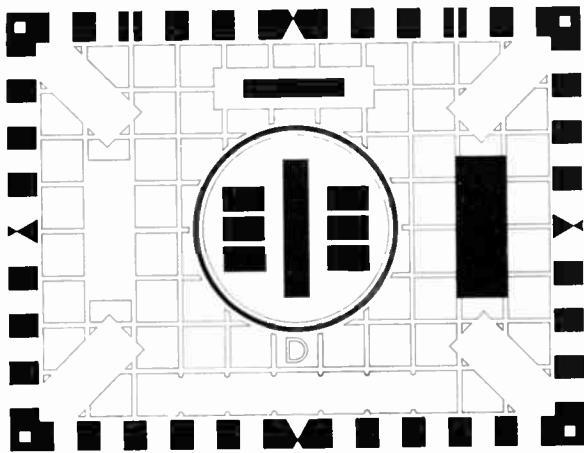
It may be imagined that in order to produce a slide transparency of a test card suitable for use in a telecine scanner all one need do is to draw the master original accurately and to specification and copy it on photographic film. This, unfortunately, is not the case, since no photographic system is capable of facsimile tonal or spatial reproduction. Photographic emulsions have a non-linear characteristic curve; they are turbid, and they both reflect and scatter internally some of the light which falls upon them; photographic lenses are imperfect in many respects, and all suffer from flare to a greater or lesser degree. Furthermore, the nature of the photographic process is such that random variables make exact reproducibility of results extremely difficult to achieve.

These factors determined the methods eventually adopted for producing 2 in × 2 in slides of Test Cards D and E, which this paper briefly describes. The fact that both 16 mm and 35 mm motion picture versions of the test cards would eventually be required influenced our thinking at many stages, though work on motion picture film is not sufficiently advanced to justify a detailed discussion at this time.

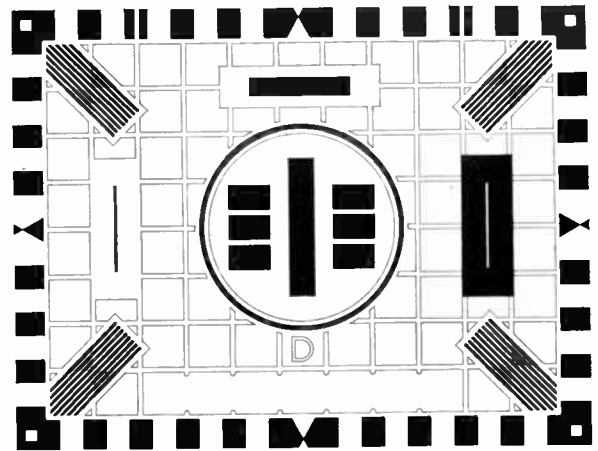
##### 15. Preliminary Work

After a considerable amount of preliminary experimental work the following basic decisions were taken:

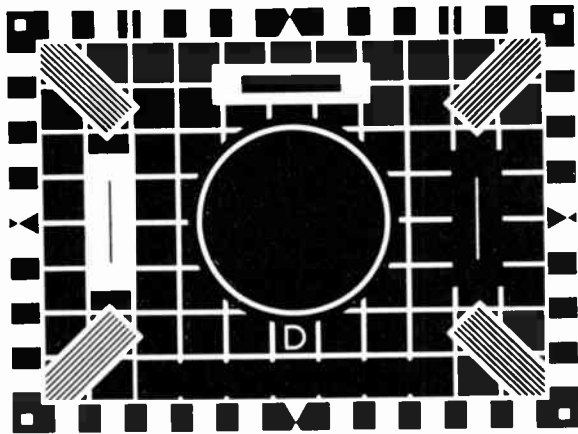
1. That the completed master original should be a negative transparency.
2. That the 2 in × 2 in slides should be made by direct photography of the master.



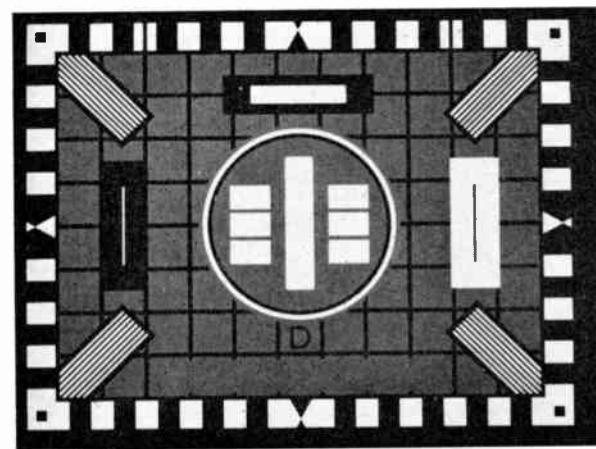
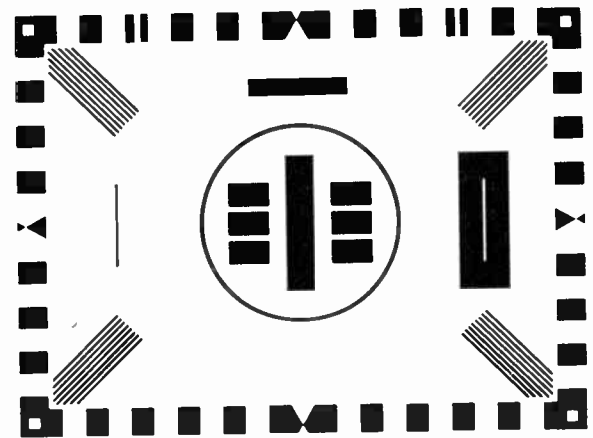
(a) The background information.



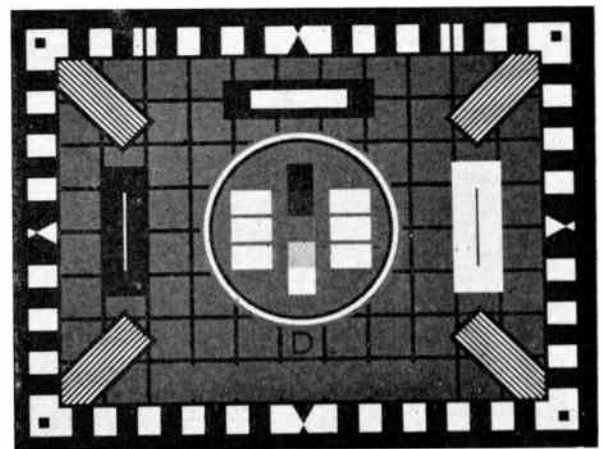
(b) Corner gratings added.



(c) The two diapositives.

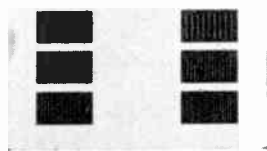


(d) The combined print from the two diapositives (not normally developed at this stage).



(e) The background master negative.

Fig. 15.



(f) The resolution bar master negative.

Fig. 15.

3. That the photographic emulsion chosen for producing the 2 in  $\times$  2 in slides should be capable of yielding the desired contrast range when processed to a gamma of 1.0.
4. That since the three groups of information on the test card—the central grey wedge, the frequency gratings and the geometrical background pattern—each presented a different problem, it was essential to keep them photographically separate, and to be able to modify them independently at each stage in the production of the master negative.
5. That caption and title information should also be kept separate.

It will be seen that the approach outlined above differs radically from that used elsewhere.

### 16. The Choice of Photographic Emulsion

The requirements of the photographic emulsion on which 2 in  $\times$  2 in slides were to be made were as follows:

- (a) Resolution should be sufficient to reproduce the high frequency sine wave grating ( $5\frac{1}{4}$  Mc/s on Card E).
- (b) Development time to yield a gamma of 1.0 should be neither inconveniently long nor uncontrollably short.
- (c) The same emulsion should be available in both 35 mm and 16 mm width.

Eastman Fine Grain Pan Duplicating Negative 5234 satisfied these requirements.

Since in common with other emulsions the response of 5234 is non-linear, the density differences between adjacent steps in the grey wedge, at both the high and low ends of the wedge, had to be 'stretched'. This meant that a density range of 2.05 was needed in the wedge on the master negative in order to give the specified range of 1.6 on the final 2 in  $\times$  2 in slide. The fact that such an overall range is unobtainable on bromide paper was one reason for not choosing a reflection type master.

## 17. The Master Negative

### 17.1. The Background

The first stage in making the master negative was to prepare a large scale drawing containing all the background information on the specification. As will be seen from Fig. 15(a), this drawing carries no diagonal corner gratings, pulse bars, grey wedge or frequency gratings. It was made with great accuracy, on dimensionally stable material, and measures approximately 30  $\times$  40 inches. To this drawing were added corner gratings and pulse bars (Fig. 15(b)).

### 17.2. The Corner Gratings

One result of the non-linearity of the photographic system is that if a series of adjacent black and white bars of equal width—that is, having equal mark/space ratio—are photographed, they will not be of equal width on the processed plate or film. The reasons for this are complex. It was found by experiment that the white bars on the drawing had to be approximately 15% wider than the black bars in order to arrive at a 1 to 1 ratio on the final 2 in  $\times$  2 in slide. These were accordingly made photographically and stuck in position on the background drawing.

### 17.3. The Pulse Bars

The required width difference between the black pulse bar and the white pulse bar were likewise determined experimentally, and turned out to be 31.7%, the white bar again being wider. These pulse bars had to be of equal width on the final slide when measured on an oscilloscope, i.e. at a density which allows for gamma correction in the television camera. This density is 0.96. The microdensitometer trace of the two pulse bars (Fig. 16) shows that width varies with density, and the exact density at which measurements are taken is therefore of great importance.

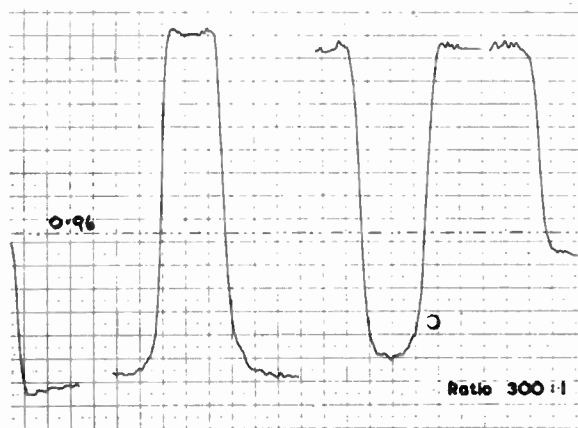


Fig. 16. A microdensitometer trace of pulse bars.

#### 17.4. *The Line Negative*

The next step was to make a line negative of the master drawing complete with corner gratings and pulse bars. This was done on a very accurate cartographic camera, using polyester-base film. From this negative two diapositives were printed in a vacuum frame, using the same type of film. These diapositives differed from one another in that one carried all the information needed to print the background grey areas, and the other carried the information needed to print the castellations, pulse bars, corner gratings and so on. The difference between them was obtained by manually blocking out relevant parts of the line negative. (Fig. 15(c).)

These two diapositives were then printed sequentially on to an Ilford Thin Film Halftone plate, using a special register jig to ensure perfect coincidence of the two images. Had the plate been processed at this stage it would have had the appearance of Fig. 15(d).

#### 17.5. *The Grey Step Wedge*

Before processing this plate, however, the grey wedge was also printed. Each step of this wedge was exposed individually by means of a mechanical device shown in Fig. 17. This consists essentially of an accurately made slot, the sides of which are chamfered, in which slides a covering bar. The bar can be located in five positions corresponding to the wedge steps, and has in it two holes which locate exactly in

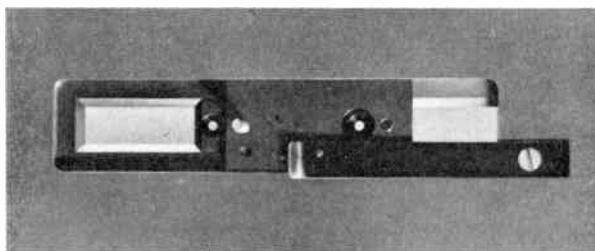


Fig. 17. The mechanism for exposing the step-wedge and dots.

the centre of the top step and the bottom step when the slot is fully closed. A second register jig enabled the wedge slot to be lined up with the latent image of the background which the photographic plate already carried. In practice, the whole of the wedge area was exposed for a time long enough to produce the required density in the lightest step then each step was covered in sequence, additional exposure being given each time. Finally, the 'spots' in the top and bottom steps were exposed by uncovering the holes in the slide bar.

The required wedge densities on the master negative were determined by plotting back from the characteristic curve of 5234 camera film developed to a gamma of 1.0, taking into account also the characteristics of the Thin Film Halftone plate. The great advantage of an independent wedge exposing device of this kind was that any density variation could be made at will. Figure 15(e) shows the appearance of the master at this stage.

#### 17.6. *The Frequency Gratings*

The next job was to insert the frequency gratings. These were supplied in the form of small bromide prints by the B.B.C. Research Department and their production has been described in Part 2. A mask plate, opaque except for the six grating rectangles, which were clear glass, was prepared from the master negative. This mask was placed in a copying camera from which the focusing screen had been removed, and an image projected through the camera lens on to the copy board. The bromide prints of the frequency gratings were then carefully positioned on the copy board within the projected rectangles. The projection lamp was removed, and the bromide prints were themselves illuminated. The mask plate was left in the camera. Behind it, and in contact with it, was placed an unexposed B 40 plate, and the bromide prints were thus photographed through the mask. The result was a negative record of the frequency gratings, the rest of the plate remaining clear (Fig. 15(f)). As with the grey wedge the precise density and contrast requirements of the master negative were determined by carrying each test through the whole process and measuring the results on the final 2 in x 2 in slide. There were thus two negatives, one (Fig. 15(e)) carrying the wedge and background information, the other (Fig. 15(f)) carrying the gratings. These were bound together in register, emulsion to emulsion, and copied on Eastman 5234 film.

#### 17.7. *The Title Plate*

The title plate, bearing the station name and any other required wording is simply placed on top of the master negative, and can readily be interchanged. It is worth noting in passing that a dummy title plate was used during all the test work previously described, so that its optical effect could be taken into account. Although the image on this plate is physically separated from the other two by one glass thickness, the depth of field of the optical system is sufficient for it to remain in focus.

### 18. The Copying Equipment

The basic photographic set-up is shown in Fig. 18. The lens used is a 4-in Repro Ultron, selected after extensive tests carried out in collaboration with

the B.B.C. Research Department. Accurate optical alignment of the copying rig is of great importance, since the dimensional tolerance on a 2 in × 2 in slide is of the order of 0.2 mm, and precise focusing is vital not only for this reason, but also because any lack of precision at this stage has a disastrous effect upon the mark/space ratio.

All densities in the specification are defined in terms of single diffuse density. As soon as the decision to use 5234 as the film stock for making the slides had been taken, therefore, three identical step wedges were made as a control. B.B.C., I.T.A. and Colour Centre each hold one copy. These were calibrated on the Westrex Densitometer at Lime Grove in terms of single diffuse density. The Colour Centre control wedge was then used for setting up a Joyce Loeb Microdensitometer each time measurements were made. The microdensitometer was thus used as a comparator.

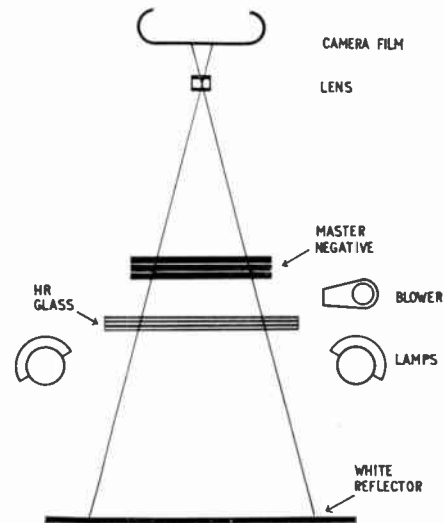


Fig. 18. The photographic set-up.

## Part 4

### 19. Conclusions

The work described in this paper has produced an accurate and repeatable test card for trade test transmissions. It has been in use for several months on the 405-line system and has proved generally acceptable despite early doubts on the subjectively visual effect of the resolution bars.

The technique for producing the latter is a precise method which can be used for producing transparent or opaque masters.

The reproduction methods used give great flexibility in production of the master negative and reasonable tolerances on the final transparencies when made in large numbers.

### 20. Acknowledgments

The various authors wish to express their gratitude to the many colleagues who assisted in this work, both in making the equipment and in measuring the innumerable trial runs during development of the processes; also to members of the B.R.E.M.A. organization who organized and collated transmitter tests.

Thanks are due particularly to Mr. W. Sproson of B.B.C. Research Department for advice and assistance on optical problems and to Mr. D. Brown of Joyce Loeb and Co. Ltd., for assistance in carrying out microdensitometer measurements.

Finally, the authors wish to thank the Director of Engineering of the B.B.C. and the Chief Engineer of the I.T.A. for permission to publish this paper.

### 21. References

1. B.B.C. Research Department Report T-069(1958).
2. N. S. Kapany and J. N. Pike, "Scanning integrator for producing sinusoidal test objects", *J. Opt. Soc. Amer.*, **46**, pp. 867-74, October 1956.
3. G. Hersee and J. T. Royle, "The new B.B.C. transparencies for testing television camera channels", B.B.C. Engineering Division Monograph No. 21, November 1958.
4. J. W. Godfrey and S. W. Amos, "Sound Recording and Reproduction", p. 215. (Iliffe, London, 1952).
5. S. W. Amos and D. C. Birkinshaw, "Television Engineering", Vol. 1, p. 272. (Iliffe, London, 1956).
6. B.B.C. Technical Memorandum T-069.
7. B.B.C. Technical Memorandum T-1039, "On Reproducing Test Card C on Motion Picture Film".
8. British Standard 3115:1959. Recommendations for density and contrast range of monochrome films and photographic opaques for television.
9. British Standard 2948:1958. Slides and opaques for television.
10. British Standard 677:1958. Motion picture film.

### 22. Appendix 1:

#### Final Specification for Test Card D Positive Transparencies

1. This specification is for the final transparent positives of the Test Chart D. Opaque positives for this pattern are not covered by this specification, and their production is not normally permitted.

2. Transparencies comply with British Standard 2948 : 1958,<sup>9</sup> motion picture film shall comply with

B.S. 677 : 1958.<sup>10</sup> The limits of the transmitted area are indicated on the layout drawing by the 'egg-timers' and by the outer corners on the small white squares; these are 1½ units inside the outer edge of the castellations. Densities shall be measured as single diffused densities.

3. *Layout: General*

The layout is shown in B.B.C. drawing PID.1000.2.14K and I.T.A. drawing H.127 sheets 1 and 2. The dimensions on these drawings are given in arbitrary units so chosen that if the test chart is scanned with a line period of 80 μs, then each horizontal unit is equivalent to 1 μs.

4. *Layout: Frequency Gratings*

The drawing shows the outlined dimensions only for the frequency gratings. They should be arranged as follows:—

Location	Frequency (405 system)	Total width of one black and one white bar
Top left-hand	1 Mc/s	1 unit
Top right-hand	1½ Mc/s	·66 units
Centre left-hand	2 Mc/s	·5 units
Centre right-hand	2½ Mc/s	·4 units
Bottom left-hand	2¾ Mc/s	·36 units
Bottom right-hand	3 Mc/s	·33 units

5. *Densities—Step Wedge*

The densities should be as follows:—

Ref. I.T.A. drawing H.127 sheet 1.

B.B.C. drawing PID.1000.2.14K.

B.B.C. Research Department Report T-069.

Ref.		Density	Tolerance
W	Background white and white spot in step 1 of step wedge	0·4	± 10%
1 & W'	Step 1 of step wedge	0·5	± 10%
2	Step 2 of step wedge	0·74	± 10%
G	Background grey	0·95	± 20%
3	Step 3 of step wedge	1·05	± 10%
4	Step 4 of step wedge		
B'	Black spot in step 5 of step wedge	1·8	± 10%
B } 5 }	Background black and step 5 of step wedge	2·0	± 10%

Note. The difference between any two densities shall be held to within +20% of the difference between their nominal values.

6. *Densities—Frequency Gratings*

"White" (for all gratings)	0·5 ± 0·05
"Black" 1, 1½, 2, 2½ Mc/s } gratings 2¾ and 3 Mc/s }	1·5 ± 0·05

7. *Densities—Pulse Bars*

White	0·5 ± 10%
Black	2·0 ± 10%

The densities of the black pulse bar and the black block of the white pulse bar shall be within 0·1 of each other.

8. *Dimensional Tolerances*

All specified dimensions shall be measured at the mid-value of the specified density range, with the exception of the pulse bar, this being measured at a density of 0·96.

All points shall lie within ±1% ± 0·1 unit of the specified point shown on H.127 sheet 1 and B.B.C. drawing PID.1000.2.14K. The width of the pulse bar, corner gratings and the overall dimensions of the frequency gratings are to be within 5% of the dimensions shown on drawing H.127 sheets 1 and 2.

9. *Test Card E*

Generally as above except the frequencies shall be:

1·5 2·5 3·5 4·0 4·5 5·25 Mc/s

when scanned on the 625-line system.

Appendix 2: *Transmission Standards*

The choice of the densities used in Test Card D was made so that the limits would comply with the densities laid down in B.S. 3115 : 1959 for television slides and film.<sup>8</sup> The choice of the densities in the step wedge was made as a result of the recommendations contained in B.B.C. Research Department Report No. T-069, on the assumption that the camera or telecine machine gamma corresponds to 0·5. The following table gives resulting voltages using a process gamma of 0·5.

	Density	Density (Relative)	Voltage gamma = 0·5
White Areas		0	·7
Step 1	·4	·1	·62
Step 2	·74	·34	·48
Pulse Bars 50%	·96	·47	·365
Background Grey G	·95	·55	·37
Step 3	1·05	·65	·33
Step 4	1·48	1·08	·20
Dark Grey Circle	1·8	1·4	·14
Black areas and Step 5	2·0	1·6	·11

Manuscript first received by the Institution on 25th November, 1964 and in final form on 18th March, 1965. (Paper No. 990/T31.)

© The Institution of Electronic and Radio Engineers, 1965

# The Dynamic Capacitor Electrometer

By

E. R. TUDOR (*Graduate*)†

**Summary:** The theory, historical development, design and construction of the dynamic capacitor electrometer are discussed. Both reed and diaphragm types are considered. Circuits are given and techniques of pH measurement described briefly.

## 1. Introduction

The dynamic capacitor electrometer has been developed to enable extremely small direct currents and potential differences to be measured in the presence of high source resistances.

## 2. Limitations of the Thermionic Electrometer Valve

In the measurement of small d.c. signals some form of amplification is necessary to enable their indication by a comparatively robust moving coil meter, or indeed to provide any proportional signal of useful power level. Thermionic electrometer amplifiers provide the most convenient method of amplification until the current to be measured approaches that taken by the control grid of the electrometer valve: fluctuations in this current then limit its further usefulness. These fluctuations are reduced to a minimum in modern electrometer valves and by careful circuit design.<sup>1</sup> An electrometer input stage may be followed by a direct-coupled amplifier employing either thermionic valves or transistors, but even with balanced circuits, negative feedback and considerable attention to maintain stable supplies, the overall performance is limited primarily by drift in the first stage.

## 3. The Dynamic Capacitor

In principle the dynamic capacitor does not have this limitation and furthermore there is no theoretical upper limit to its input resistance. However, to exploit the possibilities of a dynamic capacitor to the maximum requires the utmost care in design and manufacture. The circuitry also becomes more complicated inasmuch as a drive circuit and phase sensitive detector are required in addition to a stable a.c. amplifier which replaces the d.c. amplifier of a thermionic electrometer.

### 3.1. General Requirements

One of the most important components in a dynamic capacitor electrometer is the dynamic capacitor, which, ideally, is a perfect capacitor capable of

sustained alternating variation. For minimum zero drift the electrode surfaces should be stable, perfectly alike and unaffected by the immediate environment which also should be stable and free from all extraneous electrostatic and electromagnetic fields and ionizing radiation. Electrode insulation, besides requiring exceptional and stable insulating properties, should be free of all surface charge and piezo-electric effects. Any attempt to approach this ideal in practice requires considerable mechanical precision and special attention to insulation and electrodes.

### 3.2. Theoretical Considerations

The method of using the dynamic capacitor is illustrated in Fig. 1. Let the potential to be measured be  $V_{d.c.}$  and the internal resistance of the source be  $R_s$ . The coupling capacitor  $C_c$  may be an air dielectric capacitor but more likely will be polystyrene. The principle of operation is based on constant charge and variation of capacitance. If the dynamic capacitor

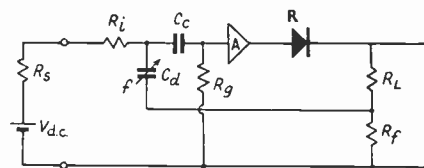


Fig. 1. Dynamic capacitor general circuit with feedback.

$R_s$	source resistance	$R$	phase-sensitive rectifier
$R_i$	isolating resistor	$R_L$	load resistance
$C_d$	dynamic capacitor	$R_f$	feedback resistor
$C_c$	coupling capacitor	$f$	frequency of $C_d$
$R_g$	grid resistor	$V_{d.c.}$	source voltage
A	stable a.c. amplifier		

$C_d$  is charged to  $V_{d.c.}$  it may be said to have received a charge  $Q$ , these quantities having the well-known relationship

$$Q = V_{d.c.} C_d$$

If  $Q$  remains constant and the capacitance changed by an amount  $dC_d$  then

$$dV_{d.c.} = -V_{d.c.} \frac{dC_d}{C_d}$$

† Formerly with W. G. Pye & Co. Ltd., Cambridge; now with Bristol Siddeley Engines Ltd., Edgware, Middlesex.

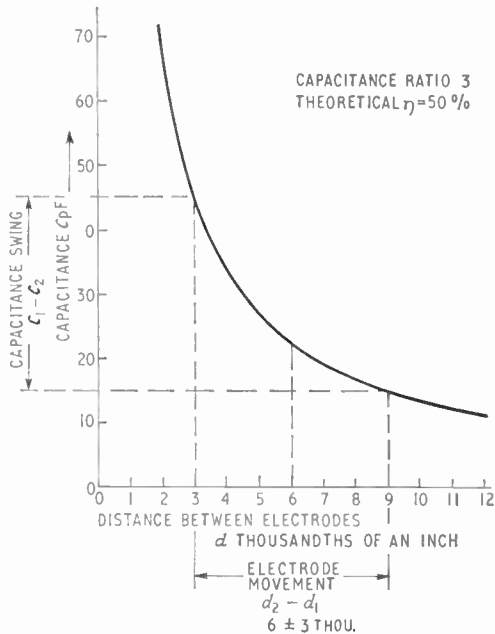


Fig. 2. Idealized capacitance swing for  $\frac{7}{8}$  in diam. electrode. Capacitance ratio 3. Theoretical  $\eta = 50\%$ .

For charge  $Q$  to be relatively steady the time-constant of the isolating resistor and dynamic capacitor should be long compared with the periodic time of operation, i.e.  $C_d R_i \gg 1/f$ , remembering that  $C_d R_i$  also influences the response time. Similarly,  $R_g C_d \gg 1/f$  and for minimum loss in coupling  $C_c > C_d$ . Since  $R_g$  is high the latter effect is small and in practice it is usual for  $C_c$  to be greater than or approximately equal to  $C_d$ . Practical considerations of size and stability also influence the value of  $R_i$  and one of the limits of measurement is set by thermal agitation or Johnson noise in this resistor which is given by

$$\epsilon^2 = 4kTR_i\delta f$$

where

Boltzmann's constant  $k = 1.38 \times 10^{-23}$  joule/deg K

$T$  = temperature deg K

$R_i$  = resistance in ohms

$\delta f$  = bandwidth in c/s.

For a set of typical values, e.g. at  $20^\circ\text{C}$  ( $293^\circ\text{K}$ ), with  $R_i = 10^9 \Omega$  and a bandwidth  $\delta f$  of 10 c/s, then  $\epsilon = 12.7 \mu\text{V}$ .

For a simple two-plate capacitor with air as the dielectric and neglecting fringing and stray effects the capacitance

$$C_d = \frac{225A}{d} \text{ pF}$$

where  $A$  = plate area in square inches

and  $d$  = distance between the plates in thousandths of an inch.

If the capacitance changes from a maximum of  $C_1 = 225A/d_1$  to a minimum of  $C_2 = 225A/d_2$ , where  $d_1$  and  $d_2$  are minimum and maximum separation respectively, then for sinusoidal motion of the moving plate the instantaneous capacitance

$$C_i = \frac{225A}{\frac{d_2 + d_1}{2} + \frac{d_2 - d_1}{2} \sin \omega t}$$

where  $\omega$  is the angular velocity of the moving plate at time  $t$ .

If the steady voltage  $V_{d.c.}$  results in a constant charge  $Q$  on the capacitor then  $V_{d.c.} = Q/C_d$  and the instantaneous voltage across the capacitor will be

$$\begin{aligned} V_i &= V_{d.c.} + V_{a.c.} \\ &= \frac{Q}{225A} \left( d_1 + \frac{d_2 - d_1}{2} \right) + \frac{Q}{225A} \left( \frac{d_2 - d_1}{2} \right) \sin \omega t \\ &= \frac{Q}{225A} \left[ \left( \frac{d_2 + d_1}{2} \right) + \left( \frac{d_2 - d_1}{2} \right) \sin \omega t \right] \end{aligned}$$

### 3.3. Conversion Efficiency

The percentage depth of modulation or the ability of the dynamic capacitor to modulate a steady potential in this way is usually termed its conversion efficiency  $\eta$  and is expressed thus:

$$\eta = \frac{\text{a.c. output (peak)}}{\text{d.c. input}} \times 100$$

Conversion efficiency sometimes is defined as the r.m.s. value of the modulation but, since in practice the modulation waveform seldom is strictly sinusoidal, peak or half peak-to-peak values are considered preferable.

From the previous consideration of instantaneous voltage

$$\eta = \frac{d_2 - d_1}{d_2 + d_1} \times 100$$

Thus for a high conversion efficiency  $d_2 \gg d_1$ .

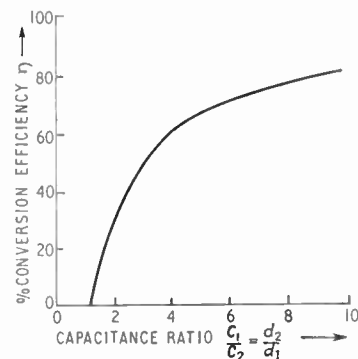


Fig. 3. Showing how conversion efficiency depends upon capacitance ratio.

Theoretically the minimum gap depends upon the maximum applied voltage. If breakdown in air occurs at 35 kV/in then for a working voltage of 10 the gap would be approximately 0.0003 in. However, due to surface irregularities and electrode malalignment it has been found in practice that the maximum capacitance corresponds to a much larger gap than that dictated by voltage breakdown considerations.

For example, if a conversion efficiency of 50% is aimed at, and the minimum gap is 0.003 in, then

$$d_2 = d_1 \left( \frac{100 + \eta}{100 - \eta} \right) = 0.009 \text{ in}$$

and the full amplitude of movement ( $d_2 - d_1$ ) = 0.006 in, i.e.  $6 \pm 3$  thousandths of an inch as shown in Fig. 2. The way in which conversion efficiency depends upon capacitance ratio is shown in Fig. 3. From this the achievement of a relatively high conversion efficiency appears deceptively simple but it is reduced by physical imperfections, coupling capacitor shunting effect and the inevitable stray capacitance. To explore briefly the effect of stray capacitance consider the arrangement depicted in Fig. 2 with the addition of 10 pF stray capacitance. Then, if this is constant, the capacitance ratio  $C_1/C_2$  is reduced to  $55/25 = 2.2$  and, from the graph of Fig. 3, this would yield a conversion efficiency of 37.5%. Expressing  $\eta$  in terms of capacitance swing

$$\eta = \frac{C_1 - C_2}{C_1 + C_2} \times 100 = \frac{55 - 25}{55 + 25} \times 100 = 37.5\%$$

Thus there is an immediate reduction of 12.5% in the conversion efficiency. In practice all deviations from the ideal contrive to detract from the theoretical conversion efficiency and result in typical values of 20 to 30%.

A high conversion efficiency is most desirable since it represents the useful output for a given input and in particular it is valuable in minimizing the effect of noise components near the vibration frequency. In Fig. 4 are shown the theoretical capacitance and voltage waveforms resulting from sinusoidal motion of the moving element for a device comprising one fixed electrode and a vibrating reed. In a practical device the waveforms are likely to be modified somewhat due to mechanical imperfections and stray capacitance. The latter cannot be eliminated completely but can be minimized by careful design and in this respect a high ratio of mean capacitance of the dynamic capacitor to stray capacitance is advantageous. Apart from stray capacitance the voltage output waveform is a direct function of the gap variation which may deviate from sinusoidal due to limitations of the drive system, low mechanical  $Q$  or cushioning effect due to trapped air or gas. Enclosing

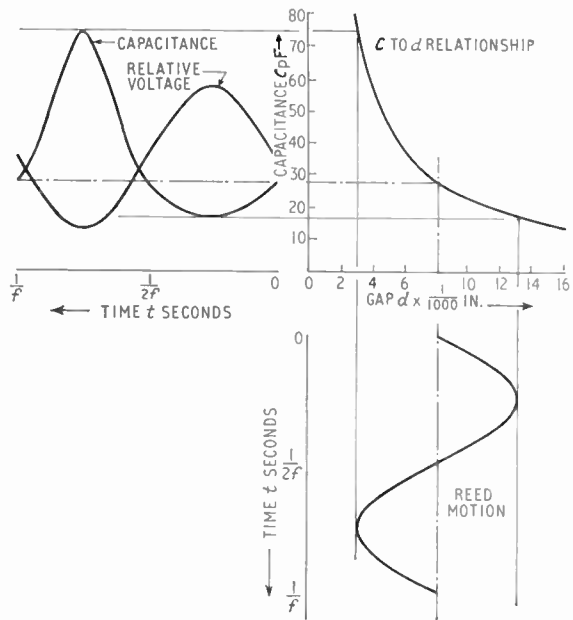


Fig. 4. Theoretical waveforms for sinusoidal motion of  $8 \pm 5 \times 10^{-3}$  in per square inch of electrode area.

the assembly in a vacuum could reduce these effects with advantage. In general the higher the conversion efficiency the more difficult is the realization of a sinusoidal output waveform.

#### 4. Types of Dynamic Capacitor

Many different physical arrangements are possible but they usually take the form of a vibrating reed or diaphragm. The single reed type uses an electromagnet to vibrate a reed or cantilever of ferromagnetic material which acts as the moving electrode vibrating in close proximity to a fixed electrode. The magnetic diaphragm type comprises a similar arrangement where the reed is replaced by a diaphragm. The moving coil diaphragm type operates in a similar fashion to a loudspeaker diaphragm whereas the fixed coil type employs the same principle as the telephone earpiece. Another method uses two similar reeds facing each other so that if both are periodically magnetized by a common field a corresponding repelling force will cause them to move apart in sympathy with the magnetizing force. In general, a moving coil system provides movement proportional to the a.c. drive signal, whereas in fixed coil systems the force on the reed or diaphragm obeys a square law. If the electromagnet in a fixed coil system is polarized the moving element will vibrate at drive frequency, if not, then it will vibrate at twice drive frequency. The reason for this effect is that if polarized the resultant magnetic field is merely varied from a maximum to a minimum at drive frequency

whereas in an unpolarized system the magnetic field alternates, having two maxima and two minima per cycle. This is shown diagrammatically in Fig. 5. The dotted curve represents the magnetic field without polarization which exerts a force on the vibrating element regardless of direction, thus causing two vibrations per cycle of drive current. The solid curve represents the magnetic field resulting from the same drive signal but with polarization (minimum). The magnetic field is now unidirectional, resulting in vibration at drive frequency. Polarization may be provided by a permanent magnet incorporated in the system magnetic circuit or it may be inherent in the drive current as in modulated d.c.

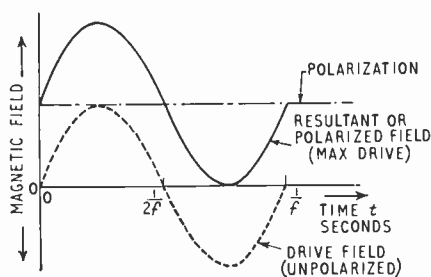


Fig. 5. Showing how polarization affects vibration frequency.

If the moving element is caused to vibrate at its natural frequency then its movement becomes more sinusoidal depending upon the mechanical  $Q$  or dynamic magnification of the system. Less drive power is required for a mechanically tuned system but for constant amplitude of vibration close agreement of frequencies, depending upon the dynamic magnification, may be important. This may be ensured by using closed loop control as for example in an electrically self-maintained tuning fork.

### 5. The Vibrating Capacitor—an Historical Review

One of the earliest published accounts of an attempt to measure small d.c. signals by means of a periodically varying capacitor was by Ross Gunn in 1932.<sup>2</sup> He used a rotating type of dynamic capacitor and in spite of commutation difficulties obtained a maximum charge sensitivity of  $4 \times 10^{-15}$  coulomb. After a number of other reports, chiefly from Europe, H. De Vries in 1947<sup>3</sup> used a self-maintained tuning fork which formed two dynamic capacitors, one used for the measurement, and a signal from the other was amplified for the drive coil. It vibrated with a frequency of 400 c/s and was used for measurements of pH. A negative feedback signal was connected to the lower plate of the capacitor and mention is

made of the need to relate the response time of the fork and amplifier.

A notable investigation by Palevsky and others<sup>4</sup> included the design of two dynamic capacitors, one of the reed type and the other of the diaphragm type. The reed driving coil was supplied at mains frequency, i.e. 60 c/s, while the diaphragm was operated at a frequency of 1000 c/s using a phase shift oscillator. The performance of both units is very commendable inasmuch as an input resistance of  $10^{15} \Omega$  with a zero drift of approximately 0.1 mV in 24 hours was recorded. The final evaluation was preceded by general design considerations and a lucid description of the many precautions necessary. An interesting article by Scherbatskoy<sup>5</sup> and others described a portable dynamic capacitor amplifier developed specially for geophysical prospecting.

A moving coil dynamic capacitor electrometer was described by van Hengel and Oosterkamp<sup>6</sup> and with overall d.c. feedback they also achieved an input resistance of  $10^{15} \Omega$ . The most sensitive range was 0–100 mV and it operated at 125 c/s.

Thomas and Finch<sup>7</sup> described a dynamic capacitor electrometer with an input resistance of  $10^{12} \Omega$  and zero drift of about 1 mV/24 hours. The most sensitive range was 0–30 mV. It used a vibrating reed which was valve maintained in resonant oscillation at approximately 550 c/s. The magnet coil assembly was polarized and divided, one half providing the controlling signal which was amplified and supplied to the other half. Precautions were taken to avoid direct coupling between the two coils.

An article by Jervis<sup>8</sup> reviewed many methods of measuring direct currents in the range of  $1 \mu\text{A}$  to  $10^{-16} \text{A}$ . After dealing with galvanometers and other low resistance devices the remainder of the article was devoted to thermionic and capacitor modulator electrometers. The range of methods described was fairly comprehensive and pertinent features included factors limiting accuracy and sensitivity. An appendix included some notes on the precautions necessary when measuring very small currents and the use of negative feedback with electrometers.

A vibrating capacitor for higher voltage measurements, namely 200 V, was described by Adler.<sup>9</sup> Here, the requirements are not as stringent and a low conversion efficiency and relatively high residual voltage become acceptable. The latter was attributed to pick up from the 60-c/s drive coil.

Ritsma<sup>10</sup> described an ingenious way of using a double dynamic capacitor connected so that the grid to cathode impedance of the first valve was constant, so minimizing grid current noise. One plate of the double capacitor was common and took the form of a thin reed, or beam supported at both ends. The fixed

plates were then placed close to this at the second harmonic antinodes. Coils were placed on the other side, one to generate an initiating signal which is amplified, reversed in phase and supplied to the other. Thus when the reed was close to one plate, i.e. maximum capacitance, it was furthest from the other. One fixed plate was connected to cathode, the other to grid and the signal applied to the moving element. The frequency of operation was about 4 kc/s and the whole system was enclosed *in vacuo* to stabilize contact potentials. The highest conversion efficiency achieved was about  $2.5 \times 10^{-2}$  and with a measuring time of 13 seconds a current of  $10^{-17}$  A was detected.

In a survey of low-level d.c. to a.c. converters for d.c. amplifiers Komolibus<sup>11</sup> devoted a short section to the vibrating capacitor. The principle of operation was outlined and typical applications and characteristics noted. A fairly comprehensive bibliography was included.

In a more recent article, modern trends in pH meter design were reviewed by Hitchcox,<sup>12</sup> and the requirements of a high performance pH meter deduced. It was shown that the performance of such an instrument is determined to a large extent by the stage which couples the electrodes to the amplifier and an example was given of a dynamic capacitor in this role.

Apart from the all-important input stage of an electrometer amplifier, semiconductor devices are finding increasing application. They may be used in a hybrid circuit where the first stage is a miniature electrometer valve which is followed by a fairly conventional transistor d.c. amplifier or they may be used in an a.c.-coupled amplifier where the electrometer input stage is preceded by a dynamic capacitor. Although the technique is not yet a serious rival to established methods, a complete semiconductor electrometer amplifier has been described by Wolff and others.<sup>13</sup> In it the voltage to be measured was used to bias a variable capacitance diode controlling the frequency of an oscillator. The output from a conventional Foster-Seeley discriminator was then amplified by two transistors arranged as a long-tailed pair. With overall negative feedback the amplifier had an input resistance of  $2.5 \times 10^{11} \Omega$ .

An advanced and interesting design of dynamic capacitor driven by a high frequency electric field has been described by van Nie and van Zelst.<sup>14</sup> The moving element consisted of a circular glass membrane carrying two electro-deposited and oxidized surfaces. This was clamped circumferentially between shaped glass insulating disks which also had deposited electrodes. One pair of adjacent surfaces was used to drive the membrane at its natural frequency of 6 kc/s and the other pair formed the dynamic capacitor proper. The coupling capacitor comprised

another similarly prepared pair of surfaces and the whole was enclosed in an evacuated bulb. The design, which involved precision glasswork, incorporated long leakage paths and stable materials capable of withstanding the temperatures necessary for successful bake-out and evacuation to a low residual pressure, so conducive to zero point stability.

## 6. Limiting Effects

Several effects conspire to limit the ultimate performance of any dynamic capacitor.

One limitation is when the zero drift becomes a significant proportion of the signal to be measured. The main source of zero drift in a dynamic capacitor is due to a phenomenon known as the contact potential effect. Basically, the dynamic capacitor may be considered as a simple two-plate capacitor in gas or vacuum with good insulation and provision made for varying the capacitance by varying the gap between the plates. Considering the capacitor alone and with constant gap, there will, in all probability, exist a small potential across the plates. Even after a temporary shorting of the plates the potential will re-appear. This potential, classically known as the Volta effect, is due to the differences in work function of the two plates at their dielectric interface and varies according to their stability.

The importance of minimizing these unwanted variations depends upon the application and stability required. The absolute potential is made small by either making the two plates of similar material, preferably cut from the same piece and with similar facing surfaces or by specially treating the facing surfaces so that they are perfectly homogeneous and as alike as possible. In the nature of things it is improbable that the two surfaces will be precisely alike and therefore there will exist an electrostatic field between the two plates and a corresponding potential. This may be compensated by deliberately introducing an external source of the same potential and opposite polarity in series with the capacitor.

However, this compensation is satisfactory only if the contact potential is constant and herein lies the difficulty. Fermi level perturbations due to random molecular agitation cause corresponding variations in the contact potential. This is almost entirely a surface effect and many surface treatments have been tried with varying success. If the surfaces cannot be made independent of the surrounding media then the latter should be made stable by sealing in a vacuum or an atmosphere of inert gas. If a vacuum is used a 'bake-out' may be necessary to minimize emission of occluded gases which could cause minute surface changes. At all times the internal structure of a dynamic capacitor must be kept scrupulously clean. The procedure usually adopted is to assemble initially

for a physical check, then to take apart, wash in methyl alcohol and re-assemble. An even breath pattern is a good indication of cleanliness since the resulting condensation is very susceptible to minor surface contamination or imperfections.

Ultimately natural radiation will set a lower limit of current measurement. If radiation is at the rate of  $0.1 \text{ r/a}$  and there are approximately  $3 \times 10^7$  seconds in a year, then radiation =  $0.1/3 \times 10^7 \text{ e.s.u./s} = 10^{-8}/3$  and one coulomb =  $3 \times 10^9 \text{ e.s.u.}$

Therefore the resulting current

$$\begin{aligned} &= \frac{10^{-8}}{3} \times \frac{1}{3 \times 10^9} \\ &\approx 10^{-18} \text{ A/cm}^3 \text{ of effective air volume.} \end{aligned}$$

Thus in a practical design and with shielding, radiation current probably could approach  $10^{-17} \text{ A}$ ; however, a practical limit due to other causes is likely to be reached before this.

### 7. Testing Techniques

In view of the very small currents associated with dynamic capacitors the cathode follower circuit of Fig. 6 was used to observe the modulation. It was constructed in the form of a probe, fully screened and with a high insulation resistance coaxial socket for the input connection from the dynamic capacitor and a polystyrene coupling capacitor which was mounted close to the input socket. In addition to the use of low capacitance coaxial cable every care was taken to reduce stray capacitances to a minimum.

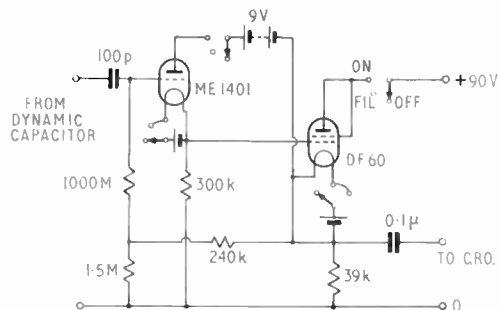


Fig. 6. Cathode follower circuit for test measurements.

Drive power for the various experimental models was obtained from an audio frequency oscillator and transistor amplifier. The capacitor input circuit is shown in Fig. 7. The first tests to which a new model is subjected are to determine its mechanical performance by observing the amplitude of modulation throughout the interested frequency range at constant drive and signal voltages. A mechanical  $Q$  of about

10 was considered a reasonable compromise between minimum drive power and being not too critical as regards frequency. It was found that the diaphragm models tended to be rather lower than this and the reed models rather higher. One reason for low mechanical  $Q$  of a diaphragm type was thought to be due to a greater cushioning effect since the displacement of air can take place round the fixed electrode only. A small hole in the centre of the fixed electrode tended to confirm this.

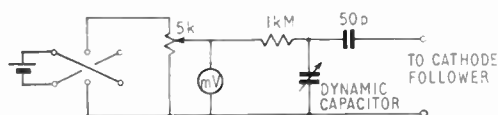


Fig. 7. Capacitor input circuit.

### 8. Experimental Data

Electrically the peak-to-peak amplitude of the modulation or output should be proportional to the d.c. input and the phase of the output is determined by the polarity of the input. The conversion efficiency is simply the ratio of half the peak to peak a.c. output to the corresponding d.c. input. A significant change in amplitude of the output for reversal of input is indicative of a high contact potential. The contact potential may be measured by adjusting the input voltage for zero or minimum output. The amplitude and waveform of this minimum output are influenced by electrode surface impurities or contamination or by extraneous pick-up, e.g. from the drive coil or circuit. The input voltage required for minimum output voltage perhaps more strictly should be called the 'back-off' voltage since it is that voltage introduced into the input circuit which opposes or cancels the inseparable capacitor voltage known as contact potential. Zero output would infer complete cancellation of contact potential whereas in practice this is seldom achieved. However, at balance a useful maximum is  $0.5 \text{ mV}$  and the waveform should be free from spikes.

The output for zero input may be regarded as the contact potential modulated in the same manner as a genuine input signal is modulated. This may be confirmed by calculating the conversion efficiency from the output voltage which results from an input equal to the back-off voltage; in all instances recorded there has been close agreement. For fresh electrodes contact potentials up to  $100 \text{ mV}$  have been observed. The results of numerous experiments have shown that if the contact potential of fresh electrodes is not more than about  $60 \text{ mV}$ , and if a good balance can be obtained, then the contact potential will diminish

exponentially to less than 20 mV. Unfortunately this remaining contact potential varies, depending upon the stability of the electrode surfaces and their immediate environment. For example, if open to the atmosphere it is susceptible to changes in relative humidity. Successful surface treatments have included various plating processes, coating with a thin even layer of colloidal graphite, surface grinding, and polishing. The electrodes also should be optically flat. Without undue expense contact potential variation or drift can be reduced to 1 mV/24 h. Much lower drift rates entail more elaborate treatment of the electrode surface.

**9. Vibrating Reed Model**

Although several experimental dynamic capacitors have been made and tested during the course of this investigation only two will be briefly mentioned here. These, however, are derived from previous models as in the usual process of development.

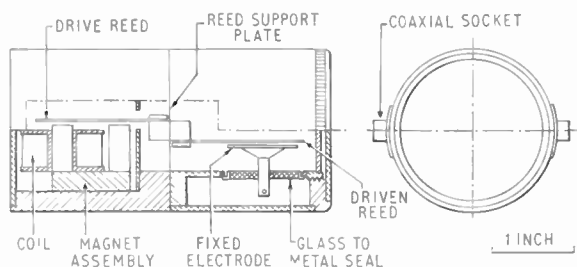


Fig. 8. Part section of the general assembly of vibrating reed dynamic capacitor.

The first is of the vibrating reed type and is somewhat unusual inasmuch as it uses two reeds in a balanced see-saw arrangement. A part sectional general assembly is shown in Fig. 8, from which it will be seen that one reed is used exclusively to impart movement to the other which is the electrically active reed. This arrangement was adopted so as to separate as completely as possible the drive circuit and associated varying magnetic field from the sensitive high resistance electrode. The reeds are supported by a 0.015 in thick stainless steel disk and are themselves attached to a block on either side of this. The reeds are 3/4 in wide, 1 1/8 in long with rounded ends and are made of 0.028 in thick stainless steel. The 3/8 in fixed electrode is made of similar material and is supported by a glass-to-metal seal which has an insulation resistance greater than 10<sup>14</sup>Ω. All other parts are of mild steel.

This mechanical arrangement may be regarded as a two-degrees-of-freedom system and as such has

two fundamental frequency resonances, one characteristic of the reed mass stiffness and the other which includes the support disk. They are well separated and as the latter is lower and has a higher amplitude of vibration it was used. The frequencies are approximately 500 c/s and 350 c/s with a mechanical Q or dynamic magnification factor of 14. Alignment of the fixed electrode was ensured by resting it on the reed which was deflected in that direction by 0.006 in and then soldering it in position. A typical set of test results are:

- drive 15 volts peak-to-peak,
- 37 ampere turns,
- 350 c/s,
- input 800 mV,
- output 450 mV peak-to-peak.

Therefore  $\eta = 28\%$

Best balance is 0.4 mV for a backing-off voltage of 5 mV and an output of 3 mV for zero input.

**10. Vibrating Diaphragm Model**

A sectional view of this model is shown in Fig. 9. The body parts are of mild steel. The diaphragm is 2 1/8 in diameter and is made of 0.006 in thick Nilo 42. The general arrangement for the fixed electrode is the same as for the reed model. The input resistor and coupling capacitor are in the top compartment as shown. The magnet pole piece is 0.006 in below the diaphragm and alignment of the fixed electrode is achieved by using a 0.006 in spacer between it and the diaphragm while soldering into position. This spacing can be reduced slightly while working during final alignment by adjusting screws deflecting the seal support plate.

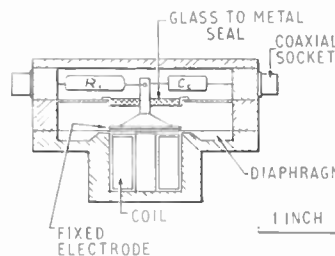


Fig. 9. Sectional arrangement of vibrating diaphragm dynamic capacitor.

The natural frequency of this unit was 850 c/s with a dynamic magnification of 9. Compared with the reed it required rather more drive power and the conversion efficiency was about half but other characteristics were similar. However, its reduced performance may be acceptable in view of its simpler construction.

### 11. Associated Circuitry

In a complete electrometer measuring instrument the dynamic capacitor requires a drive circuit, a stable a.c. amplifier with fairly high input impedance a phase-sensitive detector and an output indicator, perhaps a taut-suspension moving-coil meter. An output also should be available for other purposes, e.g. potentiometric chart recorder.

Both types of capacitor may be driven from a small transistor oscillator and amplifier. A simple two-transistor Wien network<sup>15</sup> would suffice for the oscillator or the reed type of capacitor is amenable to the fitting of a small auxiliary coil to supply a signal. Such a coil could be fitted opposite the drive coil on the other side of the same reed and with a magnetized core would provide a suitable output. Alternatively, a small strain gauge could be cemented on to the driving reed. A possible drive circuit<sup>16</sup> for a dynamic capacitor of the types described is shown in Fig. 10. A phase-shift circuit is included as some method of pre-setting the phase probably will be required to obtain the correct phase relationships in the phase-sensitive detector.<sup>17</sup> The signal amplifier also may be fully transistorized by using a high input impedance circuit<sup>18</sup> such as has been designed for use with piezo-electric strain gauges.

### 12. Application to the Measurement of pH

A particular and rather exacting application of an electrometer type of instrument is in the measurement of pH which is a measure of the effective acidity or alkalinity of a solution.<sup>19</sup> Numerically pH is the negative common logarithm of the hydrogen ion concentration in gram molecules per litre, the negative sign being understood and omitted. For example, N/10 hydrochloric acid has a hydrogen ion concentration of  $10^{-1}$  and a pH of 1, while a normal sodium hydroxide solution has a concentration of  $10^{-14}$  and thus a pH of 14. Pure water, being neutral, is at the geometric mean halfway point with a concentration of  $10^{-7}$  and a pH of 7.

The pH value of a solution may be measured electrically by measuring the voltage developed across two special electrodes dipping into the solution. In the most commonly used system and the one with widest application, the electrodes are known as the glass electrode and the reference or calomel electrode and may be regarded as active and passive respectively. The glass electrode develops a voltage with respect to the solution which is proportional to the logarithm of the hydrogen ion concentration of the solution. As its name implies, the corresponding voltage of the reference electrode is independent of the solution pH value. The net effect is a voltage across the electrodes which is proportional to the pH value of the solution and at 20°C it changes by approximately 58 mV/pH. It is positive for strongly acid solutions and passes through zero at about 7 pH, or 2 pH depending upon the type of electrodes, becoming progressively more negative for a linear increase in pH. The zero point and slope of this relationship vary with temperature. Electrically the electrode system may be regarded as a pH-dependent voltaic cell with an internal resistance which may be as high as 3000 MΩ depending upon the electrodes and temperature, in general the more robust electrodes having the higher resistance.

Thus the requirements of a pH measuring device, or pH meter, are becoming apparent. Apart from the special features of gain control and variable backing-off voltages to facilitate pH measurements over a given temperature range, essentially, a pH meter is a high input resistance millivoltmeter with ranges up to  $\pm 1000$  mV. A laboratory pH meter, sometimes a combined millivoltmeter, is expected to have a discrimination and stability of better than 0.02 pH which is equivalent to about 1.2 mV. This is 0.143% of f.s.d. and therefore the input resistance should be in the same ratio to the highest electrode resistance, i.e.

$$3 \times 10^9 \times \frac{14}{0.02} = 2.1 \times 10^{12} \Omega$$

For a thermionic valve electrometer the grid current

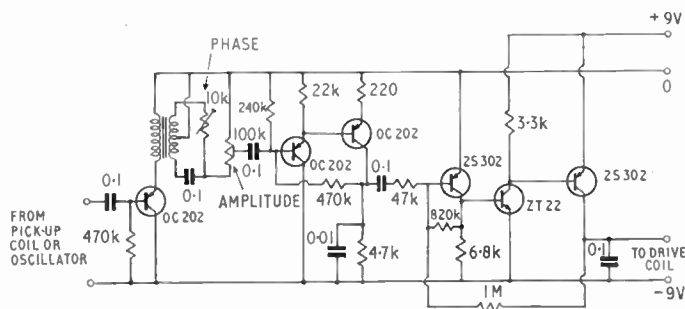


Fig. 10. Dynamic capacitor drive circuit.

and drift should not exceed  $\frac{1.2 \times 10^{-3}}{3 \times 10^9} = 4 \times 10^{-13} \text{A}$  which is sufficient to emphasize the importance of minimizing zero variations. The dynamic capacitor electrometer appears to be most nearly capable of satisfying these conditions.

### 13. Conclusion

From what is now known about dynamic capacitors and by making use of the latest techniques in transistor circuitry there appears to be scope for continued interest in the development of the dynamic capacitor electrometer.

### 14. Acknowledgment

The author wishes to thank Mr. R. B. G. Benson for guidance in the early stages of the work described, and other former colleagues at W. G. Pye & Co. Ltd.

### 15. References

1. D. Allenden, "A feedback electrometer amplifier", *Electronic Engineering*, **30**, No. 359, pp. 31-33, January 1958.
2. R. Gunn, "Principles of a new portable electrometer", *Phys. Rev.*, **40**, pp. 307-12, 15th April 1932, Series 2.
3. H. De Vries, "Measurement of small electrostatic voltages by conversion to alternating currents", *Physica, 's Grav.*, **13**, No. 8, pp. 449-52, September 1947.
4. H. Palevsky, R. K. Swank and R. Grenchik, "Design of dynamic condenser electrometers", *Rev. Sci. Instrum.*, **18**, No. 5, pp. 298-314, May 1947.
5. S. A. Scherbatskoy, T. H. Gilmartin and G. Swift, "The capacitive commutator", *Rev. Sci. Instrum.*, **18**, No. 6, pp. 415-21, June 1947.
6. J. van Hengel and W. J. Oosterkamp, "A direct-reading dynamic electrometer", *Philips Tech. Rev.*, **10**, No. 11, pp. 338-46, May 1949.
7. D. G. A. Thomas and H. W. Finch, "A simple vibrating condenser electrometer", *Electronic Engineering*, **22**, No. 271, pp. 395-8, September 1950.
8. M. W. Jervis, "The measurement of very small direct currents", *Electronic Engineering*, **26**, No. 313, pp. 100-5, March 1954.
9. J. A. Adler, "Vibrating capacitor changes d.c. to a.c.", *Electronics*, **29**, No. 6, pp. 158-9, June 1956.
10. R. J. Ritsma, "An electrometer amplifier with two dynamic condensers", *Appl. Sci. Res.*, B, **6**, No. 6, pp. 429-45, 1957.
11. E. Komolibus, "D.c./a.c. converters for d.c. amplifiers", British Scientific Instrument Research Association, Report No. R258, December 1960.
12. G. Hitchcox, "Modern trends in pH meter design", *British Commun. Electronics*, **9**, No. 1, pp. 18-22, January 1962.
13. H. S. Wolff, J. McCall and J. A. Baker, "Semiconductor electrometer amplifiers", *British Commun. Electronics*, **9**, No. 2, pp. 120-2, February 1962.
14. A. G. van Nie and J. J. Zaalberg van Zelst, "A vibrating capacitor driven by a high-frequency electric field", *Philips Tech. Rev.*, **25**, No. 4, pp. 95-103, 1963.
15. "Reference Manual of Transistor Circuits", Mullard Ltd. 1st Edition, 1960.
16. "Silicon Alloy-Junction Transistors in D.C. Amplifiers", Texas Instruments Application Note No. 8.
17. M. J. Wright, "A transistor phase sensitive demodulator of high performance", *Electronic Engineering*, **34**, No. 416, pp. 698-700, October 1962.
18. D. A. Smith and T. M. A. Lewis, "A buffer stage for piezo-electric strain gauges", *Electronic Engineering*, **34**, No. 408, pp. 99-102, February 1962.
19. R. S. Evans, "A Dictionary of pH Applications". (Herbert Publishing Co., London, 1957.)

*Manuscript first received by the Institution on 19th June 1964 and in final form on 22nd December 1964. (Paper No. 991.)*

© The Institution of Electronic and Radio Engineers, 1965

# The Analysis and Demonstration of a Method of Generating V.L.F. Noise

By

P. BRODERICK, B.Sc. †

**Summary:** The paper describes the analysis of a method of generating v.l.f. white noise based on the sampling principle. A wide-band source of noise is used and a narrow band at fairly high frequency over which the power spectrum is flat is extracted using a band-pass filter. The power spectral densities that result from sampling this band for different sampling frequencies are derived. The case of practical importance resulting in a flat spectral density around zero frequency is demonstrated experimentally for different sampling rates and the resultant maximum r.m.s. noise voltage compared with the theoretical values.

## 1. Introduction

A randomly-varying test input signal is often specified in the testing of servomechanisms and in vibrational tests on aircraft and missile systems, to mention but two applications. Such an input is a more reliable simulation of actual environmental conditions than the earlier methods of sweeping a band of frequencies expected in operation.

The frequency band of interest may be from zero to a few tenths of a cycle in automatic control equipment; to several cycles per second or in fact to a few kilocycles in vibrational testing. The problem is, however, to produce measurable noise with a flat spectrum (white noise) at vanishingly low frequencies. Over the audio band thyratrons and photomultipliers give a spectrum that is nearly white but the spectral density varies appreciably with frequency at low frequencies. The use of noise from an intrinsically white noise generator, e.g. Johnson noise in a wire-wound resistor, is restricted by the level of noise obtained. Any amplification of this is swamped by  $1/f$  noise in the amplifying devices and furthermore, if the amplifier is mains driven, the hum is difficult to reduce to negligible proportions.

Several methods have been suggested for deriving noise at very low frequency. Most of these<sup>1, 2</sup> depend upon heterodyning the noise using a local oscillator and modulator to produce beat frequencies centred about zero. Other methods have used magnetic tape or film recorders to read high frequency noise and play it back at low frequency. Another principle underlying some other methods is to apply the noise to a non-linear circuit to change the power spectrum by producing intermodulation terms. When a purely random signal with a continuous spectrum is applied to a non-linearity, the output spectrum will contain among other components intermodulation components down to zero frequency.<sup>3</sup>

† Marconi Instruments Ltd., Research Department, St. Albans, Hertfordshire.

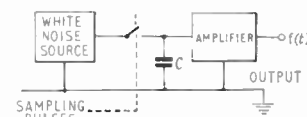
Changing the time scale of the noise by recording is perhaps too complicated a method for general purpose use while the method of producing low-frequency intermodulation terms necessitates the clipping of narrow banded noise which does not result in a power spectrum extending right down to zero frequency unless there exists a d.c. component in the clipped wave. Heterodyning is perhaps the best of the above methods provided that there is no critical dependence on the stability of the local oscillator.

The method to be described here is one which is believed to be simpler in practical detail than any of the above. It involves sampling of a band of white noise of useful level at some convenient frequency with sampling pulses of lower p.r.f. and pulse duration times set by conventional sampling technique principles.

## 2. Derivation of the Output Power Spectrum

To derive a formula for the power spectrum of the output we assume a narrow band of white noise at the input and a fixed but arbitrary sampling rate.

Consider first, however, a white noise input to an ideal sampling gate shown in Fig. 1(a).



(a). White noise applied to sampling gate.

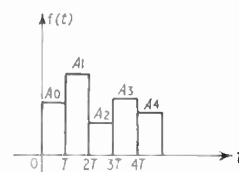


Fig. 1 (b). Output of sampling gate.

Assuming C is perfect and the amplifier input impedance is infinite, then C will not discharge between sampling pulses and the output for four sampling periods might well look like Fig. 1(b) where T is the sampling period and A<sub>n</sub> is the peak value of the sampled input at a time nT and can be either positive or negative.

The autocorrelation function of the output may be written

$$\phi(\tau) = \lim_{m \rightarrow \infty} \frac{1}{mT} \int_0^{mT} f_1(t) f_1(t+\tau) dt \quad \dots\dots(1)$$

Now

$$f_1(t) = \sum_{n=0}^{m-1} A_n f(t-nT)$$

where f(t-nT) = 1 for nT < t < (n+1)T and f(t-nT) = 0 elsewhere.

$$f_1(t+\tau) = \sum_{n=0}^{m-1} A_n f(t-nT+\tau)$$

where f(t-nT+τ) = 1 for nT-τ < t < (n+1)T-τ and f(t-nT+τ) = 0 elsewhere.

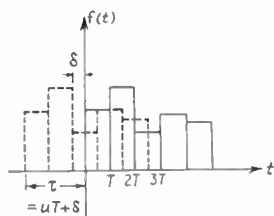


Fig. 2. Idealized output waveform of sampling gate.

The situation is now as shown in Fig. 2 where to be general τ = uT+δ with u integral and δ a fraction of T. (Alternatively it might be considered obvious that the correlation time is T in which case u = 0 and δ can lie between 0 and T. This follows in the working however.)

We can now write

$$f_1(t+\tau) = \sum_{n=0}^{m-1} A_n f(t-(n-u)T+\delta)$$

where f(t-(n-u)T+δ) = 1 for (n-u)T-δ < t < (n+1-u)T-δ

In eqn. (1) the integrand is the product of the amplitudes of the full and dotted curves in Fig. 2 for each sampling period and clearly we must refer both to the same time zero. For example in f<sub>1</sub>(t) t > 0 so in f<sub>1</sub>(t+τ) the first pulse (n = 0) to be considered is defined for -δ < t < T-δ which is obtained by putting n = u in the conditions on f<sub>1</sub>(t+τ). For the second pulse of f<sub>1</sub>(t+τ) this occurs for

$$T-\delta < t < 2T-\delta$$

which is obtained by putting n = u+1 in the con-

ditions on f<sub>1</sub>(t+τ). In general, therefore, we must replace n by (n+u) in the conditions on f<sub>1</sub>(t+τ), i.e.

$$f_1(t+\tau) = \sum_{n=0}^{m-1} A_{n+u} f[t-(n-u)T+\delta]$$

where f[t-(n-u)T+δ] = 1 for nT-δ < t < (n+1)T-δ and zero elsewhere.

Equation (1) therefore becomes:

$$\begin{aligned} \phi(\tau) &= \lim_{m \rightarrow \infty} \frac{1}{mT} \sum_{n=0}^{m-1} \sum_{n=0}^{m-1} \int_0^{mT} A_n f(t-nT) \times \\ &\quad \times A_{n+u} f(t-(n-u)T+\delta) dt \\ &\text{where the summation is taken to apply to } A_n \text{ and } A_{n+u} \text{ separately, i.e.} \\ \phi(\tau) &= \lim_{m \rightarrow \infty} \frac{1}{mT} \left[ \int_0^{T-\delta} A_0 A_u dt + \int_{T-\delta}^T A_0 A_{u+1} dt + \right. \\ &\quad \left. + \int_T^{2T-\delta} A_1 A_{u+1} dt + \int_{2T-\delta}^{2T} A_1 A_{u+2} dt + \right. \\ &\quad \left. + \dots + \int_{(m-1)T-\delta}^{mT} A_{m-1} A_{u+m} dt \right] \\ &= \lim_{m \rightarrow \infty} \frac{1}{mT} \times \\ &\quad \times \left[ \sum_{n=0}^{m-1} \int_0^{T-\delta} A_n A_{n+u} dt + \sum_{n=0}^{m-1} \int_{T-\delta}^T A_n A_{n+u+1} dt \right] \end{aligned}$$

Since in any interval A<sub>n</sub> and A<sub>n+u</sub> are constants, i.e.

$$\begin{aligned} \phi(\tau) &= \lim_{m \rightarrow \infty} \frac{1}{mT} \times \\ &\quad \times \left[ \int_0^{T-\delta} dt \sum_{n=0}^{m-1} A_n A_{n+u} + \int_{T-\delta}^T dt \sum_{n=0}^{m-1} A_n A_{n+u+1} \right] \\ \phi(\tau) &= \lim_{m \rightarrow \infty} \frac{1}{mT} \sum_{n=0}^{m-1} A_n [A_{n+u}(T-\delta) - A_{n+u+1}\delta] \quad \dots\dots(2a) \end{aligned}$$

Substituting δ = τ-uT

$$\phi(\tau) = \lim_{m \rightarrow \infty} \frac{1}{mT} \sum_{n=0}^{m-1} A_n T \{ (1+u)A_{n+u} - uA_{n+u+1} \} - A_n \tau \{ A_{n+u} - A_{n+u+1} \} \quad \dots\dots(2b)$$

If we now plot (2b) assuming the noise is white, then when τ = 0, u = 0 (from Fig. 2) and

$$\phi(\tau = 0) = \lim_{m \rightarrow \infty} \frac{1}{mT} \sum_{n=0}^{m-1} A_n^2 T = \lim_{m \rightarrow \infty} \sum_{n=0}^{m-1} \frac{A_n^2}{m} = \sigma^2$$

which is the mean square value of the input distribution. In the interval 0 to T, u = 0 but

$$\begin{aligned} \phi(\tau) &= \lim_{m \rightarrow \infty} \frac{1}{mT} \sum_{n=0}^{m-1} A_n^2 T - A_n^2 \tau + A_n A_{n+1} \tau \\ &= \lim_{m \rightarrow \infty} \frac{1}{mT} \sum_{n=0}^{m-1} A_n^2 (T-\tau) \end{aligned}$$

since A<sub>n</sub> and A<sub>n+1</sub> are uncorrelated.

This is the equation of a straight line. Also when  $T = \tau$ ,  $\phi(\tau) = 0$ . In the interval  $T$  to  $2T$ ,  $u = 1$  and  $\phi(\tau)$  is given by

$$\phi(\tau) = \lim_{m \rightarrow \infty} \frac{1}{mT} \sum_{n=0}^{m-1} A_n A_{n+1} (2T - \tau) + A_n A_{n+2} (\tau - T) = 0$$

since  $A_n$  and  $A_{n+1}$  are uncorrelated.

Similarly  $\phi(\tau) = 0$  for all  $\tau > T$ .

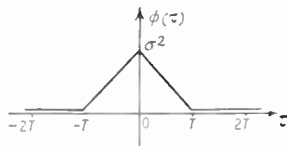


Fig. 3. The function  $\phi(\tau)$ . (The output autocorrelation function.)

The sketch of  $\phi$  is shown in Fig. 3. Since  $\phi$  is an even function the graph is symmetrical about  $\tau = 0$ .

For white noise then we need only consider the case  $u = 0$  since  $\phi$  is zero elsewhere. In this case

$$\phi(\tau) = \lim_{m \rightarrow \infty} \frac{1}{mT} \sum_{n=0}^{m-1} A_n^2 T - A_n \tau (A_n - A_{n+1}) \quad \dots\dots(3)$$

**3. The Power Spectrum of the Output**

$$P(\omega) = \int_{-\infty}^{\infty} \phi(\tau) e^{-j\omega\tau} d\tau = 2 \int_0^{\infty} \phi(\tau) \cos \omega\tau d\tau$$

Substituting  $\phi(\tau)$  we get

$$P(\omega) = \lim_{m \rightarrow \infty} \frac{1}{mT} \sum_{n=0}^{m-1} \left[ 2 \int_0^T A_n^2 T \cos \omega\tau d\tau - 2 \int_0^T A_n \tau (A_n - A_{n+1}) \cos \omega\tau d\tau \right]$$

Since  $\phi = 0$  for  $\tau > T$  the upper limits are set at  $T$ .

Therefore

$$P(\omega) = \lim_{m \rightarrow \infty} \frac{2}{mT} \left[ \sum_{n=0}^{m-1} A_n A_{n+1} \frac{T \sin \omega T}{\omega} - A_n (A_n - A_{n+1}) \left( \frac{\cos \omega T}{\omega^2} - \frac{1}{\omega^2} \right) \right]$$

but

$$\lim_{m \rightarrow \infty} \frac{1}{mT} \sum_{n=0}^{m-1} A_n A_{n+1} = 0$$

Hence

$$P(\omega) = 2 \lim_{m \rightarrow \infty} \frac{1}{mT} \sum_{n=0}^{m-1} \frac{A_n^2}{\omega^2} (\cos \omega T - 1)$$

i.e.

$$P(\omega) = T \left( \frac{\sin \frac{\omega T}{2}}{\frac{\omega T}{2}} \right)^2 \sigma^2 \quad \dots\dots(4)$$

This is sketched in Fig. 4.

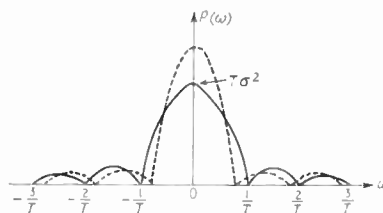


Fig. 4. Power spectrum of output. Dotted line is for a sampling rate  $< 1/T$ .

It is clear that all frequencies are present except those which are integral multiples of the sampling frequency ( $1/T$ ). It is also evident that the power in any small band near zero frequency depends upon the sampling period  $T$  and upon the r.m.s. value of the input noise ( $\sigma$ ). If the sampling frequency is reduced the graph takes on the form of the dotted curve in Fig. 4, i.e. the spectral density of the low-frequency components increases. It will be remembered that a finite spectral density at zero frequency does not mean that a d.c. component of the noise exists. For such a component to exist the spectrum would show a Dirac function at zero frequency. The spectral density is a measure of the power per unit bandwidth, the latter being small compared with the frequency. At d.c., therefore, the bandwidth becomes meaninglessly small and a finite density would produce zero power in this case.

**4. Band-limited Noise**

The situation is now as shown in Fig. 5(b).

If the band-pass filter is assumed to be ideally rectangular with a centre frequency  $f_0$ , and bandwidth  $\Delta f$  c/s then the filter transfer is

$$|H(j\omega)| = A \text{ for } f_0 - \frac{\Delta f}{2} < f < f_0 + \frac{\Delta f}{2} = 0 \text{ elsewhere.}$$

If the filter input spectral density is  $\rho$  watts/c/s over all frequencies then the output spectrum over positive frequencies is

$$P(\omega) = \rho A^2; \quad f_0 - \frac{\Delta f}{2} < f < f_0 + \frac{\Delta f}{2}$$

$P(\omega) = 0$  elsewhere (see Fig. 5(b)).

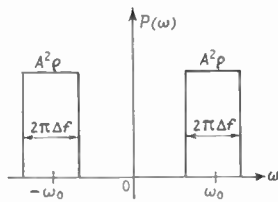
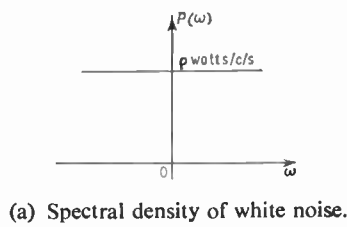


Fig. 5.

The autocorrelation function for Fig. 5(a) is an impulse at  $\tau = 0$  and is zero for all other values of  $\tau$ . This function contains an infinite amount of power. The autocorrelation function for Fig. 5(b) may be obtained by taking the inverse transform of the spectral density:

$$\begin{aligned} \phi'(\tau) &= \int_{-\infty}^{\infty} P(\omega) e^{j\omega\tau} d\omega \\ &= \int_{-f_0 - \frac{\Delta f}{2}}^{-f_0 + \frac{\Delta f}{2}} \rho A^2 e^{j\omega\tau} df + \int_{f_0 - \frac{\Delta f}{2}}^{f_0 + \frac{\Delta f}{2}} \rho A^2 e^{j\omega\tau} df \\ \phi'(\tau) &= 2\rho A^2 \Delta f \frac{\sin \pi \Delta f \tau}{\pi \Delta f \tau} \cos \omega_0 \tau \end{aligned} \quad \dots\dots(5)$$

This is shown in Fig. 6.

The problem now is to investigate the output spectrum when we sample an input with an autocorrelation function as shown in Fig. 6. We expect the spectrum to depend upon the relation of the sampling frequency to the noise bandwidth since in the limit of sampling with a frequency very much greater than any within the noise band we must get out what we put in.

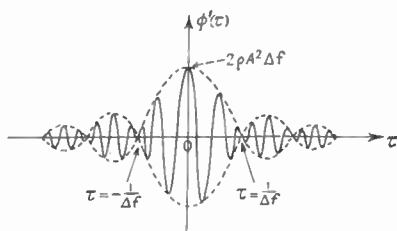


Fig. 6. Autocorrelation function of narrow band white noise.

Equation 2(b), as a function of  $\tau$  is clearly a straight line and connects the values of  $\phi(\tau)$  at  $\tau = T, 2T, 3T$ , etc. Furthermore at each sampling instant the output takes up exactly the value of the input and the autocorrelation functions are the same. Thus the output autocorrelation  $\phi_o(T)$  is equal to the input autocorrelation  $\phi_i(T)$  at the sampling times and between these times the output autocorrelation is a straight line joining the values at the sampling times.

The behaviour of the output autocorrelation function is now predictable in the special cases of interest.

(a) If the sampling frequency is very much less than the bandwidth which in the limit is the case already considered, the output autocorrelation function is that shown in Fig. 3 and is shown in Fig. 7, drawn on the same scale as the input autocorrelation.

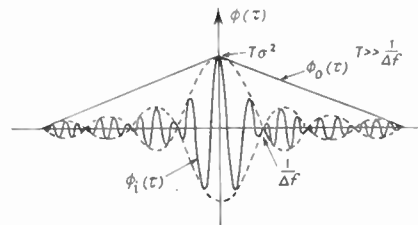


Fig. 7. Output autocorrelation function on same scale as the input autocorrelation function.

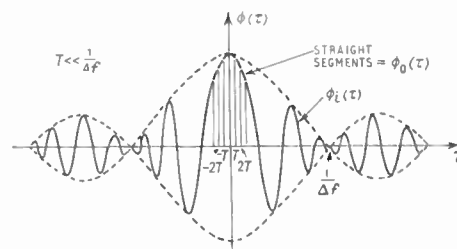


Fig. 8. Output autocorrelation function with sampling frequency much greater than bandwidth.

In this case the spectral density is shown in Fig. 4 and is given by

$$P(\omega) = T \left( \frac{\sin \frac{\omega T}{2}}{\frac{\omega T}{2}} \right)^2 \sigma^2 \quad \dots\dots(4)$$

(b) If the sampling frequency is very much greater than the bandwidth then the same rule applies with regard to the equality of  $\phi_i(T)$  and  $\phi_o(T)$  and we get the situation shown in Fig. 8.

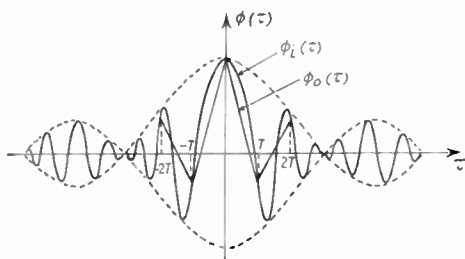


Fig. 9. General case of output autocorrelation function.

In this case the output autocorrelation function approximates to the input so that the two power spectral densities are approximately equal

$$P(\omega) = \rho A^2; \quad f_0 - \frac{\Delta f}{2} < f < f_0 + \frac{\Delta f}{2}$$

$$= 0 \text{ elsewhere.}$$

(c) In the general case we have the situation shown in Fig. 9.

The case of practical importance is, of course, the one predicting a spectrum suitable for a v.l.f. white noise generator assuming we have a source of narrow-band white noise at some convenient frequency.

This is clearly case (a) shown in Fig. 7 where the sampling frequency is very much less than the bandwidth. The density is shown in Fig. 4 and indicates that if we require a flat spectrum with calculable density we must include a low-pass filter in the output and select a portion of the curve between 0 and a frequency  $\ll 1/T$ . The lower the cut-off frequency the flatter  $P(\omega)$  over the range of interest.  $P(\omega)$  can be made flatter by decreasing  $T$ , but the cost is in the decreased magnitude of  $P(\omega)$ .

### 5. Experimental Check of Theory

A method of demonstrating case (a), showing the circuitry involved has been described by Slater.<sup>4</sup> The system used for testing the theory as put forward in the present paper is shown in Fig. 10.

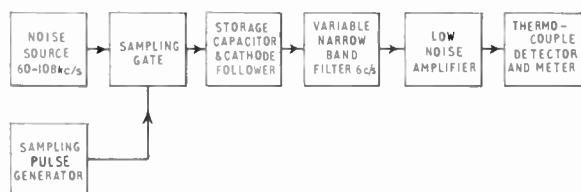


Fig. 10. Experimental arrangement for checking theory.

The circuit diagrams of the sampling gate and store and of the low-noise transistor amplifier are shown in Figs. 11 and 12. The noise source used was the noise

generator part of the Marconi white noise test set (type TF.1226B) fitted with two filters, one low-pass, the other a high-pass defining a band from 60 to 108 kc/s. For a narrow band (6 c/s) filter with a variable centre frequency from 50 c/s to 50 kc/s it was convenient to use the Marconi TF.2330 wave analyser taking the output from the system before the filtered noise is rectified for display on the meter. The sampling pulse generator was a Hewlett Packard 215A pulse generator which provides pulses up to 100 nanoseconds wide at p.r.f.'s from 100 c/s up to 1 Mc/s.

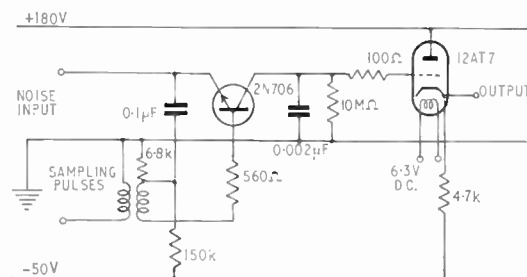


Fig. 11. Sampling gate and store.

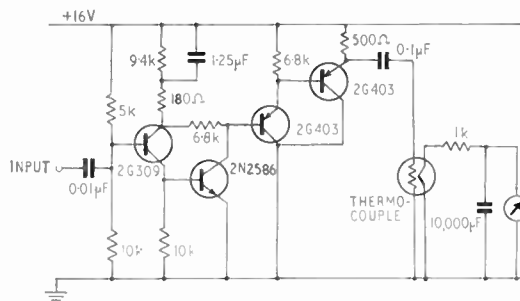


Fig. 12. Low noise transistor amplifier.

Note: The input transistor should be shown as a p-n-p device.

The sampling gate is a simple transformer-switched version where the switching time was set by the highest frequency component in the input noise, namely 108 kc/s. The pulse length for sampling a coherent signal at this frequency would need to be less than about 4  $\mu$ s (see Appendix). In the above circuit a time of 0.1  $\mu$ s was assumed in design.

An amplifier which had been used in a previous experiment requiring low-noise operation was used. All the normal precautions<sup>5</sup> for low-noise operation were observed and the resultant amplifier noise over the whole band at the output was of the order of microvolts. The gain was 36.5 at 100 kc/s with a 3 dB bandwidth extending from 7 kc/s to 350 kc/s, the low frequency cut-off being desirable so that 1/f contributions become negligible. The bandwidth could, of

course, have been greatly reduced since noise more than 40 kc/s away from the 100 kc/s carrier was not measured for any sampling rate. This would have reduced the total noise of the amplifier still further but was not necessary in view of the relative magnitudes of sampled noise (millivolts) and the total noise of the existing amplifier (microvolts).

6. Results

Readings of the output r.m.s. noise voltage were taken over the frequency range 50 c/s to 50 kc/s for sampling frequencies of 20 kc/s, 10 kc/s and 5 kc/s and the results are shown in Fig. 13(a-c).

The spectra are as predicted theoretically, the nodes corresponding to the sampling frequency used. The maximum spectral density is theoretically  $T\sigma^2$  where  $T$  is the sampling period and  $\sigma$  the r.m.s. noise voltage at the input. For a given input noise power the density at a sampling frequency  $f$  is therefore twice that at a frequency  $2f$ . The r.m.s. peak value at 5 kc/s sampling rate is therefore  $\sqrt{2}$  times that at 10 kc/s and twice that at 20 kc/s sampling rate. The effect of using a sampling rate in excess of the bandwidth may be observed by taking the limiting case of infinite sampling rate, i.e. with the gate 'held on' permanently. In this condition the only noise components less than 60 kc/s are due to the imperfect cut-off limit of the high-pass filter and no measurable noise from zero up to several kilocycles is observed.

To compare the results with the predicted values we consider the noise generator output. This produces approximately  $12.6 \mu\text{W}/\text{kc/s}$  bandwidth and for a 48 kc/s passband the input r.m.s. noise voltage was  $(300 \pm 30)\text{mV}$ , i.e.  $\sigma = (300 \pm 30)\text{mV}$ .

The mean square value of the noise at any part of the spectrum is obtained by multiplying the density ( $T\sigma^2$  at maximum) by the bandwidth of the filter (6 c/s).

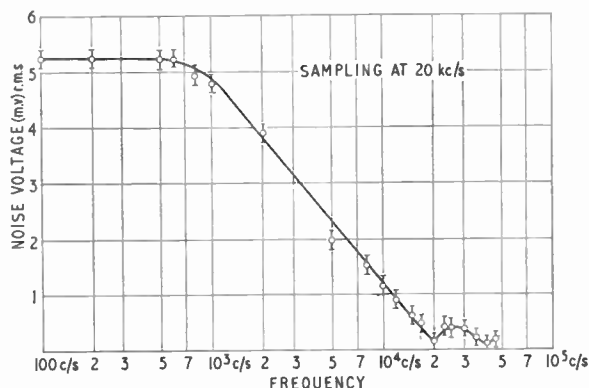
Therefore mean square noise voltage at zero frequency  
 $= 6T\sigma^2 = 6T(300 \pm 30)^2 \text{ mV}.$

The r.m.s. noise output at zero frequency (maximum value in spectrum) for each sampling frequency can now be calculated and compared with the experimental values in Fig. 13.

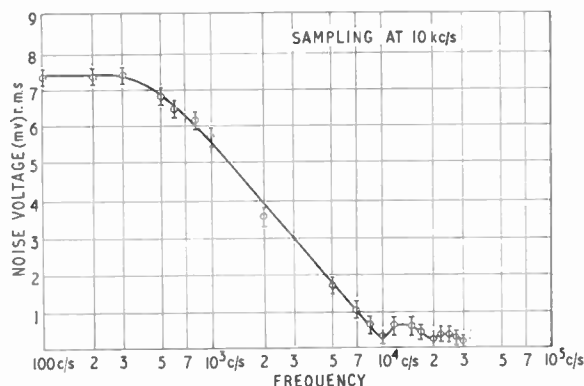
The Table shows such a comparison.

The measured values agree within the experimental error with those calculated from a knowledge of the input spectral density and the bandwidth. In a very low frequency noise generator using the above principles, therefore, the r.m.s. value of the noise at the source can be measured directly where it is wide band and converted linearly to the value obtained after sampling and low-pass filtering at the output where it

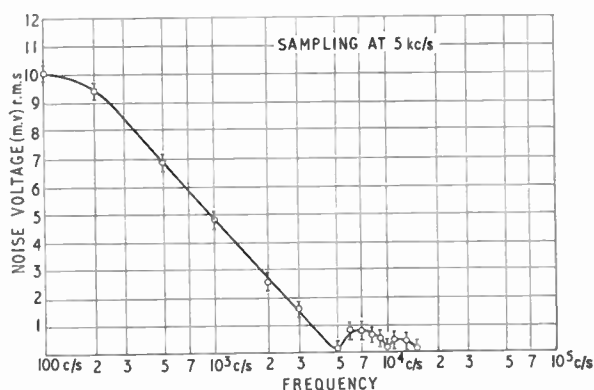
is very narrow band. In this way the problem of integrating time in very narrow band noise measurements is avoided.



(a) Sampling frequency 20 kc/s.



(b) Sampling frequency 10 kc/s.



(c) Sampling frequency 5 kc/s.

Fig. 13. Output noise voltage for various sampling frequencies.

**Table 1**  
Maximum value of r.m.s. noise voltage

Sampling frequency	Predicted voltage mV r.m.s.	Measured voltage mV r.m.s.
20 kc/s	5.2±0.37	5.3±0.17
10 kc/s	7.4±0.5	7.4±0.18
5 kc/s	10.4±0.8	10.1±0.34

As already mentioned, in obtaining a source of very low frequency white noise it would be necessary to include a low-pass filter after sampling. Thus from Fig. 13, a low-pass filter with a cut-off at about 1 kc/s would ensure an approximately flat spectrum from zero frequency to 1 kc/s, whilst in Fig. 14 the filter cut-off frequency would be set at about 500 c/s.

**7. Conclusion**

The method provides a source of white noise from zero frequency to some low frequency depending upon the sampling rate. The lower the sampling frequency the greater the spectral density but the smaller the band over which the spectrum is flat. The method conveniently derives very low frequency noise from a band of white noise at measurably high frequency which is available from a variety of sources. Furthermore the band is easily variable with either a low-pass filter or a change of sampling rate and the output known directly from a knowledge of the input r.m.s. and sampling rate. This means that the r.m.s. value of noise even at ultra-low frequencies can be displayed immediately on a meter without the necessity of measuring the output where a very long integrating time would be required to check any adjustment. Nothing elaborate is required in the design of a suitable gate for sampling narrow-banded white noise at frequencies up to tens of megacycles. Using a high-level video noise source no amplification after sampling may be required if it is, any reasonable low noise amplifier should introduce noise negligible in level to that at its input.

**8. References**

1. D. A. Bell and A. M. Rosie, "Low-frequency noise generator with Gaussian distribution", *Electronic Technology*, 37, pp. 241-5, June 1960.
2. R. R. Bennett and A. S. Fulton, "The generation and measurement of low-frequency random noise", *J. Appl. Phys.*, 22, pp. 1187-91, September 1951.

3. J. L. Douce and J. M. Shackleton, "L.f. random-signal generator", *Electronic Radio Engineer*, 35, pp. 295-7, August 1958.
4. R. J. Slater, "A low-frequency noise generator", *Electronic Engineering*, 32, pp. 473-5, August 1960.
5. P. J. Beneteau, "Designing low-noise transistor circuits", *Electronic Design*, pp. 86-8, August 1960.

**9. Appendix: Criterion for sampling pulse width assuming mean-value charge storage**

If the highest frequency in the input is

$$V = V_0 \sin \omega t$$

and the sampling period is  $T$ . Then

$$V = V_0 \sin \frac{2\pi}{T} t$$

For a sampling pulse width of  $\alpha T$  ( $\alpha < 1$ )

the mean output voltage during this time is

$$\begin{aligned} &= \frac{1}{\alpha T} \int_0^{\alpha T} V_0 \sin \omega t dt \\ &= \frac{V_0}{\alpha T} \int_0^{\alpha T} \sin \frac{2\pi}{T} t dt \\ &= \frac{V_0}{\alpha\pi} \sin \alpha\pi \sin \frac{2\pi}{T} \left( t + \frac{\alpha T}{2} \right) \\ &= V'_0 \sin \frac{2\pi}{T} \left( t + \frac{\alpha T}{2} \right) \end{aligned}$$

For the output amplitude  $V'_0$  to be 3 dB down on the input amplitude  $V_0$  then

$$\begin{aligned} 0.707 V_0 &= V'_0 \\ &= \frac{V_0}{\alpha\pi} \sin \alpha\pi \end{aligned}$$

Therefore

$$\sin \alpha\pi = 0.707 \alpha\pi$$

i.e.

$$\begin{aligned} \alpha\pi &= 79.8^\circ \\ \alpha &= 0.44 \text{ approx.} \end{aligned}$$

For an input maximum frequency of 108 kc/s,  $T \simeq 9.25 \mu\text{s}$ .

Therefore maximum sampling pulse duration  $\simeq 4 \mu\text{s}$ .

*Manuscript first received by the Institution on 26th October 1964, and in final form on 11th March 1965. (Paper No. 992/EA21.)*

© The Institution of Electronic and Radio Engineers, 1965

# *z*-Transforms and their Applications in Control Engineering

By

Y. AZAR, Dip.Eng.  
(Associate Member)†

**Summary:** The paper describes the *z*-transform theory and its application. The background theory is built up in four stages from the continuous convolution integral, through the real-time impulse theory, to the *z*-transform. It is stressed that, unlike the Laplace transform, the *z*-transform is only an approximation. Engineering units are used throughout and emphasis is given to the correct representation of the sampler. The finite time of sampling is taken into account and it is shown how to make practical use of it. Illustrations of practical systems show good agreement with the calculations and attention is called to some common errors in the literature. The stability criteria are stated and methods of stability investigations are described. It is shown that for systems with zero-order hold circuits, the continuous Laplace transform is a more useful tool than the *z*-transform. The paper concludes with a practical approach to the design of discrete controllers.

## 1. Introduction

Sampled data theory is a very useful and rather simple tool for the evaluation of continuous and pulsed systems. For continuous systems, the computation can be greatly simplified by artificially transferring the continuous function to an impulse train, and computation then is done by a desk calculator or by an electronic digital computer. For a pulsed system or, as it is also called, a sampled system, the theory is actually 'cut' for it since the narrow width pulses of information resemble the theoretical impulses. Two points must be borne in mind at this early stage:

- (1) *Sampled* systems with impulse trains exist only on paper and in practice we have *pulsed* systems with narrow pulse width trains.
- (2) Even if we use pure impulses in our assumptions to simplify the mathematics, the result is only an approximation whose accuracy depends on the chosen sampling rate. Unlike the Laplace transform which gives an exact solution, the sampled data theory and the '*z*-transformation' is an approximation.

The principle of this method is the Convolution Integral, but actual hard labour integration is avoided by replacing the continuous function by an impulse train. We shall first calculate the response of a continuous system using the continuous function convolution integration, then show how to avoid the tedious integration by the impulse approximation, and lastly, how the same theory applies to pulsed systems (multiplexing, etc.). A helpful introduction to the convolution integral is given by J. G. Holbrook.<sup>1(a)</sup>

† The Solartron Electronic Group Ltd., Chessington, Surrey.

## 2. The Convolution Integral

The convolution integral is defined as

$$c(t) = \int_{-\infty}^{\infty} g(x) \cdot e(t-x) dx = \int_{-\infty}^{\infty} e(x) \cdot g(t-x) dx \quad \dots\dots(1)$$

Since we deal with engineering problems and the same functions as the Laplace transform, i.e. both  $g(x)$  and  $e(x)$  are zero for negative values of time, we may write

$$c(t) = \int_0^t g(x) \cdot e(t-x) dx = \int_0^t e(x) \cdot g(t-x) dx \quad \dots\dots(2)$$

If we compare this method with the Laplace transform method, we realize how more difficult it is in comparison—for the Laplace transform of eqn. (2) is:

$$\mathcal{L}[c(t)] = C(s) = E(s) \cdot G(s) \quad \dots\dots(3)$$

In other words, the complicated convolution integral in the time domain is replaced by simple multiplication in the complex variable  $s$  domain.

We shall first demonstrate how to find the response of a given system in the time domain using the convolution integral and then show how to simplify the calculation by introducing the sampled data theory approximation.

### Example 1

Find the response of a simple RC filter to a known function of time whose Laplace transform is very difficult to obtain.

Figure 1 shows how to find the value (amplitude) of  $c(t)$  at time  $t = 3$  seconds.

Step 1: draw  $e(t)$  as  $e(x)$  (Fig. 1(c))

Step 2: draw  $g(t)$  as  $g(-x)$  (Fig. 1(e))

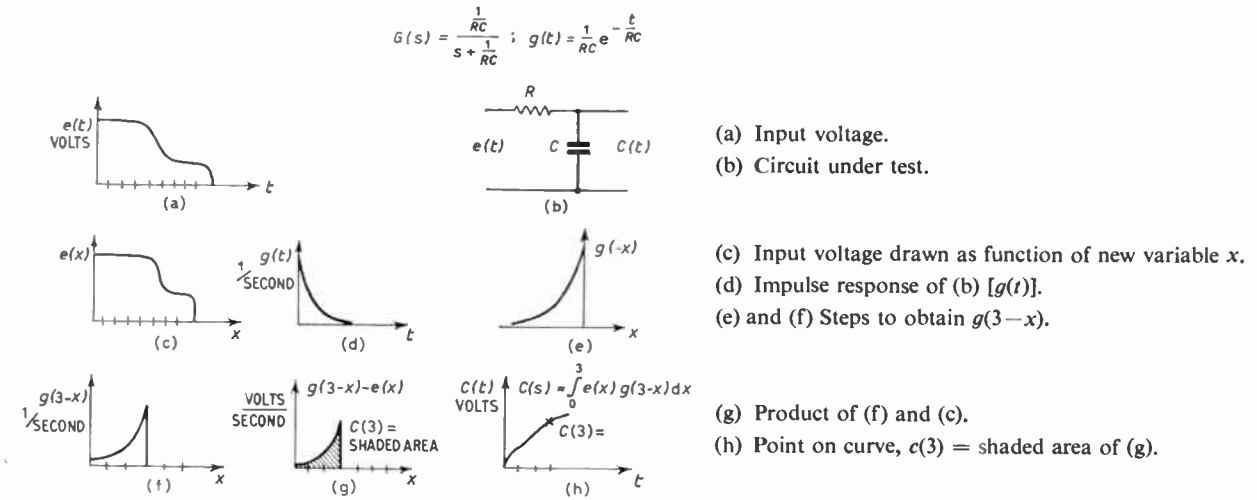


Fig. 1. Graphical determination of the continuous convolution integral (eqn. (2)).

- Step 3: draw the delayed impulse response at the desired point, ( $t = 3$  s) (Fig. 1(f))
- Step 4: multiply  $e(x)$  by  $g(t-x)$  (Fig. 1(g))
- Step 5: integrate  $\int_0^t e(x)g(t-x) dx = c(t)$  (Fig. 1(h)).

Although this procedure is exact and can be done graphically, every point on the curve  $c(t)$  has to be integrated separately. This snag is overcome if we draw  $e(t)$  as an impulse train of equally spaced impulses, where each impulse area is equal to the corresponding value (i.e. amplitude) of the given continuous function. If, for example, the value of  $e(t)$  is, say, 4 volts, then the area of the corresponding impulse is also 4 volts.

The simplification stems from the definition of the unit impulse:

$$\int_{-\infty}^{\infty} \delta(t) dt \triangleq 1 \quad \dots\dots(4)$$

(Note that the dimension of the impulse is 1/second.)

Thus, the value of the convolution integral of  $g(t)$  times an impulse of area  $A$  is

$$\int_0^{t_1} A\delta(t_1-x)g(x) dx = Ag(t_1) \quad \dots\dots(5)$$

Since  $g(x)$  can be treated as constant during the interval that the impulse exists (which tends to zero), the integration can be avoided.

Fortunately, we do not even have to reflect or 'turn back' one of the functions, since an impulse turned back is equal to the original impulse.

Thus

$$\begin{aligned} c(t_1) &= \int_0^{t_1} g(x) \cdot a \cdot \delta(t_1-x) dx \\ &= \int_0^{t_1} g(t) \cdot a \delta(t-t_1) dt \\ &= g(t_1) \cdot a \quad \dots\dots(6) \end{aligned}$$

### 3. The Sampled Data Theory Approximation

We shall now show how to convert a continuous function into an impulse train. First approximate the function by the 'stair-case' function:<sup>1(b)</sup>

$$\begin{aligned} e(t) &\simeq e(\theta)[u_1(t)-u_1(t-T)] + \\ &\quad + e(T)[u_1(t-T)-u_1(t-2T)] + \dots \\ &= \sum_{k=0}^n e(kT)\{u_1(t-kT)-u_1[t-(k+1)T]\} \quad \dots\dots(7) \end{aligned}$$

where  $e(t)$  is the continuous function

$u_1(t)$  is a step function

$T$  is the sampling period.

Both  $n$  and  $k$  are integers and  $nT \leq t < (n+1)T$ .

Note that the accuracy of the approximation depends on the choice of a small enough  $T$  compared with the dominant time constant of  $c(t)$ . Figure 2(a) shows the graphical procedure.

Multiplying each  $e(kT)$  by  $\delta(t-kT)$  turns each value of the staircase function into an impulse—this is called *sampling*. The impulse at time  $kT$  is

$$e^*(kT) = e(kT) \cdot \delta(t-kT) \quad \dots\dots(8)$$

and, in general, the impulse train is described by

Fig. 2(c):

$$e^*(nT) = \sum_{k=0}^n e(kT) \cdot \delta(t - kT) \quad \dots\dots(9)$$

To convert back from impulses to the staircase function, we perform the integration:

$$e(nT) = \int_{(n-1)T}^{nT} e^*(nT) dt = e^*(nT) \cdot T \quad \dots\dots(10)$$

From eqns. (6), (7), (8), (9) and (10), we may write:

$$\begin{aligned} c(t_n) &\simeq c(nT) = \int_0^{t_n} g(t) \cdot e^*(nT - t) dt \\ &= \int_0^{t_n} g(t) \sum_{k=0}^{\infty} e(kT) \cdot \delta(t_n - t) dt \\ &= \int_0^{t_n} g(t) \cdot \sum_{k=0}^{\infty} e(kT) \cdot \delta(t - t_n) dt \triangleq \int_0^{t_n} c^*(nT) dt \\ &= c^*(nT) \cdot T \quad \dots\dots(11) \end{aligned}$$

We can summarize now the advantages of this technique:

- (1) No 'turning back' of the function is necessary (see eqn. (6)).
- (2) The convolution integral is replaced by a product (see eqn. (11)).
- (3) The resultant staircase output is obtained by merely multiplying the impulse produce by the sampling period  $T$ .

The only disadvantage is that the output is an approximation which depends on the sampling rate.

The following example demonstrates this technique.

**Example 2**

Apply the above technique to the problem given in Example 1.

The construction of  $c(Tn)$  is quite simple. Attention is called to Fig. 2(e) where the construction of  $c^*(2T)$  is shown enlarged,  $c^*(2T) = a + b + c$ . The importance of choosing  $T/RC \rightarrow 0$  is apparent from Fig. 2(f), where the initial step is not zero as expected.

From the above graphical construction we see that we did not use the values of  $g(t)$  in the in-between sampling and we can tell by intuition that the calculation can be further simplified if we also draw  $g(t)$  as a series of impulses, in other words, sample it.

We have mentioned before that a product in the complex variable plane is equal to the convolution integral in the time domain. However, as is shown later in eqn. (17), the value of each impulse in the time domain is equal to the value of the translated impulse in the  $s$  domain, i.e.

$$g^*(t) = g^*(0) + g^*(T) + g^*(2T) + \dots + g^*(nT) \quad \dots\dots(12)$$

$$\begin{aligned} G^*(s) &= g^*(0)e^{-s \cdot 0} + g^*(T)e^{-sT} + g^*(2T)e^{-2sT} + \\ &\quad + \dots + g^*(nT)e^{-sTn} \quad \dots\dots(13) \end{aligned}$$

$$\begin{aligned} G(z) &= g^*(0)z^0 + g^*(T)z^{-1} + g^*(2T)z^{-2} + \\ &\quad + \dots + g^*(nT)z^{-n} \quad \dots\dots(14) \end{aligned}$$

Thus the product of two impulse trains in the complex variable plane, say  $G^*(s) \cdot E^*(s)$ , gives a new impulse train:

$$C^*(s) = G^*(s) \cdot E^*(s) \quad \dots\dots(15)$$

The value of each term in the series  $G^*(s)$  and  $E^*(s)$  are obtained from the corresponding functions in the time domain, i.e.  $g^*(t)$  and  $c^*(t)$ .

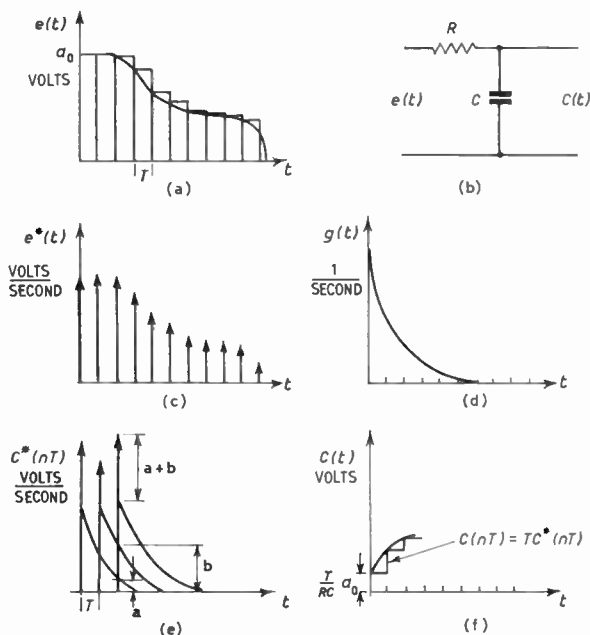
Finally,  $c(t)$  is obtained by using eqn. (6):

$$\begin{aligned} c(t_n) &\simeq c(nT) = \int_0^{t_n} g^*(t) \cdot e^*(t_n - t) dt \\ &= \int_0^{t_n} g^*(t) e^*(t - t_n) dt \\ &= \int_0^{t_n} c^*(t) dt = c^*(nT)T \quad \dots\dots(16) \end{aligned}$$

Example 3 demonstrates this further simplification.

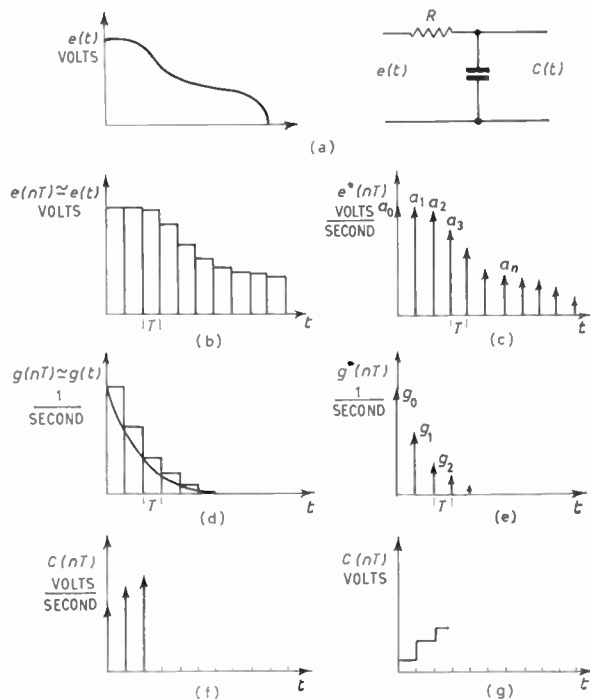
**Example 3**

Use the above technique to solve the problem given in Example 1.



- (a) Rectangular approximation of the input voltage.
- (b) Circuit under test.
- (c) Input voltage after sampling.
- (d) Impulse response of circuit.
- (e) Construction of the convolution product.
- (f) Plot of resultant output voltage (compare with Fig. 1(h)).

**Fig. 2.** Graphical determination of the sampled convolution integral (eqn. (11)).



- (a) Input voltage and circuit under test.
- (b) } Sampling procedure of input voltage.
- (c) }
- (d) } Sampling procedure of impulse response of circuit.
- (e) }
- (f) Construction of the convolution product.
- (g) Plot of the derived output voltage (compare with Fig. 2(f) and 1(h)).

Fig. 3. Graphical determination of the sampled convolution integral (eqn. (16)).

The same graphical procedure is used as in the previous example. We shall show now why this method is so suitable for digital computation.

Figure 3(c) describes equation (9):

$$e^*(nT) = \sum_{k=0}^n e(kT) \cdot \delta(t - kT) = a_0\delta(t) + a_1\delta(t - T) + a_2\delta(t - 2T) + \dots$$

while Fig. 3(e) describes:

$$g^*(nT) = \sum_{k=0}^n g(kT) \cdot \delta(t - kT) = g_0\delta(t) + g_1\delta(t - T) + g_2\delta(t - 2T) + \dots$$

The convolution multiplication is arranged as shown in Table 1.

It is quite simple to program an electronic digital computer to perform the above computation and

simple problems can also be done with great ease on a standard desk calculator.

#### 4. The z-Transform

The 'z-transform' is a shorthand form for the long impulse train discussed before. Instead of multiplying term by term and adding them up, we can use the condensed form of the 'z-transform' and just multiply two polynomials of a new variable z.

We shall first transform the sampled function from the time domain to the complex variable s domain. From eqn. (9):

$$F^*(s) = \mathcal{L}[f^*(t)] = \mathcal{L}\left[\sum_{k=0}^{\infty} f(kT) \cdot \delta(t - kT)\right] = \sum_{k=0}^n f(kT) e^{-sTk} \dots (17)$$

since  $\mathcal{L}[\delta(t - kT)] = e^{-sTk}$  and  $f(kT)$  is constant during the infinitesimal time that the impulse exists.

If we put  $e^{sT} = z$  we can rewrite eqn. (17):

$$F(z) = F^*(s) = \sum_{k=0}^n f(kT)z^{-k} \dots (18)$$

This is the definition of the z-transform from the time domain. There is another definition of a transform from the s plane which is discussed elsewhere.<sup>4-8</sup>

Table 1

$a_0$	$a_1$	$a_2$	$a_3$	$a_4$	$a_5$	$a_6$	$a_7 \dots$	
$g_0$	$g_1$	$g_2$	$g_3$	$g_4$	$g_5$	$g_6$	$g_7 \dots$	
$g_0a_0$	$g_0a_1$	$g_0a_2$	$g_0a_3$	$g_0a_4$	$g_0a_5$	$g_0a_6$	$g_0a_7 \dots$	
	$g_1a_0$	$g_1a_1$	$g_1a_2$	$g_1a_3$	$g_1a_4$	$g_1a_5$	$g_1a_6$	$g_1a_7 \dots$
		$g_2a_0$	$g_2a_1$	etc.				
$c^*(0) = g_0a_0$								
$c^*(T) = g_0a_1 + g_1a_0$		$c^*(nT) = \sum_{k=0}^n g_k a_{n-k}$						
$c^*(kT) = g_0a_k + g_1a_{k-1} + g_2a_{k-2} + \dots$								

Let us now build up a table of z-transform pairs.

(1) Unit step function  $f(t) = u_1(t)$ , i.e.  $F(s) = 1/s$ .

$$f^*(nT) = \sum_{k=0}^{\infty} 1 \cdot \delta(t - kT)$$

hence

$$F^*(s) = 1 + e^{-sT} + e^{-s2T} + \dots = \frac{1}{1 - e^{-sT}} = \frac{1}{1 - z^{-1}} = \frac{z}{z - 1} \dots (19)$$

(2) Exponential decay,  $e^{-at} = f(t)$  i.e.  $F(s) = 1/(s + a)$ .

$$f^*(nT) = \sum_{k=0}^n e^{-kTa} \cdot \delta(t - kT)$$

hence

$$F^*(s) = 1 + e^{-Ta} \cdot e^{-sT} + e^{-2Ta} \cdot e^{-2sT} + \dots$$

$$= \frac{1}{1 - e^{-Ta} \cdot e^{-sT}} = \frac{1}{1 - e^{-aT} \cdot z^{-1}} = \frac{z}{z - e^{-aT}} \quad \dots\dots(20)$$

For other common forms the table of conversion may be found, for example, in references 2, 4-8, 14, 16a.

Example 4 demonstrates how to use the short-form notation of the z-transform to save the long multiplication and summation shown in Table 1. Obviously the form in Table 1 is most suitable for digital computers, while the z-transform method is more suitable for human and analogue computation.

**Example 4**

Find the step response of a single lag R-C filter.

We shall assume that an ideal sampler is interposed between the driving generator and the network so that we can use the same procedure as in Fig. 3, but this time do the computation with the z-transform method.

We aim at finding

$$c^*(nT) = e^*(nT) * g^*(nT) \quad \dots\dots(21)$$

(\* denotes convolution product).

Taking the z-transform of eqn. (21) we write:

$$C(z) = E(z) \cdot G(z) \quad \dots\dots(22)$$

Now from eqns. (19) and (20):

$$E(z) = \frac{z}{z-1} \quad \text{and} \quad G(z) = \frac{za}{z - e^{-aT}}$$

Thus

$$C(z) = z \frac{za}{(z-1)(z - e^{-aT})}$$

$$= az \left[ \frac{1}{(z-1)(1 - e^{-aT})} - \frac{e^{-aT}}{(z - e^{-aT})(1 - e^{-aT})} \right]$$

$$= \frac{a}{1 - e^{-aT}} \left[ \frac{z}{z-1} - \frac{z e^{-aT}}{z - e^{-aT}} \right] \quad \dots\dots(23)$$

We recognize the first term in the square bracket of eqn. (23) as  $f(t) = 1$  and the second as

$$f(t) = e^{-aT} \cdot e^{-at}$$

Hence the inverse z-transform of eqn. (23) is:

$$\mathcal{Z}^{-1}[C(z)] = c^*(nT) = \frac{a}{1 - e^{-aT}} (1 - e^{-aT} \cdot e^{-at}) \quad \dots\dots(24)$$

and finally we can find the approximated output voltage from eqn. (11)

$$c(nT) = c^*(nT) \cdot T = \frac{aT}{1 - e^{-aT}} (1 - e^{-aT} \cdot e^{-at}) \quad \dots\dots(25)$$

The plot of eqn. (25) is similar to Figs. 2(f) and 3(g). The initial value is not zero as the exact Laplace method yields, but  $c(0) = aT$ . The final value is again not 1, but:

$$c(\infty T) = \frac{aT}{1 - e^{-aT}}$$

In both cases the accuracy of the approximation depends on making

$$aT = \frac{T}{RC} \rightarrow 0$$

Although the Laplace transform gives an exact and quicker solution than the z-transform, the z-transform has the following advantages:

- (a) It is easier to program a digital computer to solve a z-transformed function rather than an s-transformed function (see Table 1).
- (b) It is the most suitable theory for pulsed system, as will be shown later.

Before we start to analyse pulsed systems, we must show how to convert a function of z, i.e.  $F(z)$  back into the series from which is suitable for digital computers.

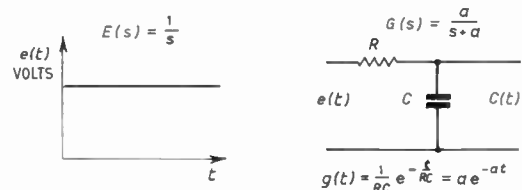


Fig. 4. Circuit and input voltage for Example 4.

**Example 5**

In the process of evaluating  $C(z) = G(z) \cdot E(z)$ ,  $E(z)$  was quantized (i.e. digitized in a form of an impulse train) and it was necessary to write  $G(z)$  as a longhand series so that the multiplication and summation of Table 1 can be carried out on a digital computer.

First transfer  $G(s)$  to get

$$G(z) = \frac{d_0 + d_1 z^{-1} + d_2 z^{-2} + \dots}{1 + b_1 z^{-1} + b_2 z^{-2} + \dots}$$

and write:

$$G(z) = \frac{d_0 + d_1 z^{-1} + d_2 z^{-2} + \dots}{1 + b_1 z^{-1} + b_2 z^{-2} + \dots}$$

$$= g_0 + g_1 z^{-1} + g_2 z^{-2} \quad \dots\dots(26)$$

Equate equal powers of z, thus

$$z^0: \quad d_0 = g_0$$

$$z^{-1}: \quad d_1 = b_1 g_0 + g_1 b_0$$

Therefore

$$g_1 = d_1 - d_0 b_1$$

$$z^{-2}: d_2 = g_0 b_2 + g_1 b_1 + g_2$$

Therefore

$$g_2 = d_2 - d_1 b_1 - d_0 b_2 + d_0 b_1^2$$

$$z^{-n}: d_n = \sum_{k=0}^n g_k \cdot b_{(n-k)} \dots\dots(27)$$

When all the required values of  $g$  are found, the computation is done as shown in Table 1. A numerical example is given by Pierre.<sup>13</sup>

Thus we have seen that we can calculate the response to a complicated input driving function without the need of the Laplace transform. The driving function can be preserved in the time domain while the system transfer function is converted to a condensed  $z$ -function and then to a longhand series of impulses. The digitizing of the driving function can be done by analogue-to-digital converters.

**5. The Analysis of Pulsed (Sampled) Systems**

Pulsed systems are systems whose information's transmission is carried out by relatively short duration intervals. Under this category would fall carrier modulated signals or interrupted d.c. After demodulation, there is no difference between the two, so we shall discuss the latter only.

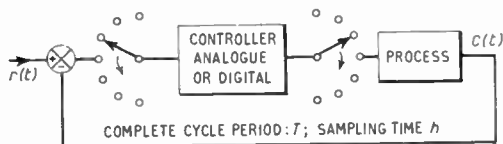


Fig. 5. Essentials of a multiplexed system.

Figure 5 shows the essentials of a physical 'sampler' of a pulsed system where a single controller is time shared (multiplexed) among many loops.

At this point we must pay careful attention to the right description of the 'sampler'. When we deal with passive electrical circuits we must use a double-pole switch for the sampler (Fig. 6). The reason is that from the definition of the sampling function,  $f(t)$  exists during the sampling period but is zero elsewhere. In the simple example of Fig. 6 the network will act as a peak detector and would not follow the input otherwise.

If we want to simulate the problem of Example 2 on an analogue computer, we would have to use the network of Fig. 6. (The switch is often drawn as a single-pole switch—an eye-sore to the practical engineer.) The switch remains in position 1 for  $h$

seconds and assumed to transfer instantaneously to position 2 for the remaining  $T-h$  seconds.

For certain active circuits such as the zero order hold circuit we must use a single-pole switch, while for some operational amplifier applications it is immaterial which switch we use. Thus the type of switch used must be considered for every application.

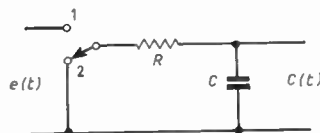


Fig. 6. Correct sampler configuration.

Another point to note is that the practical sampler does not produce impulses whose area is equal to the value of the original continuous function, as this would necessitate fantastic amplitudes. It is obvious that the energy of the practically sampled function is  $h/T$  smaller than the continuous function and this gain factor must be included. More detail and comparison between the solutions of the step response of the pulsed system of Fig. 6, using the exact Laplace transform and  $z$ -transform have been given elsewhere,<sup>3</sup> where the effect of  $T/RC$  on the accuracy is also demonstrated.

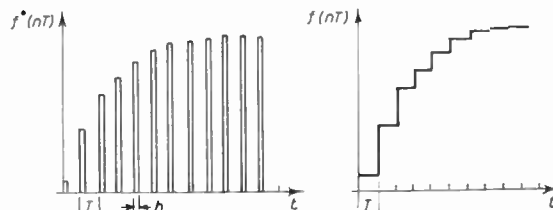


Fig. 7. Input and output of zero order hold circuit.

Before dealing with stability analysis in the  $z$ -plane and showing the importance of  $z$ -transform, it will be shown that in most cases the Laplace transform of continuous systems still holds for pulsed systems as well. This applies to all analogue computed cases where a zero-order hold circuit is used and the correct repetition rate is chosen. On the other hand, when digital computers are used as controllers, the longhand  $z$ -transform is a necessity for both multiplexing and continuous systems.

**5.1. The Zero-order Hold Circuit**

We have seen that a switch performed the function of sampling and we shall now see how the zero-order hold circuit builds up a staircase function from the applied impulses or, more accurately, from the applied short duration pulses.

Mathematically, each narrow pulse (or sample) is held constant, i.e. multiplied by  $1/s$  for a period  $T$ . In mathematical notation, we multiply the pulsed function by:

$$\frac{1 - e^{-sT}}{s} \dots\dots(28)$$

Thus, if we start with a continuous function  $f(t)$ , and sample it, we have  $f^*(nT)$  and cascading it with the zero-order hold circuit we get  $f(t) \simeq f^*(nT)T = f(nT)$  provided that  $T$  is small in comparison with the dominant time constant of  $f(t)$ .

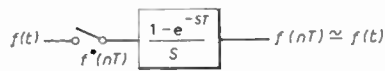


Fig. 8. Mathematical representation of zero-order hold circuit.

In other words, there is no point in applying the z-transform to systems where the sampler is followed by the zero order hold circuit: if we chose a high repetition rate, the resultant staircase function is a good approximation to the original continuous function and, if not, the z-transform approximation is not valid anyhow. The same applies to the higher order hold circuits.

Figure 9 shows a practical zero-order hold circuit.

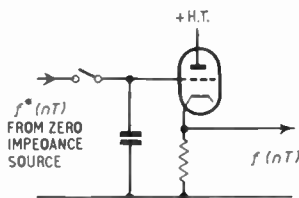


Fig. 9. Basic diagram of zero-order hold circuit.

5.2. The Effect of the Position of the 'Sampler'

When the z-transform of a system is taken, the position of the samplers must be taken into account. In Fig. 10 we must consider the impulse response of both  $G_1(s)$  and  $G_2(s)$ . Thus the z-transform is:

$$\mathcal{Z}[G(s)] = \mathcal{Z}[G_1(s).G_2(s)] = G_1 G_2(z) \dots\dots(29)$$

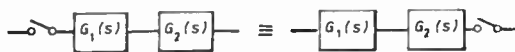


Fig. 10. Cascaded system as described by eqn. (29).

If another sampler is interposed between  $G_1(s)$  and  $G_2(s)$  (Fig. 11), we must consider the impulse response of each function individually, and the z-transform would be:

$$\mathcal{Z}[G(s)] = \mathcal{Z}[G_1(s)]. \mathcal{Z}[G_2(s)] = G_1(z). G_2(z) \dots\dots(30)$$

Tables of different combinations of sampled data system are given in references 2, 4-8, 14 and 16b.



Fig. 11. Cascaded system as described by eqn. (30).

6. Stability Criteria

Consider the system shown in Fig. 12:

The closed loop transfer function is:

$$\frac{C(z)}{R(z)} = \frac{G(z)}{1 + GH(z)} \dots\dots(31)$$

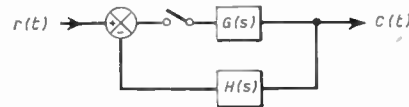


Fig. 12. Closed loop sampled system.

The criteria for stability are the same as for continuous systems, and both the Nyquist and root locus plots can be applied to determine the stability margins, etc.

$$\text{Since } z = e^{sT} = e^{\sigma} \cdot e^{j\omega T} \dots\dots(32)$$

the  $s$  plane ( $s = \sigma + j\omega$ ) is conformally transported to the  $z$  plane, by using eqn. (32).

The  $j\omega$  axis ( $\sigma = 0; -\infty < \omega < \infty$ ) is transformed to a unit circle in the  $z$  plane (Fig. 13). All the points on the left of the  $j\omega$  axis in the  $s$ -plane are located to the left of the unit circle as we go from  $-\infty$  to  $+\infty$  (i.e. anti-clockwise) or, in other words, confined inside the unit circle. The origin  $s = 0 + j0$  is transformed by eqn. (32) to  $z = 0^0 = 1$ . The real axis (i.e.  $-\infty < \sigma < \infty$ ) is transformed to the real axis line going from the origin ( $e^{-\infty} = 0$ ) to  $\infty(e^{\infty} \rightarrow \infty)$ .

For stable systems, the closed loop poles of  $F(s)$  must lie to the left of the  $j\omega$  axis in the  $s$ -plane, hence the closed loop poles of  $F(z)$  must lie inside the unit axis. The root locus is defined in a similar manner, i.e. the locus of the points whose angle to all the singular points of the open loop function  $F(z)$  is 180 deg.

The Nyquist plot is done in a similar manner by substituting  $z = 1 / \theta$  in the open loop equation.

For example, if the point corresponding to  $z = e^0 \cdot e^{j\pi/2} = 1 / 90^\circ$  is plotted in a given  $F(z)$ , say:

$$F(z) = \frac{(a_0 + z)(a_1 + z)}{(b_0 + z)(b_1 + z)(b_2 + z)}$$

then

$$F(j) = \frac{(a_0 + j)(a_1 + j)}{(b_0 + j)(b_1 + j)(b_2 + j)}$$

For various analytical treatments and discussions on stability of pulsed systems, the reader is referred to reference 14.

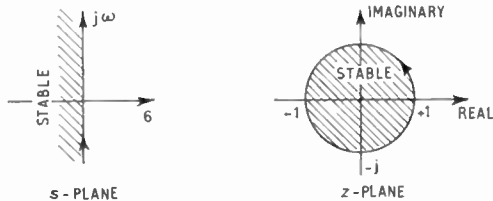


Fig. 13. Transformation of the s-plane to the z-plane.

Several Nyquist plots are given by Gibson<sup>4</sup> and root-locus plots are given by Jury<sup>5(a)</sup> and Tou.<sup>6(a)</sup> In all these examples there is one common error which they all make when they analyse pulsed systems with a zero order hold. They all say that the z-transform of the system, shown in Fig. 10, is  $G_1 G_2(z)$ , but when it comes to the zero-order hold, they treat it differently and arrive at very serious errors.

Consider the system of Fig. 14, which is identical to Fig. 10 in all respects, except that  $G_1(s)$  is detailed as:

$$G_1(s) = \frac{1 - e^{-sT}}{s} = \text{zero-order hold}$$

The customary way of writing the transfer function of Fig. 14 is:

$$\begin{aligned} G(z) &= \frac{C(z)}{E(z)} = \mathcal{Z}[G_1(s) \cdot G_2(s)] \\ &= \mathcal{Z}\left[\frac{1 - e^{-sT}}{s} \cdot G_2(s)\right] \end{aligned} \quad \dots\dots(33)$$

and then to write eqn. (33) as:

$$\begin{aligned} \frac{C(z)}{E(z)} &= G(z) = (1 - e^{-sT}) \cdot \mathcal{Z}[1/s \cdot G_2(s)] \\ &= (1 - z^{-1}) \cdot \mathcal{Z}[1/s \cdot G_2(s)] \\ &= \frac{z - 1}{z} \cdot \mathcal{Z}[1/s \cdot G_2(s)] \end{aligned} \quad \dots\dots(34)$$

The term  $1/s$  in the square brackets indicates that we perform integration with respect to time on the continuous function  $g_2(t)$ . However, the term  $(z - 1)/z$  indicates that we differentiate the pulsed function with respect to time. Ideally the overall effect would be to leave the time function intact. Unfortunately the discrete differentiation is far from ideal (being only an approximation) and an error has crept in. For more detailed analyses, see Section 11 and the paper by Salzer.<sup>12</sup>



Fig. 14. A sampler and hold circuit drive.

Physical considerations show us that the sample and hold circuit (or the zero-order hold) merely increases the ratio  $h/T$  towards unity. In other words we need only to take the z-transform of  $G_2(s)$  and treat  $\mathcal{Z}\left[\frac{1 - e^{-sT}}{s}\right]$  as unity. As is explained elsewhere<sup>3</sup>, we had to multiply the transfer function by  $h/T$  when the zero-order hold was not used. In digital computation the matter does not arise since the hold circuit is intrinsically incorporated by virtue of the function of the computer (or paper) store, where the data are stored for at least one sampling period. From the above discussion we conclude that for physical systems the hold circuit acts as an amplifier of unity gain while for digital computation the hold function is carried out by virtue of the store. In both these cases its z-transfer function is unity.

To check this argument the example given by Tou<sup>6</sup> was simulated on the analogue computer (Fig. 15(a)). The gain was increased until continuous oscillations were maintained. The measured gain agrees with that predicted from the root locus plot in the z-plane shown in Fig. 15(b).

The system's transfer function for  $T = 0.1s$ , is:

$$\begin{aligned} \mathcal{Z}\left[\frac{K}{s(1 + 0.1s)(1 + 0.05s)}\right] \\ = \frac{Kz(z + 0.368)0.399}{(z - 1)(z - 0.368)(z - 0.135)} \end{aligned}$$

From the root locus plot (Fig. 15(b)) we find that the ultimate gain  $k_u$  for continuous oscillation is approximately 3.5, which agrees with the measured result. On the other hand, according to Tou,  $k_u = 13.2$ . Note that this correction affects only the location of the zeros and the gain factor.

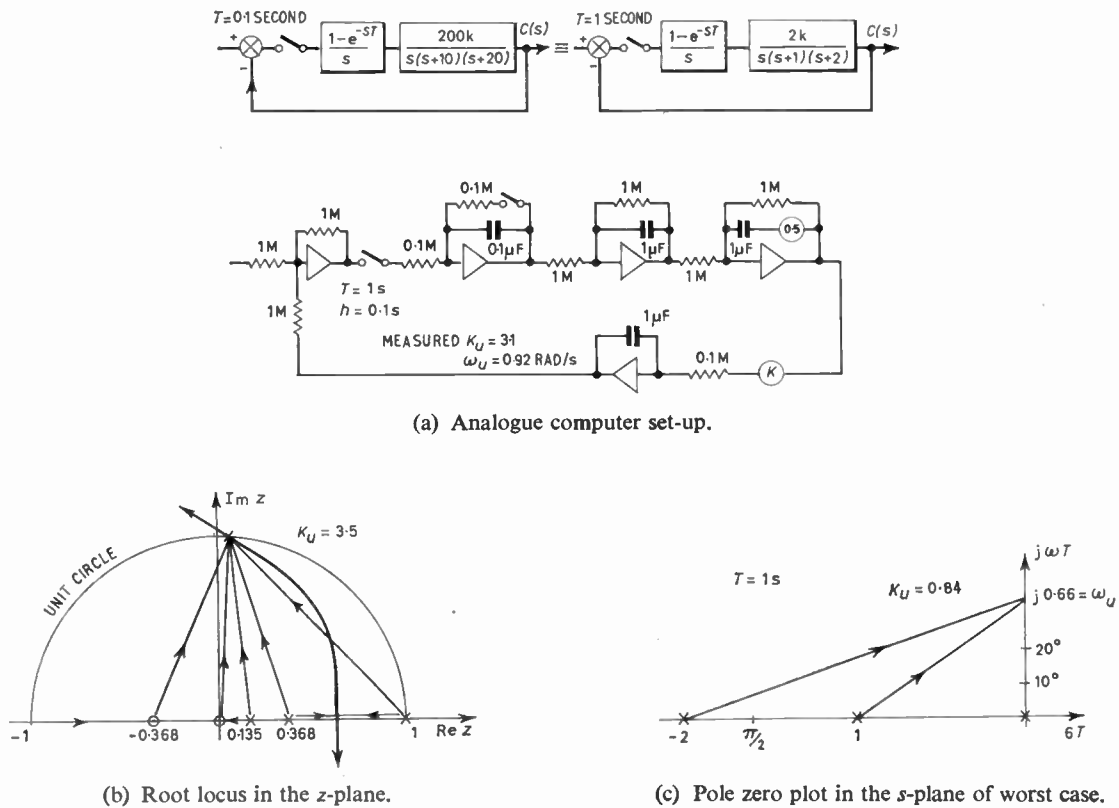


Fig. 15. Simulation of third-order sampled data system.

If the designer does not want to use z-transform he may apply the continuous Laplace transform technique, but must take into account the dead time involved due to sampling. The worst case is the whole of the sampling period  $T$ .

Thus:

$$G(s) \simeq e^{-sT} \cdot G_2(s) \quad \dots\dots(35)$$

Figure 15(c) shows the pole-zero plot in the s-plane. The calculated ultimate gain is found to be  $k_u = 0.84$ , which allows for a safety factor of 4 for this case.

**7. The Choice between Discrete and Continuous Controllers**

The temptation to design systems in the z-plane is quite great because it is so easy to convert the impulse train from the z to the time domain (eqn. (14)). A few authors (Tou<sup>6(b)</sup> and Raggazzini and Franklin<sup>7</sup>) give some design criteria for finite settling time, maximum overshoot, etc., for defined inputs. Unfortunately, the requirements for different inputs, say step and ramp, conflict (Tou<sup>6(c)</sup>) and a compromise is sought with one eye kept on the stability. For

random inputs, the discrete controller is treated on the same lines as continuous controllers and need no further discussion here. Thus from the control theory viewpoint, there is no advantage in using discrete controllers. The design is carried out in the s-plane as a continuous system. Once the pole-zero configuration of the controller is decided, the z-transformation of the controller transfer function takes place. That is, if we have decided to use discrete control at all. The choice between a discrete or continuous controller is made on engineering grounds only.

The points to be taken into account are: time-sharing (multiplexing), reliability, long- and short-term drifts, long time-constants and power dissipation. All these points are met easily by the discrete controller, while the use of derivatives and other phase advance networks are more easily met by a continuous controller.

The discrete controller lends itself more readily to integration in a data-logging system, but this topic is outside the scope of this paper.

**8. The Realization of the Discrete Controller**

Once the decision has been made in favour of a discrete controller, methods are investigated to find the best way to realize the z-transform of the desired controller. But before attempting to realize the transfer function, a simple check should be applied to verify that the function is physically realizable.

The necessary and sufficient condition for the general pulsed transfer function

$$G(z) = \frac{\sum_{k=0}^m a_k z^{-k}}{b_0 + \sum_{k=1}^n b_k z^{-k}} \dots\dots(36)$$

to be physically realizable is that the coefficient  $b_0$  is not zero.

If the function is expressed as a ratio of two polynomials in  $z^k$  instead of  $z^{-k}$  (as in eqn. (36)), the condition is that  $G(z)$  contains no more zeros than poles. The proof is based on the fact that otherwise the transfer function would depend on the unknown future values of the input, rather than the past values. The full proof is given elsewhere.<sup>5-8</sup>

The condition of realizability does not imply that eqn. (36) is stable. The condition for this is that the poles of  $G(z)$  should lie inside the unit circle in the z-plane.

There are two basic approaches to synthesize  $G(z)$ , namely analogue and digital. The digital technique is further divided into:

- (1) direct programming
- (2) iterative programming
- (3) parallel programming.

The analogue technique is divided into:

- (1) delay circuits and potentiometers
- (2) R-C active and non-active networks.

**8.1. Direct Programming**

Equation (36) is rewritten as:

$$\frac{E_o(z)}{E_{in}(z)} = G(z) = \frac{a_0 + a_1 z^{-1} + a_2 z^{-2} + \dots + a_m z^{-m}}{1 + b_1 z^{-1} + b_2 z^{-2} + \dots + b_n z^{-n}} \dots\dots(37)$$

Cross-multiplying eqn. (37) and taking the inverse z-transform yields:

$$e_o^*(t) = \sum_{k=0}^m a_k \cdot e_{in}^*(t - kT) - \sum_{k=1}^n b_k e_o^*(t - kT) \dots\dots(38)$$

Eqn. (38) contains:

- $m + n + 1$  terms,
- $m + n$  additions and subtractions,
- $m + n + 1$  multiplications,
- $m + n$  transfers.

**8.2. Iterative (Series) Programming**

If eqn. (36) can be factorized to  $m$  real and simple zeros ( $\alpha$ ) and  $n$  real and simple poles ( $\beta$ ), we may write:

$$G(z) = \frac{E_o(z)}{E_{in}(z)} = \frac{K(z + \alpha_1)(z + \alpha_2) \dots (z + \alpha_m)}{(z + \beta_1)(z + \beta_2) \dots (z + \beta_n)} \dots\dots(39)$$

and if  $m < n$ , we can rewrite eqn. (39):

$$G(z) = \frac{z + \alpha_1}{z + \beta_1} \cdot \frac{z + \alpha_2}{z + \beta_2} \dots \frac{z + \alpha_m}{z + \beta_m} \frac{1}{z + \beta_{m+1}} \frac{K}{z + \beta_n} \\ = G_1(z) \cdot G_2(z) \dots G_m(z) \dots G_n(z) \dots\dots(40)$$

Put

$$G_1(z) = \frac{E_1(z)}{E_{in}(z)} = \frac{1 + \alpha_1 z^{-1}}{1 + \beta_1 z^{-1}} \dots\dots(41)$$

Cross-multiplying eqn. (41) and taking the inverse transform yields:

$$e_1^*(t) = e_{in}^*(t) + \alpha_1 e_{in}^*(t - T) - \beta_1 e_1^*(t - T)$$

where  $e_1^*(t)$ ,  $e_2^*(t)$  and so on are shown in Fig. 16.

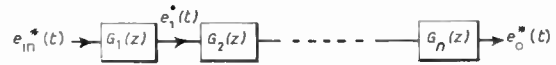


Fig. 16. Iterative programming.

Similarly,  $e_2^*(t)$ ,  $e_3^*(t)$  and so on, are found and the computer is set to solve the set of the following equations:

$$\left. \begin{aligned} e_1^*(t) &= e_{in}^*(t) + \alpha_1 e_{in}^*(t - T) - \beta_1 e_1^*(t - T) \\ e_2^*(t) &= e_1^*(t) + \alpha_2 e_1^*(t - T) - \beta_2 e_2^*(t - T) \\ &\vdots \\ e_m^*(t) &= e_{m-1}^*(t) + \alpha_m e_{m-1}^*(t) - \beta_m e_m^*(t - T) \\ e_{m+1}^*(t) &= e_m^*(t) + \alpha_{m+1} e_m^*(t) - \beta_{m+1} e_{m+1}^*(t - T) \\ &\vdots \\ e_o^*(t) &= K e_{n-1}^*(t - T) - \beta_n e_o^*(t - T) \end{aligned} \right\} \dots\dots(42)$$

To solve this set of equations we need to perform:

- $m + n$  additions and subtraction,
- $m + n + 1$  multiplications,
- $n$  transfers.

**8.3. Parallel Programming**

The third method is based on partial fraction expansion of  $G(z)$ . Let the partial expansion of  $G(z)$  be

$$\frac{E_o(z)}{E_{in}(z)} = G(z) = G_a(z) + G_b(z) + G_c(z) + \dots + G_n(z)$$

where

$$\left. \begin{aligned} G_a(z) &= \frac{E_a(z)}{E_{in}(z)} = \frac{K_a}{z + \beta_a} = \frac{K_a z^{-1}}{1 + \beta_a z^{-1}} \\ G_b(z) &= \frac{E_b(z)}{E_{in}(z)} = \frac{K_b}{z + \beta_b} = \frac{K_b z^{-1}}{1 + \beta_b z^{-1}} \\ &\vdots \\ G_n(z) &= \frac{E_n(z)}{E_{in}(z)} = \frac{K_n}{z + \beta_n} = \frac{K_n z^{-1}}{1 + \beta_n z^{-1}} \end{aligned} \right\} \dots\dots(43)$$

Cross-multiplying and taking the inverse of each of the above equations, we get:

$$\left. \begin{aligned} e_a^*(t) &= K_a e_{in}^*(t-T) - \beta_a e_a^*(t-T) \\ e_b^*(t) &= K_b e_{in}^*(t-T) - \beta_b e_b^*(t-T) \\ &\vdots \\ e_n^*(t) &= K_n e_{in}^*(t-T) - \beta_n e_n^*(t-T) \end{aligned} \right\} \dots\dots(44)$$

The desired output is obtained by summing up all the individual values:

$$\begin{aligned} e_o^*(t) &= e_a^*(t) + e_b^*(t) + e_c^*(t) + \dots + e_n^*(t) \\ &= \sum_{k=1}^n K_k e_{in}^*(t-T) - \sum_{k=1}^n \beta_k e_k^*(t-T) \end{aligned} \dots\dots(45)$$

The construction of eqn. (43), as illustrated in Fig. 17, explains the term 'parallel programming'.

To solve the set of eqns. (44), the digital computer is required to perform:

- 2n-1 additions and subtractions,
- 2n multiplications,
- n+1 transfers.

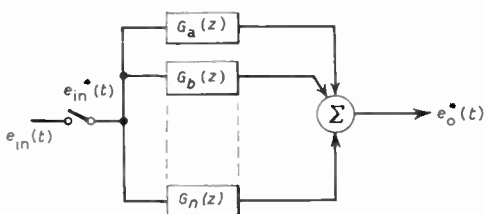


Fig. 17. Parallel programming.

8.4. Relative Merits

The relative merits of each method can best be judged according to the problem and computer facilities. The direct method minimizes the computation delay since all the terms of eqn. (38) except  $a_0 e_{in}^*(t)$  can be computed from previous stored data  $e_{in}(t-T)$ ,  $e_{in}^*(t-2T)$ , etc. Thus the computer needs to compute only one term from present sampled information and digest all the other terms from its store. This saving in computation time is offset by the requirement of a large store. On the other hand,

the importance of minimizing the delay cannot be overstressed for on-line control.

The iterative method is the slowest, but needs the least number of storage cells. It also enables us to obtain intermediate data, for instance, velocity when computing distance from acceleration. This technique is widely used in analogue computers.

The parallel method is faster than the iterative method but needs more stores.

Further discussion on these methods can be found in the literature.<sup>8</sup>

8.5. Delay Circuits and Potentiometers Method

We have dealt so far with digital synthesis where the information was digitized. We shall investigate analogue systems where the information is presented in terms of interrupted continuous variables.

Consider the synthesis of:

$$\frac{E_o(z)}{E_{in}(z)} = G(z) = \frac{a_0 + a_1 z^{-1}}{1 + b_1 z^{-1}} \dots\dots(46)$$

and write:

$$\begin{aligned} G(z) &= \frac{a_0 + a_1 z^{-1}}{1 + b_1 z^{-1}} = \frac{a_0}{1 + b_1 z^{-1}} + \frac{a_1 z^{-1}}{1 + b_1 z^{-1}} \\ &= \frac{1}{1 + b_1 z^{-1}} (a_0 + a_1 z^{-1}) \end{aligned} \dots\dots(47)$$

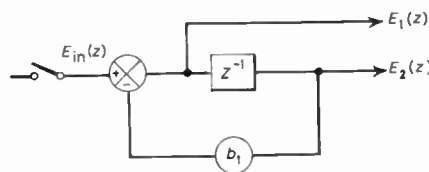


Fig. 18. Realization of  $\frac{1}{1 + b_1 z^{-1}}$

The factor  $\frac{1}{1 + b_1 z^{-1}}$  can easily be constructed using basic feedback theory, as shown in Fig. 18 which yields

$$\frac{E_1(z)}{E_{in}(z)} = \frac{1}{1 + b_1 z^{-1}} \quad \text{and} \quad \frac{E_2(z)}{E_{in}(z)} = \frac{z^{-1}}{1 + b_1 z^{-1}}$$

Hence, by summing the outputs in Fig. 17 and multiplying by the appropriate coefficient we get:

$$\begin{aligned} G(z) &= \frac{E_o(z)}{E_{in}(z)} = \frac{a_0 E_1(z)}{E_{in}(z)} + \frac{a_1 E_2(z)}{E_{in}(z)} \\ &= \frac{a_0}{1 + b_1 z^{-1}} + \frac{a_1 z^{-1}}{1 + b_1 z^{-1}} \end{aligned} \dots\dots(48)$$

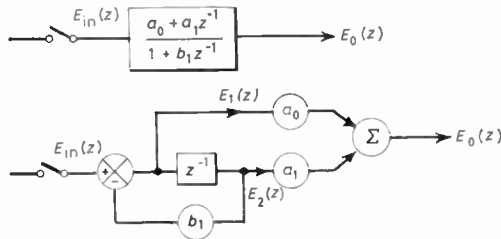


Fig. 19. Realization of eqn. (46).

Equation (47) is thus realized. Figure 19 shows the complete circuit.

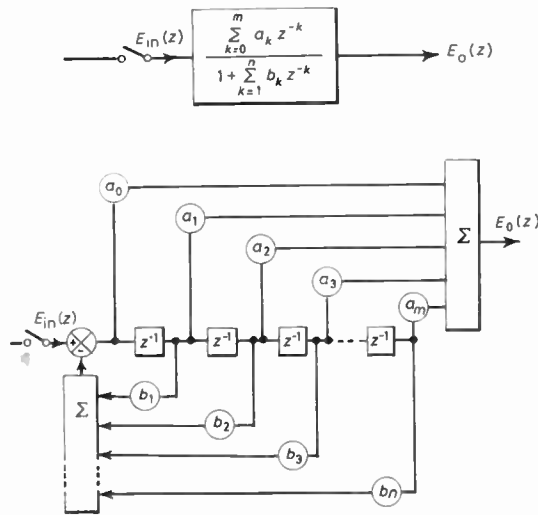


Fig. 20. Realization of the general pulsed transfer-function using delay circuits and potentiometers.

Applying the same principle to eqn. (49), we can synthesize the general transfer function as shown in Fig. 20.

$$G(z) = \frac{\sum_{k=0}^m a_k z^{-k}}{1 + \sum_{k=1}^n b_k z^{-k}} \quad \dots\dots(49)$$

Utilization of this technique is described by Togino.<sup>9</sup> The delay circuit must not exhibit a continuous delay such as a delay line, but can use zero order hold circuits as shown in Fig. 21. The system works as an ‘analogue shift register’ where the information is transmitted from one stage to the other, every pulse.

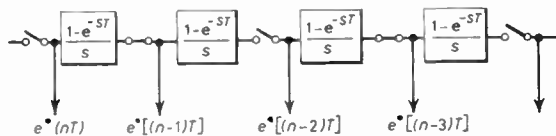


Fig. 21. Realization of discrete delay.

### 8.6. Realization of a Discrete Controller by R-C and Hold Circuits

This method utilizes conventional continuous R-C networks in series with a sampler and zero-order hold circuits. The approach is similar to a.c. servo compensation, where the input a.c. signal is demodulated; compensation is performed on the demodulated ‘envelope’ and then the resulting output is modulated again. In pulsed systems, the modulator is replaced by the sampler and the demodulator by the zero-order hold (Fig. 22).

The use of derivative action in  $G(s)$  would cause some trouble because the staircase waveform which is applied to  $G(s)$  contains high-frequency components. This snag is overcome by interposing a low-pass filter between the hold circuit and the controller.

The subject is well covered in the literature on a.c. and d.c. control systems, to which the reader is referred for further details.

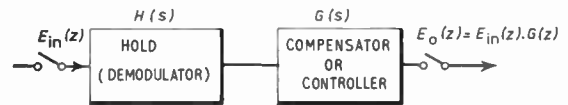


Fig. 22. Direct transformation of  $G(s)$  to  $G(z)$ .

### 8.7. Realization of Discrete Controllers by R-C Circuits Only

The finite width of the pulses plays an important part in this case, and the correction factor mentioned in reference 3 should be applied. Consider the realization of a discrete proportional+integral controller, whose continuous transfer function is:

$$G(s) = K \left( 1 + \frac{1}{sT_i} \right) \quad \dots\dots(50)$$

Now the z-transform of 1 is 1 and

$$\mathcal{Z} \left[ \frac{1}{sT_i} \right] = \frac{z}{(z-1)T_i}$$

Bearing in mind that we are going to generate this term by a continuous circuit element, we shall multiply by  $T$  to comply with eqn. (11) and change the scale factor  $T_i$  as explained in ref. 3, i.e.  $T_i^* = \frac{h}{T} T_i$  where  $h$  is the sampling time and  $T$  the sampling period.

From the above discussion, we write the desired pulsed transfer function as

$$G(z) = K \left( 1 + \frac{zT}{(z-1)T_i^*} \right) \quad \dots\dots(51)$$

Equation (51) is realized in Fig. 23.

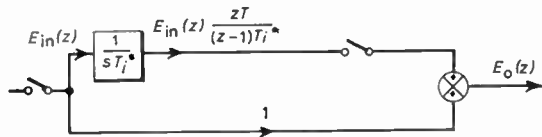


Fig. 23. Realization of eqn. (51).

Let us find out now the response of this controller to a unit step:  $e_{in}(t) = u_1(t)$ .

$$E_o(z) = E_{in}(z) \cdot G(z) = K \frac{z}{z-1} \left( 1 + \frac{zT}{(z-1)T_i^*} \right)$$

$$= K \left[ \frac{z}{z-1} + z \frac{T}{hT_i} \cdot \frac{zT}{(z-1)^2} \right] \dots\dots(52)$$

$\downarrow$   
train of unit impulses
 $\downarrow$   
time advance
 $\downarrow$   
unit ramp train of impulses

Taking the inverse transform of eqn. (52), and plotting it, we have Fig. 24.

The controller shown in Fig. 23 can be realized by a single operational amplifier, shown in Fig. 25.

The continuous transfer function  $G(s)$  is given by:

$$G(s) = \frac{R_2 + \frac{1}{sC_2}}{R_1} = \frac{R_2}{R_1} + \frac{1}{sCR_1} = \frac{R_2}{R_1} \left( 1 + \frac{1}{sCR_2} \right)$$

$$= K \left( 1 + \frac{1}{sT_i^*} \right) \dots\dots(53)$$

where  $K = \frac{R_2}{R_1}$  and  $T_i^* = CR_2$

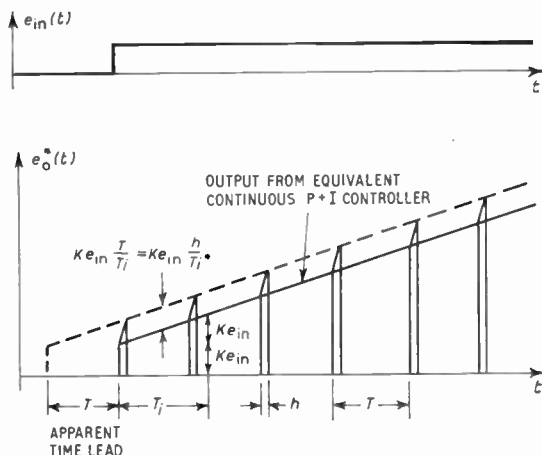


Fig. 24. Step response of a pulsed proportional+integral (p+i) controller.

Note that due to sampling, we achieved very long integrating time constants with relative small components. This is due to the effective integral time  $-T_i$ ,

being  $T/h$  larger than  $T_i^*$ . That is quite noticeable in Fig. 24. If a continuous output is desired, a hold circuit can be connected after the second sampler in Fig. 23. This technique enables us to exploit the sampled data theory to achieve long-time integration. The application of this theory to drift-corrected chopper amplifiers is widely known and needs no further discussion. An application of this theory to voice multiplexing is described by Kamp.<sup>15</sup>

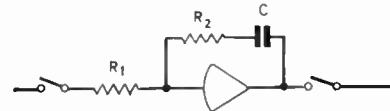


Fig. 25. Realization of pulsed p+i controller.

### 9. z-Transform Theorems

A short list of important theorems is given below. For proofs and more details, reference should be made to the literature.<sup>4-8</sup>

(1) *Linearity:*  
 $\mathcal{Z}[ag(t)] = aG(z) \dots\dots(54)$

$\mathcal{Z}[g_1(t) + g_2(t)] = G_1(z) + G_2(z) \dots\dots(55)$

(2) *Real Translation:*  
 $\mathcal{Z}[g(t \pm nT)] = z^{\pm n} \cdot G(z) \dots\dots(56)$

(3) *Scale Change in the z-Domain:*  
 $\mathcal{Z}[e^{\pm at} \cdot g(t)] = G(e^{\pm at} \cdot z) \dots\dots(57)$

(4) *Final Value:*  
 $\lim_{t \rightarrow \infty} f(t) = \lim_{z \rightarrow 1} \left[ \frac{z-1}{z} \cdot G(z) \right] \dots\dots(58)$

(5) *Initial Value:*  
 $\lim_{t \rightarrow 0} f(t) = \lim_{z \rightarrow \infty} G(z) \dots\dots(59)$

### 10. z-Transforms versus Other Numerical Approximations

We have shown that the z-transform is based on the replacement of the continuous function by the staircase function (i.e. rectangles approximation) and sampling the latter. We have emphasized before that this method is an approximation whose accuracy depends on the sampling rate. We shall now compare the conventional z-transform which is based on the rectangle approximation to other numerical approximation based on other criteria. It has been shown (10-12) that other approximations give much better accuracy for the same sampling rate and the only advantage of the conventional z-transform is its simplicity (a factor which is very important in

analysing and synthesizing complicated systems), and higher degree of stability.

Consider the function of integration in the time domain:

$$\mathcal{L} \left[ \int_0^{\infty} f(t) \cdot dt \right] = \frac{1}{s} F(s) = C(s) \cdot F(s)$$

According to the conventional z-transform which is based on the rectangles approximation, the computer is programmed to perform:

$$C(z) = \frac{Tz}{z-1} \quad \dots\dots(60)$$

Using the trapezia approximation we have:

$$C(z) = \frac{T}{a} \cdot \frac{z+1}{z-1} \quad \dots\dots(61)$$

Simpson's  $\frac{1}{3}$  method yields:

$$C(z) = \frac{T}{3} \cdot \frac{z^2+4z+1}{z^2-1} \quad \dots\dots(62)$$

Simpson's  $\frac{2}{3}$  method yields:

$$C(z) = \frac{3T}{8} \frac{1+3z^{-1}+3z^{-2}+z^{-3}}{1-z^{-3}} \quad \dots\dots(63)$$

Weddle's method gives:

$$C(z) = \frac{3T}{10} \frac{1+6z^{-1}+6z^{-2}+6z^{-3}+z^{-4}}{1+z^{-1}+z^{-3}+z^{-4}} \quad \dots\dots(64)$$

Note that the factor  $T$  has already been included in the programs to comply with eqn. (11).

Table 2 shows the relative error when integrating an harmonic function of angular frequency:

$$\omega = \frac{1}{T} \cdot \frac{\pi}{3} \quad \text{and} \quad \omega = \frac{1}{T} \cdot \frac{\pi}{2}$$

A comparison between the five methods and pure integration is given by Salzer<sup>12</sup> where amplitude/frequency and phase/frequency are plotted.

In general, the reader is advised to apply the conventional z-transform for their simplicity and

higher stability, and try to achieve the highest sampling rate possible.

### 11. Conclusion

The z-transform theory enables the response of known systems to recorded data to be computed without transforming the data to the s-plane and without the use of the tedious Convolution Integral. The results have been shown to be an approximation whose accuracy depends on the sampling rate.

The common error in the analysis of the systems incorporating zero-order hold circuits has been exposed. It has also been shown that in the case where a sampler is followed by a hold circuit, the system may be treated in the continuous s-plane with the inclusion of a small time delay  $e^{-sT}$ .

The application of the z-transform theory to pulsed systems was demonstrated by the realization of discrete controllers. Attention has been called to the fact that the z-transform theory is based on the rectangles approximation which is not the best approximation to continuous functions.

The choice between pulsed or continuous systems should be made on engineering merits only. Consideration should be given to economics, multiplexing, reliability, power dissipation, drift and long time integrations. The z-transform is a useful tool in these applications, but not necessarily the most accurate one. In due course perhaps the numerical analysis theory will be developed to give a more accurate technique which is as easy to apply as the z-transform.

### 12. References

1. J. G. Holbrook, "Laplace Transforms for Electronic Engineers", (Pergamon Press, London, 1958.) (a) pp. 105-11; (b) p. 171.
2. J. R. Raggazzini and L. A. Zadeh, "The analysis of sampled data servo systems", *Trans. Amer. Inst. Elect. Engrs*, 71, Part 2, pp. 225-34, 1952.

**Table 2**  
Relative errors for different methods of integration of an harmonic function

Frequency	Method				
	Rectangles (Conventional z-transforms)	Trapezia approximation	Simpson's $\frac{1}{3}$	Simpson's $\frac{2}{3}$	Weddle's
$\omega = \frac{1}{T} \frac{\pi}{3}$	+4.7%	-9.3%	+0.77%	+1.12%	-0.25%
$\omega = \frac{1}{T} \frac{\pi}{2}$	+9.5%	-7.9%	+1.05%	+1.19%	-0.93%

3. Y. Azar, "Some pitfalls in the application of z-transforms", *Control*, 8, No. 76, pp. 571-3, October 1964.
4. J. E. Gibson, "Non-linear Automatic Control", pp. 112-20. (McGraw-Hill, New York, 1963.)
5. E. I. Jury, "Sampled Data Control Systems". (John Wiley, New York, 1958.)  
(a) pp. 123-30.
6. J. T. Tou, "Digital and Sampled Data Systems". (McGraw-Hill, New York, 1959.)  
(a) pp. 481-98; (b) pp. 501-34 and (c) p. 521, Fig. 10.4-1.
7. J. R. Ragazzini and G. F. Franklin, "Sampled Data Control Systems". (McGraw-Hill, New York, 1958.)  
(a) pp. 148-80.
8. Ya. Z. Tsypkin, "Sampled Systems Theory and Applications". (Pergamon Press, Oxford, 1964.)
9. K. Togino, "Sampling controllers pace Japanese sintering mill", *Control Engineering*, 11, No. 5, pp. 86-94, May 1964.
10. W. K. Linvill and R. W. Sittler, "Extension of conventional technique to the design of sampled data systems", *I.R.E. Convention Record*, 1, Part 1, pp. 99-104, 1953.
11. W. K. Linvill and J. R. Salzer, "Analysis of control systems involving digital computers", *Proc. Inst. Radio Engrs*, 41, pp. 901-6, July 1953.
12. J. M. Salzer, "Frequency analysis of digital computers operating in real time", *Proc. Inst. Radio Engrs*, 42, No. 2, pp. 457-66, February 1954.
13. D. A. Pierre, "A tabular algorithm for z-transform inversion", *Control Engineering*, 10, No. 9, p. 110, September 1963.
14. E. I. Jury, "Theory and Application of the z-Transform Method". (John Wiley, New York, 1964.)
15. H. A. Kamp, "Time-division multiplexing simplifies voice relay switching", *Control Engineering*, 11, No. 1, p. 101, January 1964.
16. J. G. Truxal, "Automatic Feedback Control Synthesis". (McGraw-Hill, New York, 1959.)  
(a) p. 511; (b) p. 521.

*Manuscript first received by the Institution on 25th July 1964, and in final form on 2nd October 1964. (Paper No. 993/C81.)*

© The Institution of Electronic and Radio Engineers, 1965

# Radio Engineering Overseas . . .

The following abstracts are taken from Commonwealth, European and Asian journals received by the Institution's Library. Abstracts of papers published in American journals are not included because they are available in many other publications. Members who wish to consult any of the papers quoted should apply to the Librarian, giving full bibliographical details, i.e. title, author, journal and date, of the paper required. All papers are in the language of the country of origin of the journal unless otherwise stated. Translations cannot be supplied.

## P.C.M. ENCODING

Instantaneous companding is a useful technique for the improvement of the transmission quality of p.c.m. systems. In a Japanese paper various non-linear encoding and decoding techniques without using diode companders are discussed, with particular emphasis on logarithmic decoders, which are composed of cascaded attenuators. A hyperbolic sinusoidal law is derived from the logarithmic law, and is obtained by an attenuation line decoder. These non-linear laws are attained on the attenuation-linear basis. Likewise, various passive decoders on the immittance-linear basis can be considered. In this case the non-linear law is expressed by a rational function of the digital variable  $x$ . Also a decoder based on the multinomial expansion is introduced, whose non-linear law is given by a polynomial of  $x$ .

It is shown that the hyperbolic sine curve provides more uniform signal/noise characteristics for some range of the mean speech volume, while the modified hyperbolic law yields as high signal/noise ratio as is obtained by the exponential law without great loss in the signal/noise ratio for louder speech. Several experimental studies of these decoders are described.

"Logarithmic p.c.m. encoding without diode compander" Hisashi Kaneko and Tadahiro Sekimoto, *N.E.C. Research and Development*, No. 7, pp. 12-25, November 1964. (In English.)

## U.H.F. TELEVISION

The November 1964 issue of *L'Onde Électrique* is devoted to "Decimetric Television". The following are some of the papers:

"Television on decimetric wavelengths", L. A. Lamoitier, pp. 1091-2.

"French standards for the second channel", M. L. Goussot, pp. 1093-8.

"The propagation of decimetric waves (from the television point of view)", J. F. Arnaud, pp. 1099-1106.

"The specification of transmitting equipment for television at decimetric wavelengths", S. Lacharnay, pp. 1107-14.

"The Stockholm plan for decimetric wavelengths", M. Huet, pp. 1115-20.

"Klystrons for high power television transmitters at decimetric wavelengths", P. Aucouturier, pp. 1121-7.

"Klystron decimetric television transmitter", C. Babillon, pp. 1128-38.

"Power tetrodes for television transmitters in Bands IV and V", M. Gerlach, pp. 1139-44.

"C.F.T.H. television transmitters using tetrodes for decimetric waves", R. Depaillat, pp. 1145-56.

"C.S.F. antennas for television at decimetric wavelengths", M. Renoir, R. Dassonville, M. Destrade and L. Pham van Cang, pp. 1157-1163.

"C.F.T.H. television antennas for decimetric waves (Bands IV and V)", R. Chesneau, pp. 1164-76.

"Slot antennas: principles and practice", M. Rateau, pp. 1177-88.

"Problems arising in the installation of transmitting aerials for decimetric wavelengths", L. Kaiser, pp. 1189-96.

"Phase distortion in waveguides", R. Martin, pp. 1197-1200.

"Waveguides and their use in television", L. Le Davay, pp. 1201-8.

"Television receivers for transmissions in the metric and decimetric wave bands", A. Dubec, pp. 1209-19.

*L'Onde Électrique*, 44, No. 452, pp. 1091-1219, November 1964.

## MEASUREMENT OF F.M. INTERMODULATION NOISE

Intermodulation noise generated in f.m. signals carrying noise modulation of arbitrary pre-emphasis by linear amplifier and discriminator networks having polynomial frequency characteristics is discussed in a recent Swedish monograph and a consistent first order theory is derived. Special attention is paid to the cases of no pre-emphasis and C.C.I.R. pre-emphasis. The theory is applied to evaluate the distortion of 960-channel and 1800-channel f.d.m. signals in amplifiers consisting of stagger-tuned pairs, stagger-tuned triples and equal- $Q$  double-tuned stages, and it is demonstrated that double-tuned amplifiers are vastly superior.

The exact transmission properties and design equations for double-tuned circuits having maximally-flat selectivity curves are derived, and elements of a pole-zero synthesis procedure for wideband discriminator networks are outlined.

The design of a new type of instrument for measuring f.m. intermodulation noise generated in 70 Mc/s i.f. amplifiers is described, and a high-resolution group-delay meter for the frequency range 60 to 80 Mc/s is presented.

"On Intermodulation Noise and Group-Delay in Wideband Radio-Relay Systems Carrying Frequency-Division Multiplex Telephony", R. I. Magnusson, *Transactions of Chalmers University of Technology, Gothenburg, Sweden*, No. 285, 1964. (177 pages) (In English.)